Tectonic Geomorphology and Paleoseismology of the Lake Heron Fault, New Zealand

A thesis submitted in partial fulfillment of

the requirements for the degree of

Master of Science in Geology

at the

University of Canterbury

by

David Samuel Jacobson

July 2015

Abstract

New Zealand's South Island is actively deforming as a result of oblique continental collision between the Pacific and Australian Plates. Within the central portion of the island, this results in reverse faulting, including earthquake rupture on the previously unreseached Lake Heron Fault. Because few of these faults have been studied, there is a major gap in knowledge on the paleoseismicity of the region.

In this thesis, I use structural mapping, deformation analysis, geophysics, topographic contouring, fault measurements, Monte Carlo simulations, and paleoseismic trenching, in conjuction with geochronologic approaches including Schmidt hammer exposure age dating, and radiocarbon dating to characterize the earthquake history and behavior of the Lake Heron Fault.

Measurements of Pleistocene-Holocene displacement of discrete and distributed deformation indicate that along the Lake Heron Fault, total vertical deformation is approximately 20 m since the Last Glacial Maximum. This deformation can be constrained, using Schmidt hammer exposure age dating, to the last 10.15 ± 2.95 ka, and is consistent across surfaces which could differ in age by up to 15 ka. This suggests that a period of quiescence was followed by increased activity, and using Monte Carlo simulations, a vertical slip rate of 2.25 ± 1.05 mm/yr was calculated. This is more than double published vertical uplift rates, though when the fault dip within bedrock (60°) is integrated, net slip falls within published geodetic slip rates. While the fault was seen to dip 60° in bedrock, near surface dip measurements indicate a deflection and shallowing of fault dip by up to 80% in some locations in Late Quaternary sediments.

Further structural calculations indicate that while the Lake Heron Fault has a strike (200°), preferential to pure dip-slip motion, which is seen on discrete fault scarps, microtectonic measurements from crestal grabens show that along the fault, near-surface stress and localized surface rupture is not representative of the regional stress or the structure at depth.

From paleoseismic trenching, evidence of 2-3 earthquakes was discovered, and using radiocarbon dating, the timing of the last events is constrained to the last 2.6 ka, with the most recent event occurring approximately 0.6 ± 0.2 ka. Large single event displacements (2.75 ± 0.25 m), earthquake magnitudes (Mw 7.4 ± 0.3), and a short recurrence interval (1.45 ± 0.42 ka) indicate that the Lake Heron Fault has been highly active in the Holocene.

Results of this study in conjunction with others also show there is a possibility the Lake Heron and Forest Creek fault represent an 80 km long, segmented reverse fault, capable of generating Mw 7.7 earthquakes. However, because of variability in the timing of paleoearthquakes, the structures more frequently ruptures independently in magnitude 7.0+ earthquakes. Lastly, I propose that changing crustal stress provides a possible mechanism for apparent temporal variability in the earthquake recurrence on the Lake Heron Fault.

Acknowledgements

During my MSc study both my research and I were supported by the New Zealand Earthquake Commission, and Environment Canterbury for which I am very grateful.

First and foremost, I would like to thank my supervisor, Mark Quigley. Mark, thank you for supporting, and teaching me for the last 2.5 years. The last year during the course of my thesis has been a wild time for many reasons, and I am grateful you took a chance and committed to me. You provided necessary feedback, while also trusting and challenging me to always make my project better.

Further discussions with University of Canterbury staff, including Jarg Pettinga, Stefan Winkler, and Andy Nicol provided useful insights, while also reining me in when I strayed too far outside the box. David Nobes also assisted with GPR processing and interpretations of geophysics done with Matt Cockcroft.

Two people I continue to be in debt to are Ellyse Gore and Alec Wild. Ellie, thank you for helping with so much field work even as temperatures fell below zero, and for providing support when things were hardest. You helped get me out in the field when I wasn't sure I could go. Alec, thank you for helping with field work, especially Schmidt hammering, keeping me sane through rough times, and for the soccer discussions during our many coffee breaks. I will surely miss those.

The technical staff at UC, namely Pat Roberts, Janet Warburton, Sacha Baldwin-Cunningham were all fantastic and helped my Masters run smoothly. Sacha, a special thank you for your help when I repeatedly ran into problems during my field work. I would also like to thank Anekant Wandres for aiding me with GPS processing and for always keeping me on edge with his jokes.

The landowners of the Lake Heron Basin and the Department of Conservation have been receptive, and I thank them for allowing me to conduct research on their land. While DOC didn't allow my project to progress as planned, I still managed to get useful results.

Another group of people that deserve a special thanks are members of the Christchurch ultimate frisbee community. Being able to get out and away from distractions, and playing a sport in which I was always surrounded by such amazing people was great. Plus, winning two national championships was icing on the cake. Thank you to everyone for challenging me in another facet of my life.

I would also like to thank my flatmates. While there has been turnover, everyone at 38

Hansons Lane has always be extremely supportive, and provided me a welcoming environment that I felt I could truly go home to.

Last, but certainly not least I would like to thank my family in the U.S.. The support I have received during my last 3 years in New Zealand helped me get through this, and I couldn't have done it without you.

Contents

List of Figures

List of Tables

1 Introduction

1.1 Background

Situated on the plate boundary between the Australian and Pacific plates, New Zealand has numerous locations where research into tectonic geomorphology and paleoseismology can be conducted. Its short geologic history, tectonic variability, and abundant associated hazards means these studies are vital for understanding and quantifying deformation and seismic hazard at plate boundaries.

Within the central South Island, numerous reverse faults are clearly exposed at the surface through the geomorphology of the landscape. However, with the exception of a few studies (Van Dissen et al., 1993; Amos and Burbank, 2007; Amos et al., 2007, 2010, 2011; Stahl, 2014), slip rates, recurrence intervals, coseismic slip, and earthquake magnitudes for many active faults are unknown. This is a clear gap in knowledge, especially for a region where the deformation and seismic hazard is dominated by these NE-striking reverse faults (Stahl, 2014). Additionally, within the area, limited dating has been done, and most slip rates, and moment magnitudes are based off relative and extrapolated surfaces, and scaling relationships rather than paleoseismic investigation (Barrell and Strong, 2009). Furthermore, while geodetic measurements are valuable, where geologic studies have been conducted, there is great disparity between the reported slip rates (Wallace et al., 2007). Finally, recurrence intervals assigned to most of these faults have been generated using scaling laws that were designed for strike slip and oblique faults rather than reverse faults (Stirling et al., 2012). Therefore, there is a need to complete more of these studies to determine the tectonic model for Canterbury and New Zealand as a whole.

While there have been few studies on faults in the foothills of the Southern Alps, those elsewhere have provided constraints on the paleoseismic history of many of New Zealand's major faults (Howard, 2001; Nicol et al., 2001; Norris and Cooper, 2001; Howard et al., 2005; Hornblow et al., 2014; Khajavi et al., 2015). Each of these studies provided valuable data, furthering knowledge on deformation and seismicity within New Zealand.

Despite 75% of the average slip across the South Island being taken up by the Alpine Fault, there is debate as to how the remaining 25% is distributed (Norris and Cooper, 2001). As it currently stands, faults such as the Lake Heron Fault, within New Zealand's compressive regime of the foothills of the Southern Alps, account for some of this deformation (Pettinga et al., 1998, 2001; Wallace et al., 2007). The Lake Heron Fault is also of importance as it lies near a zone where reverse faulting transitions to strike-slip, and it is the largest reverse fault in the northern part of the central South Island (Stahl, 2014). Therefore, understanding

the paleoseismology, structure, and kinematics in the region could help further the structural model for Canterbury.

To date, no study has thoroughly investigated the Lake Heron Fault. Only preliminary field mapping has been completed, no active fault research has taken place, and all data is based primarily on potential surfaces ages, scaling relationships, and similarities with faults of similar size or in the region (Pettinga et al., 1998; Barrell and Strong, 2009).

A comprehensive study of the Lake Heron Fault will provide additional insight into a fault lacking comprehensive analysis, and the compressive regime of the eastern foothills, including but not limited to: relationships with nearby faults (Stahl, 2014), how changing stress could have influenced the tectonic history, and how rheology and sediment thickness can effect fault surface rupture.

1.2 Aims and Methodology

The principle aims of this study are to gain a greater understanding of the behavior of the Lake Heron Fault since the Last Glacial Maximum, and to use this information to better understand fault dynamics in west-central Canterbury. To date, there is a sufficient lack of evidence detailing the characteristics of reverse faults. This is attributed to the fact that they are often blind, have discontinuous surface traces, and/or zones of distributed faulting (Roering et al., 1997; Stahl, 2014). Nevertheless, research must be done on them to better understand their earthquake hazards and associated paleoseismicity. Outcomes of this project will include a revised understanding of the structures and deformation associated with the Lake Heron Fault, an approximated late Quaternary earthquake fault rupture history, and insights into how regional strain is taken up throughout the area.

Research methods used in this study include:

1. Aerial photo analysis using KiwiImage, DigitalGlobe imagery, and 1940's aerial photography. This was combined with detailed field mapping of structural and geomorphic features in the Lake Heron Basin.

2. Radiocarbon (^{14}C) dating of charcoal samples to constrain the late Quaternary rupture history of the Lake Heron Fault. These samples were analyzed by the radiocarbon lab at GNS.

3. Hand-dug trenching along the main trace of the Lake Heron Fault on the Paddle Hill Creek Fan. This was done to obtain samples suitable for radiocarbon dating, as well as

additional measurement of the fault's slip rate, and information required to calculate the Lake Heron Fault's recurrence interval, coseismic slip, and timing of paleoearthquakes.

4. Geophysical surveying using 100 MHz pulsEKKO and 200 MHz shielded GPR systems. Surveys were done at the trench location, and others on the Paddle Hill Creek Fan.

5. Topographic contouring of a moraine along the Lake Heron Fault in order to determine fault morphology and the kinematics required to produce offset seen.

6. Fault scarp analysis through surveying using a differential GPS (GeoXH 2008).

7. Analysis of geomorphic features using approximate ages to determine slip rates, recurrence intervals, single event displacements, and approximate earthquake magnitudes along the Lake Heron Fault.

8. Schmidt Hammer exposure dating of modern and relict fluvial terraces using the techniques proposed by Winkler (2005), Shakesby et al. (2006), and Stahl et al. (2013) in order to constrain the Lake Heron Fault's recurrence interval.

9. Fault measurements taken at in situ greywacke, and piercing points in order to constrain the near surface fault dip of the Lake Heron Fault in order to show its variability.

10. Monte Carlo paleoseismic analysis using @Risk software.

Thesis Goal	Research Questions	Relevant Chapter
Determine slip rates and deformation to identify recent fault activity on the Lake Heron Fault.	How is fault-associated deformation distributed along the fault?	Chapters 2 & 3
	How do ages calculated using Schmidt hammer exposure age dating compare with published ages?	Chapter 2
	How do calculated slip rates compare with geodetically derived ones?	Chapter 5
Obtain ages and single event displacement of earthquakes to determine a recurrence interval and potential earthquake magnitudes of the Lake Heron Fault	How does sediment thickness/type/rheology effect fault behavior at/near the surface?	Chapters 2 & 3
	What type of motion is observed along the Lake Heron Fault and what are the implications?	Chapter 3
	Is it possible, that the Lake Heron Fault links with the Forest Creek Fault to the south-west? If so, what are the implications?	Chapters 4 & 5

Figure 1.1: Thesis aims and questions

1.3 Geological Setting

1.3.1 Plate Boundary Tectonics

The motion between the Australian and Pacific plates is accommodated predominantly (75%) along the Alpine Fault, a NE-SW-striking dextral reverse fault (Norris and Cooper, 2001). This fault, which extends for over 400 km through the South Island from just NE of Milford Sound to the Marlborough Region has a recurrence interval of a few hundred years, each time generating Mw 7.8 ± 0.5 earthquakes (Sutherland and Norris, 1995; Sutherland et al., 2007; Langridge et al., 2010). This means that of the approximately 40 mm/yr of fault-parallel interplate motion that occurs in the central South Island, 30 mm takes place along the Alpine Fault, with the rest of it distributed amongst numerous faults across the region. Much of this leftover motion is accommodated in the Marlborough Fault System and the eastern foothills of the Southern Alps (Norris and Cooper, 2001; Wallace et al., 2007; DeMets et al., 2010) (Figure 1.2).

Outside of the Alpine Fault, Canterbury is broken up into eight fault domains (Pettinga et al., 1998) (Figure 1.3). The Lake Heron Fault lies on the border of Domains 5 and 6, which are regions of thrust/reverse faulting. These domains mark the margin with the Southern Alps, which were created by continent-continent collision, and have the geometry of a double-sided wedge (Norris et al., 1990). Domains 5 and 6 lie just southwest of the highly active Porters Pass-Amberley Fault Zone, an area of hybrid strike-slip and thrust faulting, representing the beginning of a transition from thrust to strike-slip faulting in New Zealand (Pettinga et al., 1998).

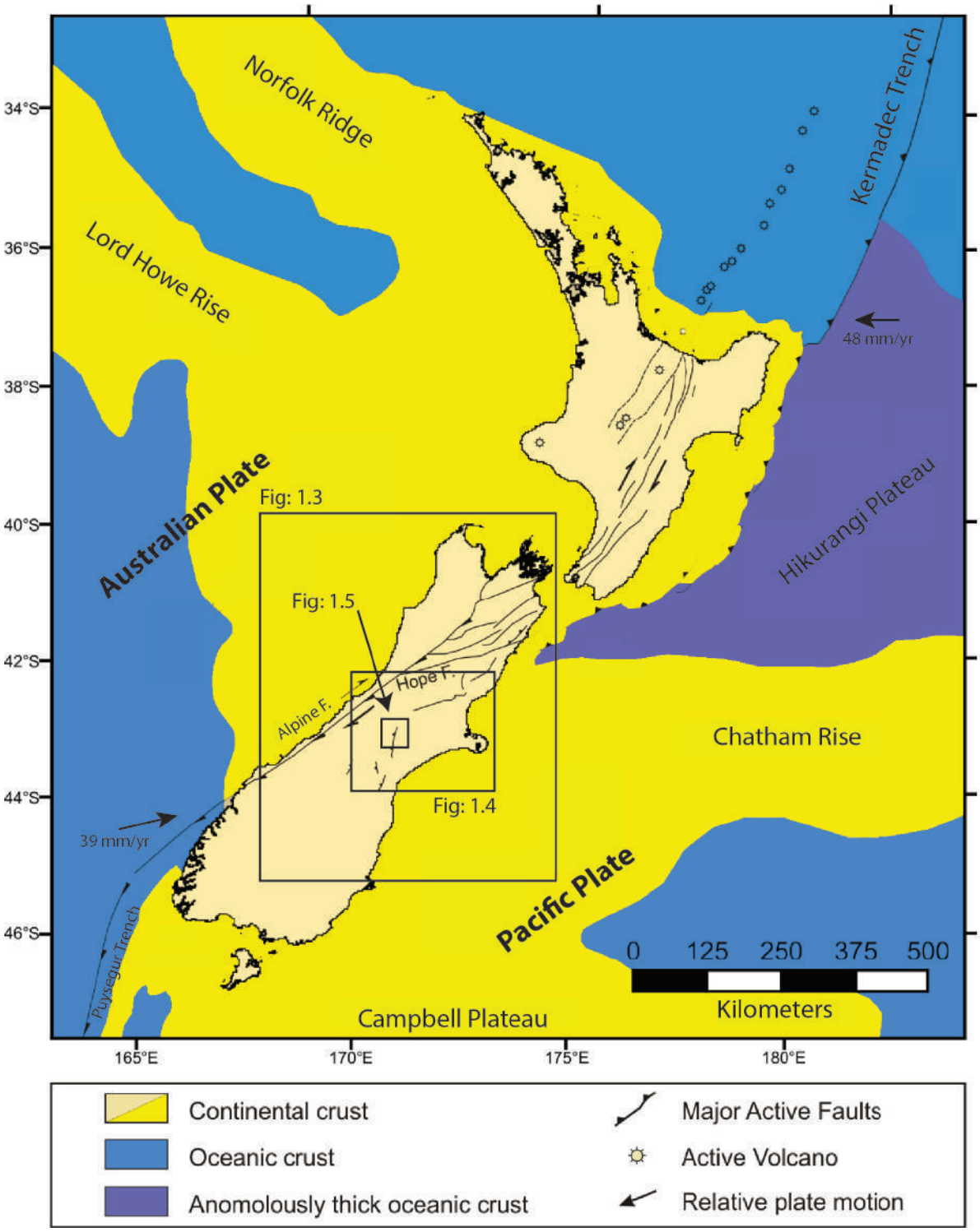

Figure 1.2: Structural map of New Zealand illustrating relative plate motion and large-scale faults (Pettinga et al., 1998; Beavan et al., 2002). Of the 40 mm/yr of plate motion, 75% of it is accommodated along the dextral-reverse Alpine Fault.

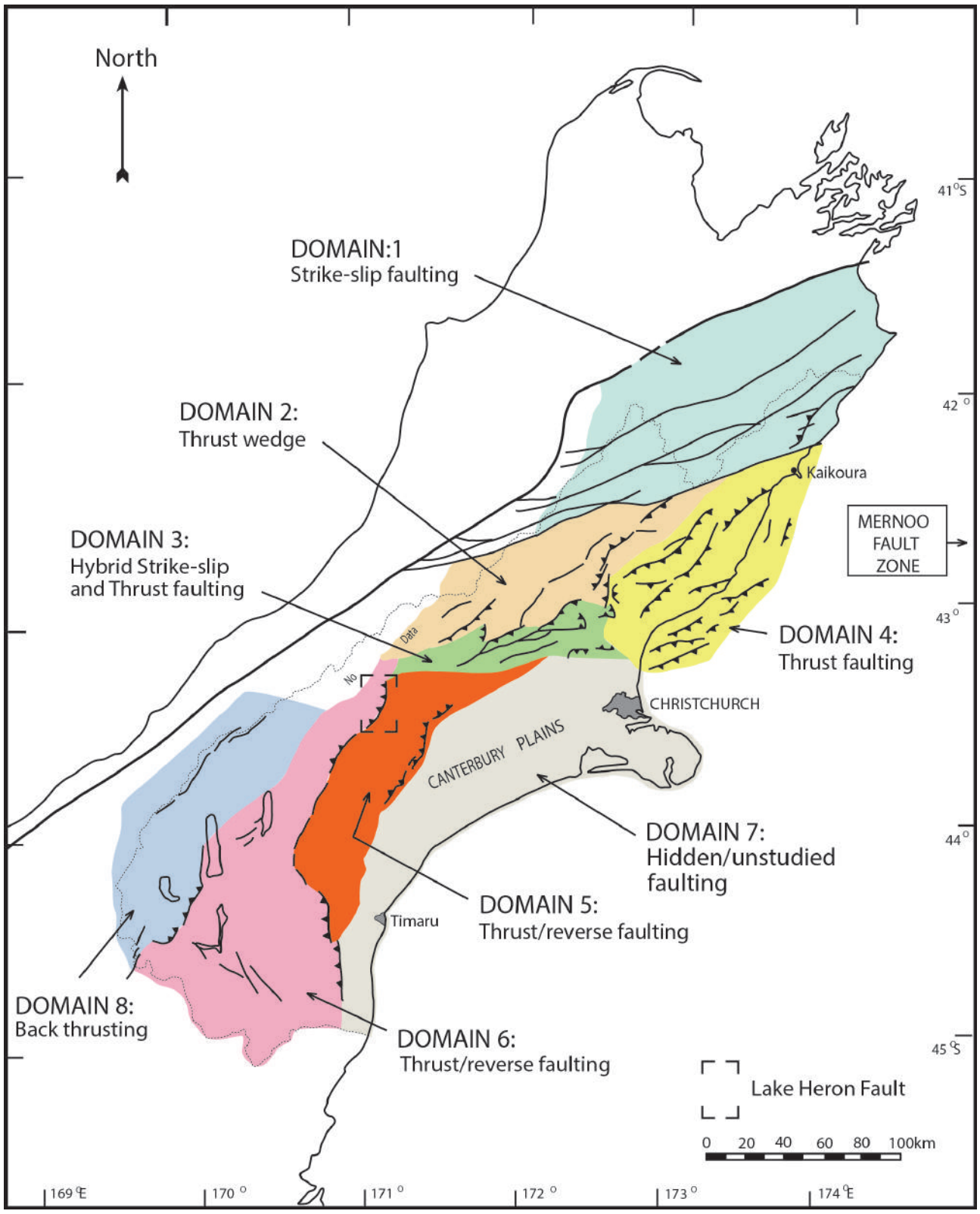

Figure 1.3: Fault domain map of the Canterbury region. The Lake Heron Fault is located on the border between domains 5 and 6, though officially it is in Domain 6 (Pettinga et al., 1998). These domains mark the transition from thrust/reverse faulting to strike-slip faulting to the northeast in the Porters Pass/Amberley Fault Zone.

1.3.2 Geology of Western Canterbury

The geology of western Canterbury is made up predominantly of Mesozoic greywacke, which is part of the Torlesse Supergroup (Cox et al., 2007). Within the study area, the rocks are "non-schistose to schistose quartzofeldspathic sandstone interbedded with siltstone-mudstone" (Cox et al., 2007). Overlying much of the basement rock is a veneer of Quaternary sediments, dominated by Holocene and Pleistocene glacial and glacial outwash deposits, of which limited absolute dating has been done (Barrell et al., 2011; Rother et al., 2014).

The area of active thrust faulting, which includes the Lake Heron Fault, is within a zone of secondary maximum convergence and elevated strain rates when compared to regions outside the Alpine Fault (Beavan and Haines, 2001; Wallace et al., 2007). Some surveys suggest these faults, which are often moderate to steeply dipping, and inferred to shallow into a decollement at 10-20 km depth, represent backthrusts off the Alpine Fault (Berryman et al., 2002; Wannamaker et al., 2002; Beavan et al., 2007).

1.4 Previous Work

Despite being the northernmost major reverse fault in the Central South Island, no paleoseismic or structural investigation has taken place on the Lake Heron Fault (Stahl, 2014). The fault was first mapped, though not named, by Gair (1967), and then Mabin (1980). Oliver et al. (1990) published a more detailed map, which included the then named Lake Heron Fault. This map included fault scarps as well as the nearby Maori Lakes Fault. While Oliver et al. (1990) published this map for the Department of Scientific and Industrial Research, Sarah Beanland was credited with the mapping. Though these maps gradually became more detailed, this is the first study in which the fault has been mapped in great detail, aided by high resolution satellite imagery.

While there has been more recent research into the area (Pettinga et al., 1998, 2001; Cox et al., 2007; Barrell and Strong, 2009; Barrell et al., 2011) it relies primarily on scaling relationships and relative ages. Aerial photo mapping and preliminary field reconnaissance was done to locate active faults and other structural features (Pettinga et al., 1998, 2001). These studies suggest that the Lake Heron Fault is approximately 40 km long with an average strike of 205°. Additionally, they indicate the fault dips 45° to 60° west, last ruptured 2,700 years ago, and generates Mw 7.4 $\pm$ 0.3 earthquakes. However, these studies were done in an attempt to catalogue and compile all existing records with some new supplementary material rather than conduct entirely new investigative research.

Another such compilation is the GNS QMAP of the Aoraki region, created in 2007 to synthesize existing geologic data and provide insight into regional geology and location of faults (Cox et al., 2007). More recently, two GNS reports (Barrell and Strong 2009; Barrell et al. 2011) gave much more focus to the region. In one, all known active faults within the Ashburton District were identified, with approximate slip rates and recurrence intervals given (Barrell and Strong, 2009). However, uplift per event (2 m) was proposed in order to place the features within a previously published recurrence interval classification. Additionally, the age of the deformed landscape was estimated, rather than provided by means of absolute ages. In Barrell et al. (2011) the glacial geomorphology of the region was interpreted. This research, which compiled over 10 years of data, subdivided glacial units while providing estimations of ages. However, these ages were not calculated from dating, and were done instead through surface correlation and known ages of glacial advances.

In addition to these works, two glacial geomorphology theses were completed in 2008 at the University of Canterbury. Jeremy Pugh and Mike Evans researched the glacial history of the Lake Heron and nearby Lake Clearwater basins respectively (Evans, 2008; Pugh, 2008). These theses identified and dated glacial advances and retreats found throughout the valleys. More recently, much of this work was reanalyzed, with additional surface exposure ages to determine the extent of New Zealand's Last Glacial Maximum (Rother et al., 2014).

1.5 Location and Characteristics of Study Area

The Lake Heron Fault study area lies north of the Rangitata River, in the northwest portion of the Ashburton District. The area is 25 km northwest of Mt. Somers, and 120 km west of the city of Christchurch (Figure 1.4). The majority of field work was done just south of Lake Heron in the DOC-run Hakatere Conservation Park. Additionally, work was completed on the Castle Ridge and Mt. Arrowsmith Stations, which are used predominantly as pasture land.

The Lake Heron Basin is a relatively cool climate region, and receives limited rainfall (Figure 1.7). Though the models in Figure 1.7 indicate that the basin is on average 13.8° C, and receives 74 cm of rainfall per year, the interpolations were created using no climate stations within the basin. Therefore, while they provide useful information, their limitations are to be noted. Because of this climate, it is likely that rocks in the area weather slowly, which will become applicable to the Schmidt hammer exposure age dating done in Chapter 3.

Due to the alpine climate, the area contains sparse vegetation. The only trees are those planted on station land while the rest of the non-station land is dominated by grasses, tussock, matagouri and Spaniard Grass.

The topography of the field site varies significantly. To the east and west are the Mt. Somers and Dogs Ranges respectively, which reach 2,200 meters in elevation. Along the majority of the Lake Heron Fault, the elevation is approximately 700 m, with some variability along alluvial fans and glacial moraines.

The surface geology within the basin is dominated by Quaternary sediments of glacial and fluvial origin (Cox et al., 2007) (Figures 1.5 & 1.6). The only bedrock found within the field site is in the ranges and along the fault in the active channel of the South Branch of the Ashburton River.

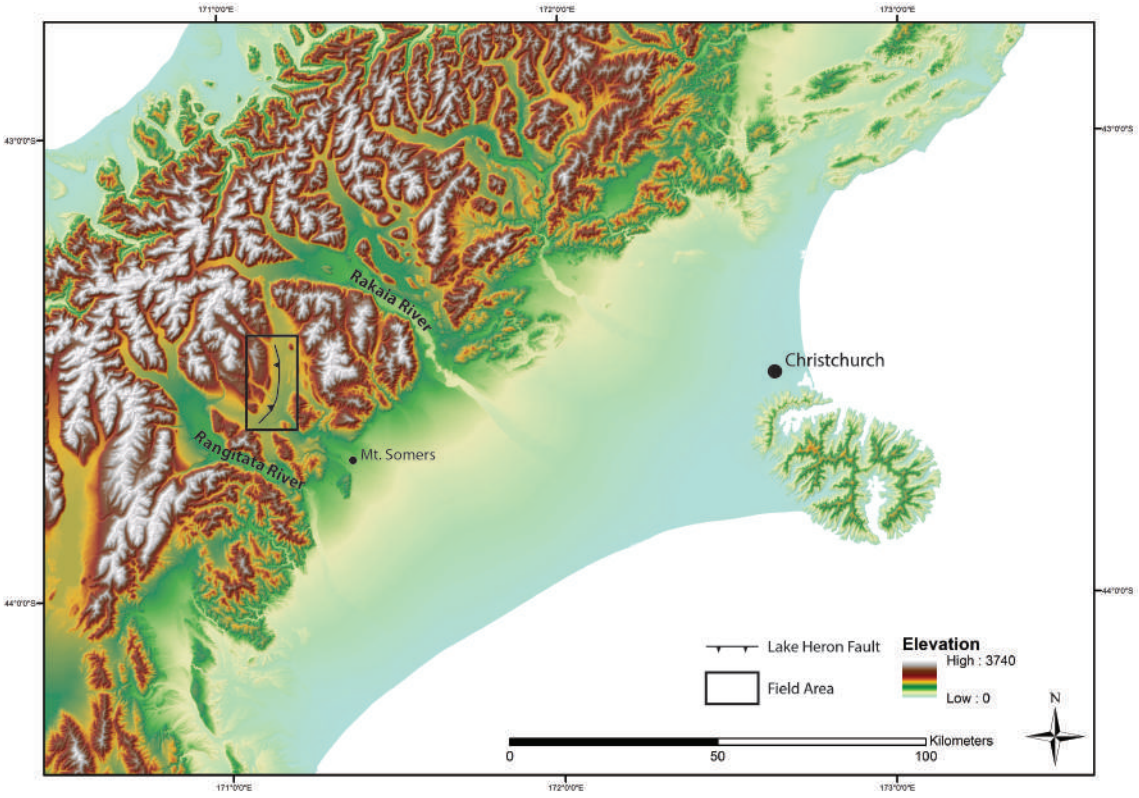

Figure 1.4: Surface DEM map showing the location of the Lake Heron Fault.

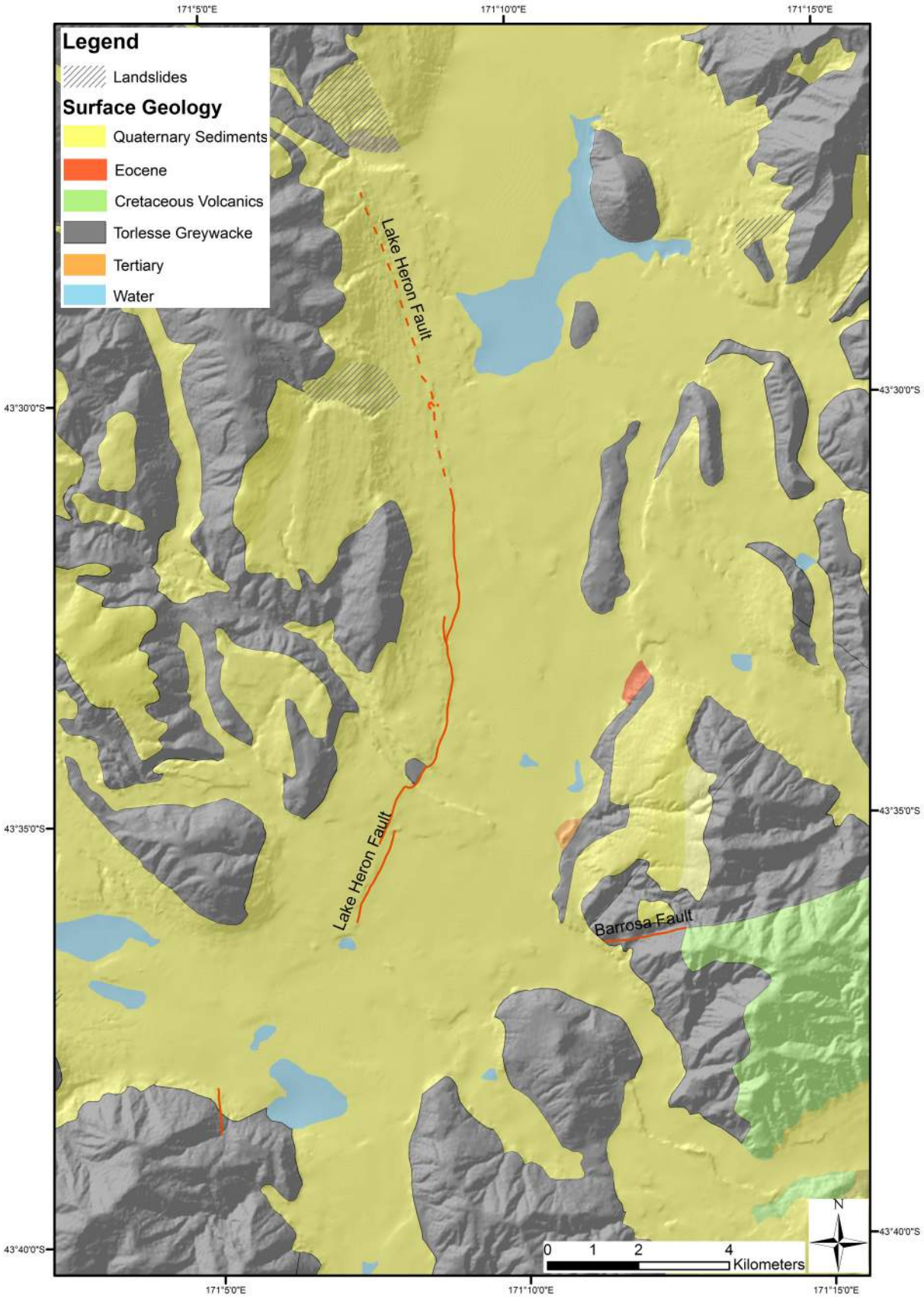

Figure 1.5: Simplified surface geology of the Lake Heron Basin (Modified from Cox et al. (2007)).

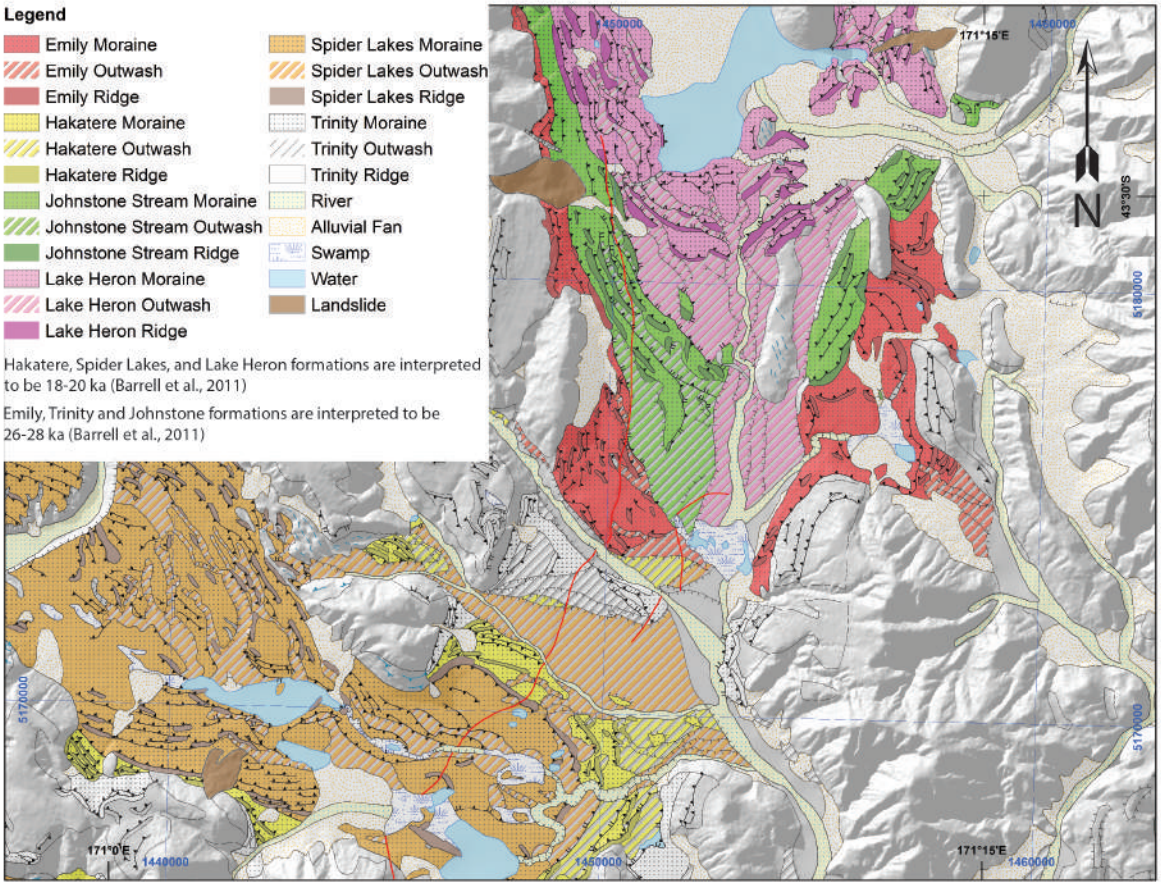

Figure 1.6: Geomorphic map of the Lake Heron and Lake Clearwater basins from Barrell et al. (2011). In this figure, the red lines represent structural features, while all black lines represent riser types.

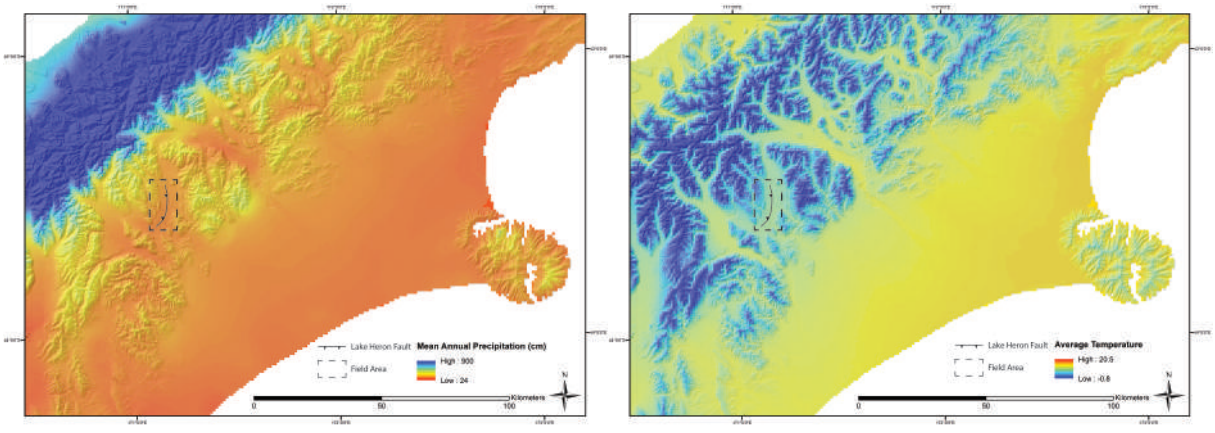

Figure 1.7: Precipitation (left) and temperature maps for the central South Island. It is important to note that these are interpolations generated using climate stations from around the South Island.

1.6 Thesis Format and Logistical Explanation

Chapter 2 investigates the structural geology and surface deformation of the Lake Heron Fault. Within this chapter, the fault will be broken up into three study areas: Spider Lakes, Paddle Hill Creek and Castle Ridge. Each of these sections will be examined individually and collectively to determine the reasons behind the variability seen. Challenges in determining the structure and extent of deformation in regions such as the Lake Heron Basin exist due to varying topography and orientation of geomorphic features. Therefore, field mapping, fault dip measurements, geophysics and surveying using dGPS units provided excellent means of determining the structure and deformation. Understanding these characteristics and the kinematics required to produce the features along the Lake Heron Fault required addressing several questions:

1. Does the Lake Heron Fault exhibit typical reverse fault behavior? How do microtectonic stresses acting on the Lake Heron Fault compare with regional stress, and what are the implications?
2. How does sediment thickness and rheology affect fault exposure at the surface? This exposure includes a combination of the size of the deformation zone, coupled with the structures seen. In order to determine this, numerous cross sections will be produced to analyze changing fault surface expressions.
3. How does deformation vary throughout the Lake Heron Basin?

Chapter 3 investigates the chronologic history of the Lake Heron Fault. This was done through both Schmidt hammer exposure-age dating (SHD) and paleoseismic trenching of the Lake Heron Fault. To date, very few absolute ages have been acquired for the Lake Heron Basin. Cosmogenic ages have been reported for the area (Rother et al., 2014) though several vital locations have yet to be dated. Therefore, being able to use SHD on fluvial terraces allowed for a reliable technique to apply to the region. Additionally, within this chapter, two Schmidt hammer methods were used to calibrate ages in the area, to show potential variation. Prior to this study, SHD on fluvial terraces had only been done once before (Stahl et al., 2013) and was found to yield consistent ages. Therefore, the technique was applied in the Lake Heron Basin to constrain the timing of faulting. Lastly, within this chapter, variation in slip rates using acquired ages is shown using a Monte Carlo analysis.

This chapter also investigates the paleoseismology of the Lake Heron Fault. This fault is recognized as the most active feature in the Ashburton District. However, no paleoseismic study has ever been completed. Therefore, this provided an excellent locality to study an

earthquake history. I used mapping, surveying and trenching to derive fault parameters, which were then used to calculate recurrence intervals, single event displacements and earthquake magnitudes. The results show that the Lake Heron Fault is likely capable of Mw 7.0+ earthquakes at intervals significantly shorter than originally expected.

Chapter 4 summarizes the main conclusions of the thesis, prioritizing those most important to the understanding of the structural diversity of paleoseismicity of the Lake Heron Fault. Findings that relate to the tectonic regime of Western Canterbury are also included.

Digital Appendices are also included, and contain additional relevant information such as Schmidt hammer data, high resolution structural maps, survey lines, raw geophysics files, and radiocarbon results.

1.7 Related Work and Originality

1.7.1 Structural Analogues

This thesis benefitted primarily from the Ph.D thesis written by Stahl (2014), which focused on the active tectonics and geomorphology of reverse faults in the central South Island. In this work, which revolves around the Fox Peak and Forest Creek Faults, the Lake Heron Fault was noted as an area where future work would be valuable. Additionally, many of the techniques used in this thesis were either used or created in Stahl (2014). This thesis also benefitted from work done on the Ostler Fault (Amos and Burbank, 2007; Amos et al., 2007, 2010, 2011). This is one of the few other paleoseismic studies done on a central South Island reverse fault. Therefore, methodologies were mimicked in this study as well.

Because all of these faults are in the South Canterbury Fault Zone, they can be viewed as structural analogues (Wallace et al., 2007; Stahl, 2014). The Fox Peak and Forest Creek faults are NE-SW striking reverse faults located SW of the Lake Heron Fault, and are each approximately 40 km in length (Stahl, 2014). These faults are each highly segmented at the surface, though at depth, merge, creating a larger structure capable of rupturing simultaneously with a magnitude up to 7.4. Similarly, the Ostler Fault is highly segmented, is N-S striking, predominantly dip-slip fault which is 60 km in length (Davis et al., 2005; Amos and Burbank, 2007; Amos et al., 2010, 2011). Because these faults are all in in proximity to one another, and are therefore undergoing similar regional stress (Wallace et al. (2007)) characteristics were often compared in an attempt to interpret both localized and regional features.

1.7.2 Originality

In addition to these works, this thesis benefitted from many discussions with my supervisors and collaborators, including Mark Quigley, Jarg Pettinga, Andy Nicol, Stefan Winkler, and David Nobes. In Chapters 2 and 3, Ellyse Gore and Alec Wild assisted with field work, while Stefan Winkler and David Nobes aided with interpretation. In Chapter 3, Mark Quigley helped with trenching, though all other work is my own. The final text is also my own, though my principal supervisor, Mark Quigley, provided editorial assistance and made himself available for valuable scientific discussions. Apart from this, and preliminary work done by Tim Stahl, all work constitutes my own personal research into a mostly unresearched fault.

2 Structural Geology and Surface Deformation

2.1 Introduction

The Lake Heron Fault is a highly complex reverse fault within New Zealand's rangefront fault system. In order to understand various characteristics, detailed structural and deformation analyses were done to highlight key traits. By first completing structural maps, and then combining them with detailed surveying, a comprehensive dataset could be compiled, aiding in interpretation. Before this study, all prior work which included the Lake Heron Fault highlighted a significant difficulty in determining certain characteristics, its unknown length. Depending on which study is examined, fault length ranges from 18-80 km (Pettinga et al., 1998, 2001; Upton et al., 2004; Upton and Koons, 2007; Upton et al., 2009; Barrell and Strong, 2009; Stahl, 2014). Therefore, this study hoped to shed light on this uncertainty.

For the purposes of this thesis, the fault is divided into three study areas. This was done because of variability in deformation, and surface age (Chapter 3). From south to north, they are: Spider Lakes, Paddle Hill Creek, and Castle Ridge (Figure 2.1). Within this chapter, the study sites will be analyzed individually, and collectively in an attempt to uncover the reasons behind differences seen. Because the dominant reason behind differentiating them was deformation and age, greater emphasis on overall site characteristics will be given in Section 2.3 and Chapter 3.

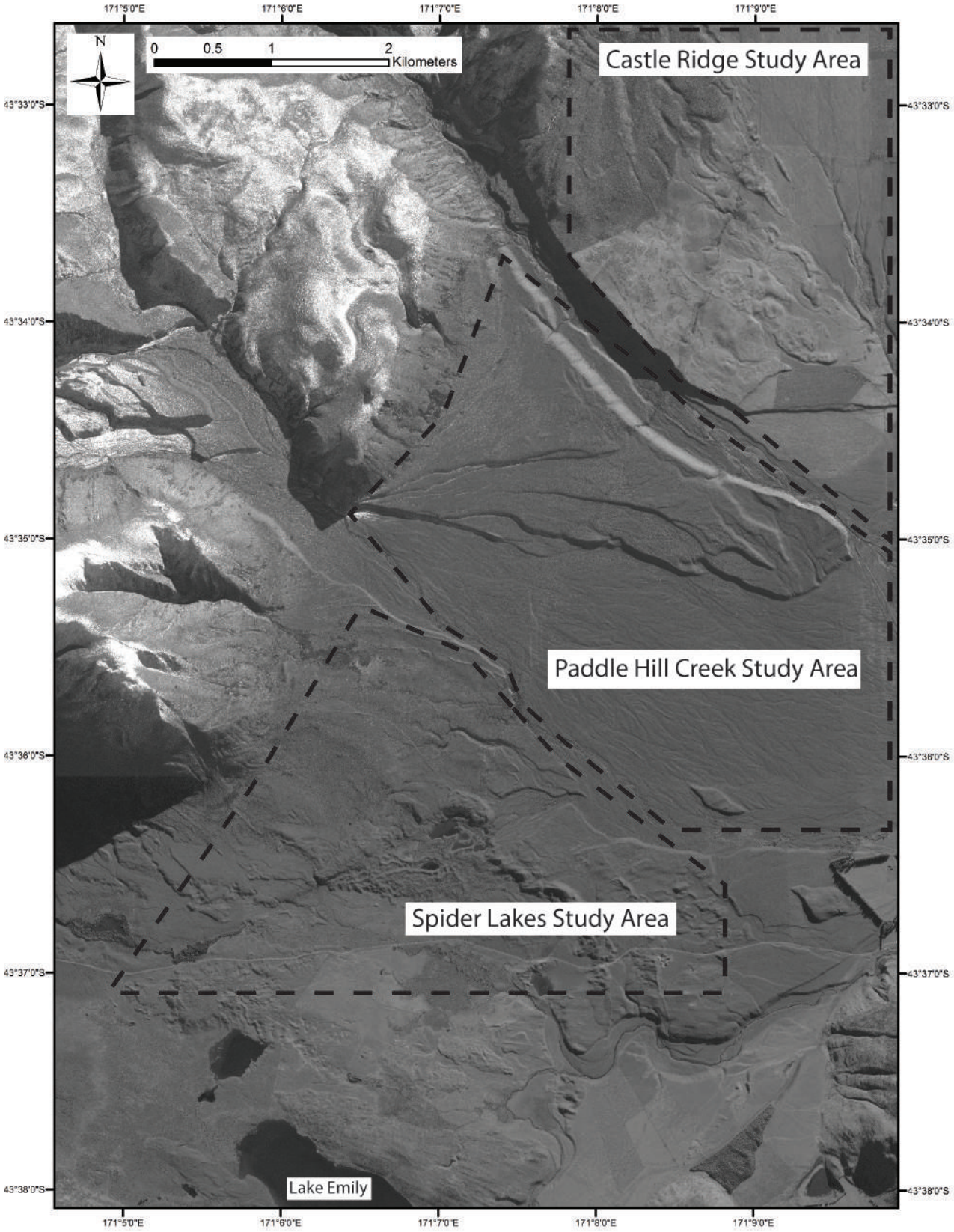

Figure 2.1: Lake Heron field are with study site subdivisions. These subdivisions show regions where work was done, and how research in each of these locations will be kept separate from one another.

2.2 Structural Geology

Along the western margin of the Lake Heron Basin are numerous faults and folds which comprise the Lake Heron Fault. By carefully analyzing the surface expression through field mapping, near-surface measurements, and topographic contouring, characteristics such as fault dip, sense of motion (strike-slip vs. dip-slip), and why the tectonic geomorphology (e.g. folds) appears the way it does could be determined. Within this chapter, select outcrops will be categorized and discussed together, based on which technique was used to analyze them (Figure 2.2). Though large-scale maps will be shown, enlarged sections will be prioritized in order to demonstrate specific structural characteristics.

Prior to this study, little was known about the fault, limited to its presence as a NE-SW trending reverse fault within New Zealand's rangefront fault system (Pettinga et al., 1998, 2001; Barrell and Strong, 2009; Stahl, 2014). Because of the predominant orientation of σ^1, thrust/reverse faulting dominates in this region, and could also be confirmed from the nature of tectonic fractures (Figure 1.3). Some previous works (Litchfield et al. 2013) have speculated that the Lake Heron Fault dips 60° to the west, has a small component of sinistral motion, and a rake of 250°.

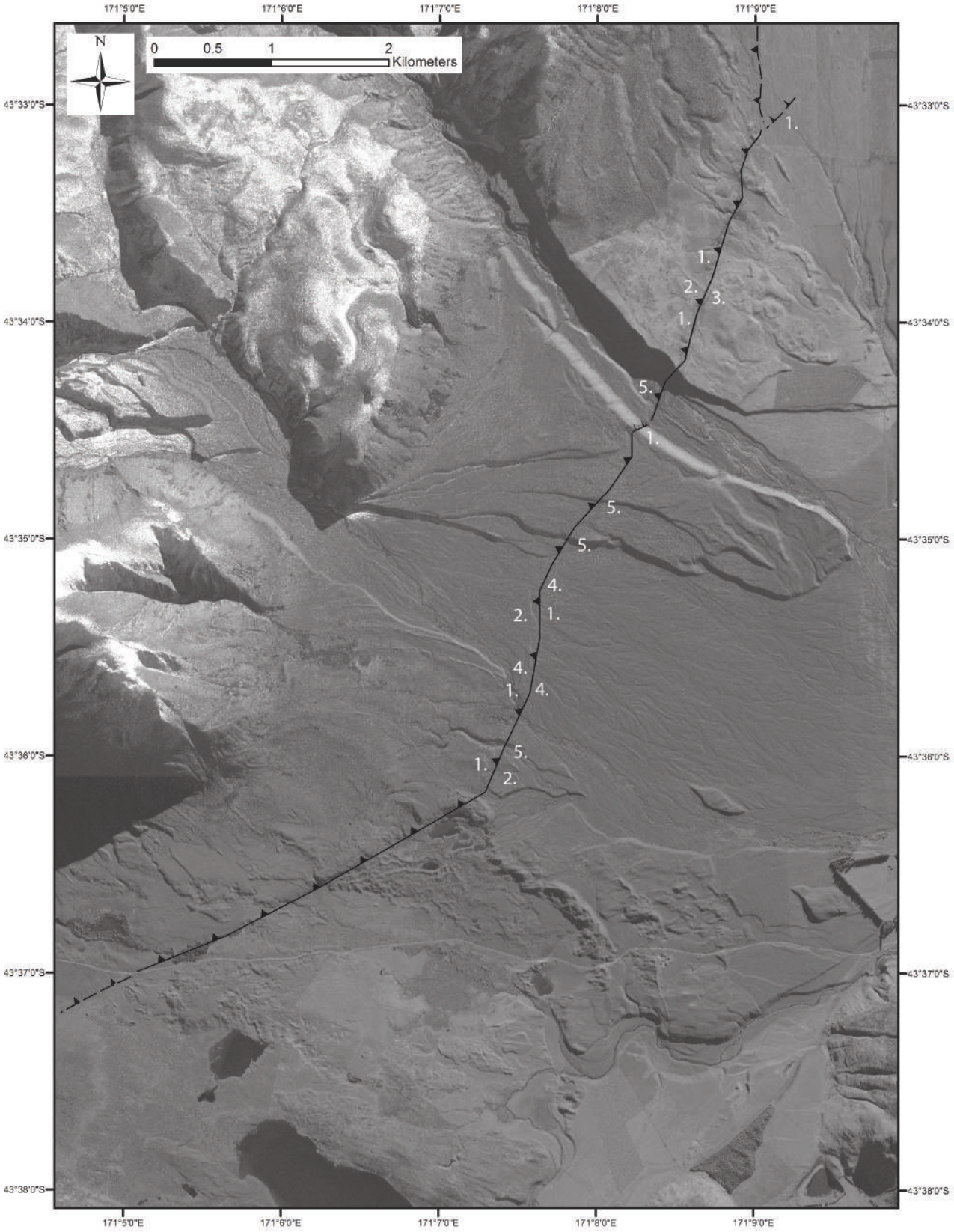

Figure 2.2: Generalized structural map of the Lake Heron Fault, showing locations analyzed using (1) structural mapping, (2) cross sectional analysis, (3) topographic contouring, (4) geophysics, and (5) fault dip measurements.

2.2.1 Structural Mapping and Topographic Contouring

The first step used to determine the structural geology was compiling detailed field maps. Care was taken to note all possible traces, and features were only included if they could be confidently attributed to be of tectonic origin. However, because of the clear tectonic geomorphology, error remained limited, aiding in the reliability of structures noted.

2.2.1.1 Structural Mapping

In order to map the entire site in great detail, it was broken into the three study areas (Figure 2.1). From here, imagery acquired through a DigitalGlobe Foundation imagery grant was enlarged to pick out individual faults and folds. Features were heavily scrutinized during labelling, in order to ensure every possible structure had the correct symbol (e.g. definite and approximate).

Within the Castle Ridge Section, the majority of the fault 3 km north of the South Branch of the Ashburton River is listed as approximate, as geomorphic features trending parallel to the strike of the fault made differentiation difficult (Figure 2.8). Though small sections will be prioritized, the total surface rupture length of the mapped portion of the fault is approximately 10 km, significantly less than the 18-80 km range given in multiple publications (Pettinga et al., 1998, 2001; Upton et al., 2004; Upton and Koons, 2007; Upton et al., 2009; Barrell and Strong, 2009; Stahl, 2014).

From structural mapping, various surface features could be clearly labelled, and used to interpret broad-scale structures. Within this section, such tectonic features more carefully examined include:

1. Topographic flexure
2. Apparent fault step-overs
3. Fault discontinuity
4. Significant alteration in the type and number of faults exposed at the surface

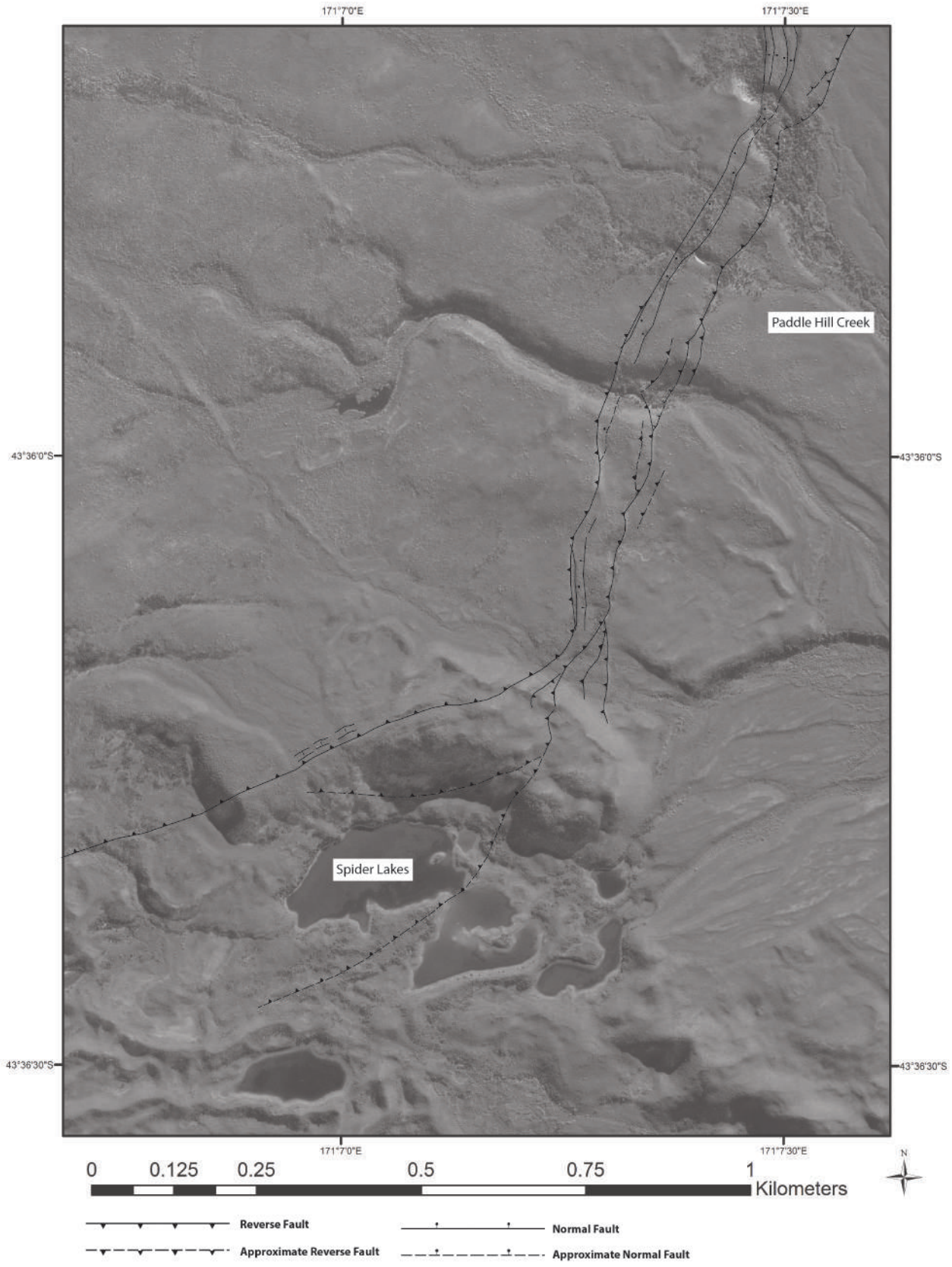

Figure 2.3: Structural geology map of Spider Lakes study site

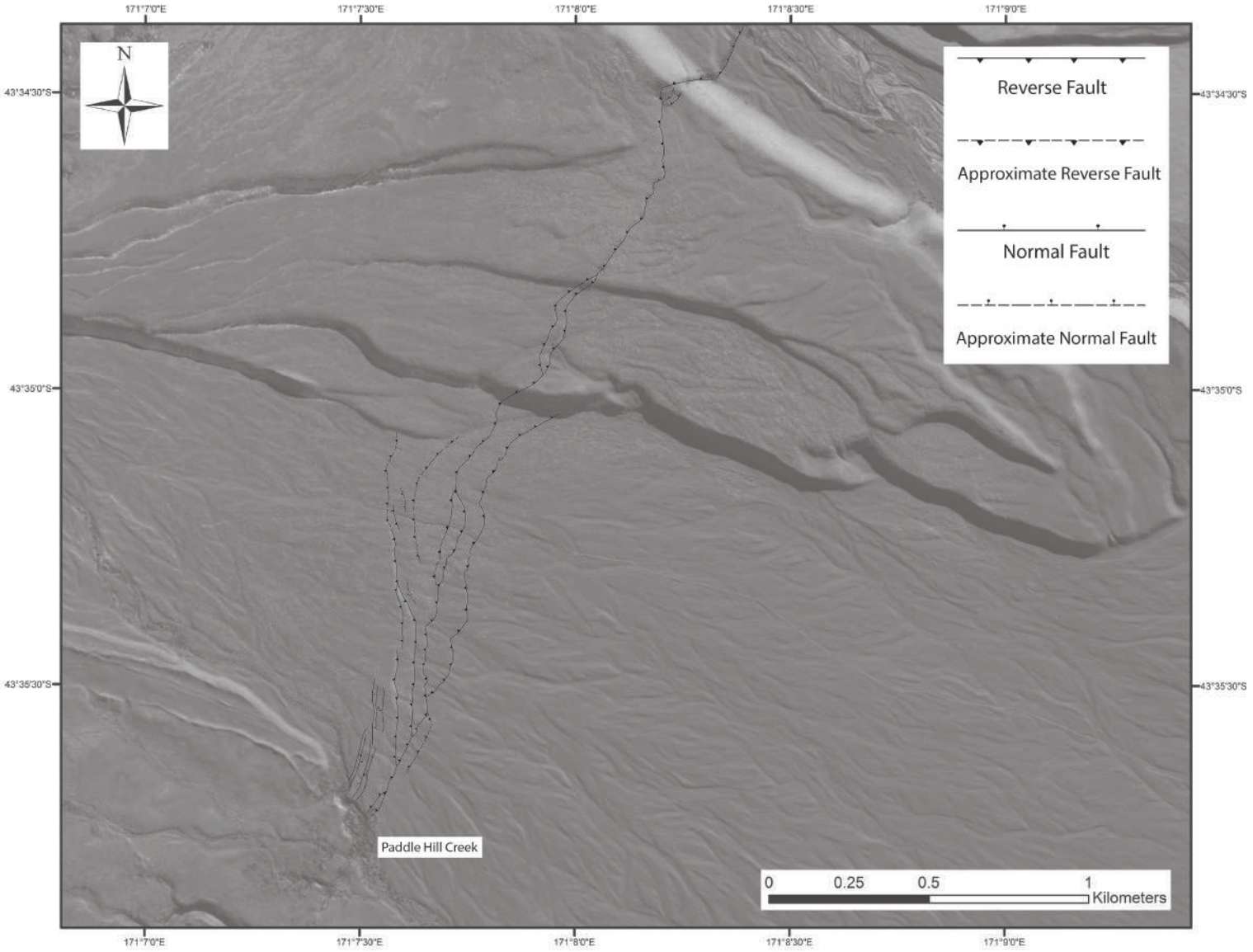

Figure 2.4: Structural geology map of the Paddle Hill Creek study site

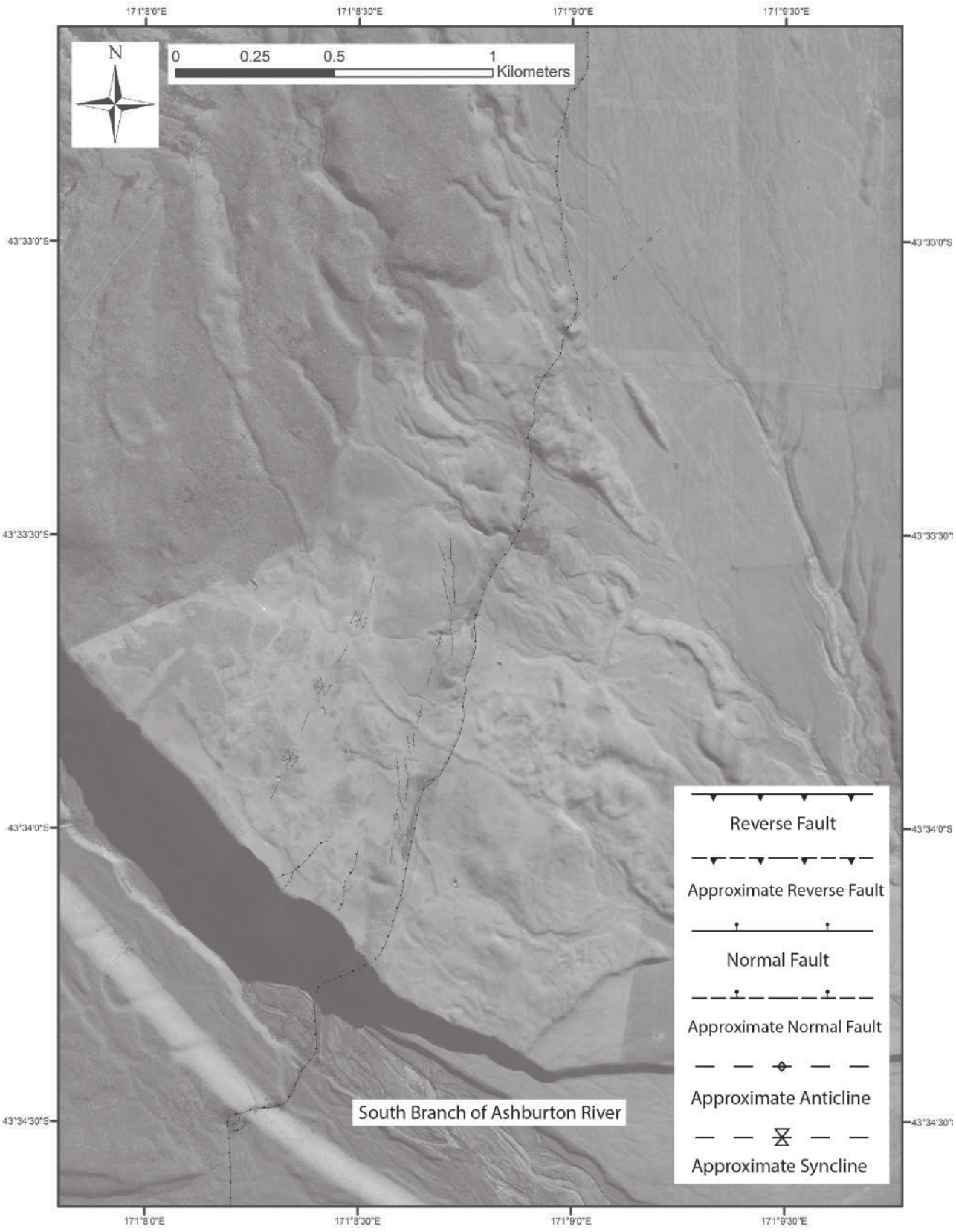

Figure 2.5: Structural geology map of the Castle Ridge study site

Throughout the field site, areas of topographic flexure were often noted on structural maps through fold symbols. Topographic flexure is also often characterized by tensional cracks of varying nature (Philip and Meghraoui, 1983). Within the Lake Heron Fault field site, these cracks take the form of crestal graben, which are found in all three study areas (Figure 2.6). These graben, which are comprised of series of normal faults, are primarily useful as their orientation indicates the instantaneous principle stress direction at the time of their formation.

Though the area is as a whole compressional, these small-scale, near-surface, extensional features on the hanging wall all lie at least 75 m west of the main trace, with the exception of the graben at Site 1. While large crestal graben have been noted on thrust systems worldwide, the ones in this field site are 25-50 m wide. Though on a broad scale, the normal faults which make up these graben appear continuous, when closely examined, they are actually en echelon, often making for poorly-defined boundaries.

A structural trait which can be determined by these crestal graben is what the near-surface extensional direction was at the time of their formation (Philip and Meghraoui, 1983). Though these graben only indicate the stress direction at a particular location, when combined, they give an indication of how stress varies throughout the field site. It must be stated, that the orientations will be on a mircotectonic scale, and cannot be used to interpret the maximum regional compression direction.

In order to determine the instantaneous local extensional direction required to produce each graben, their orientation had to be known. Once determined, the near-surface tensional component of stress was assumed to be perpendicular. Additionally, according to Philip and Meghraoui (1983) tensional cracks such as crestal graben often form perpendicular, or slightly oblique to the localized deep compressive forces which created the fold on which the graben formed. This can be concluded as while crestal graben are extensional features, they are a product of folding which requires compression. This also means that the localized deep component of compression and the localized near-surface extension have the similar orientations.

In total, seven crestal graben were analyzed to determine instantaneous principle horizontal extension and compression (Figure 2.6). From this figure, it is clear there is large variation, in some place differing by over 80°. Having said that, each graben trends roughly subparallel to the fault trace they correspond to.

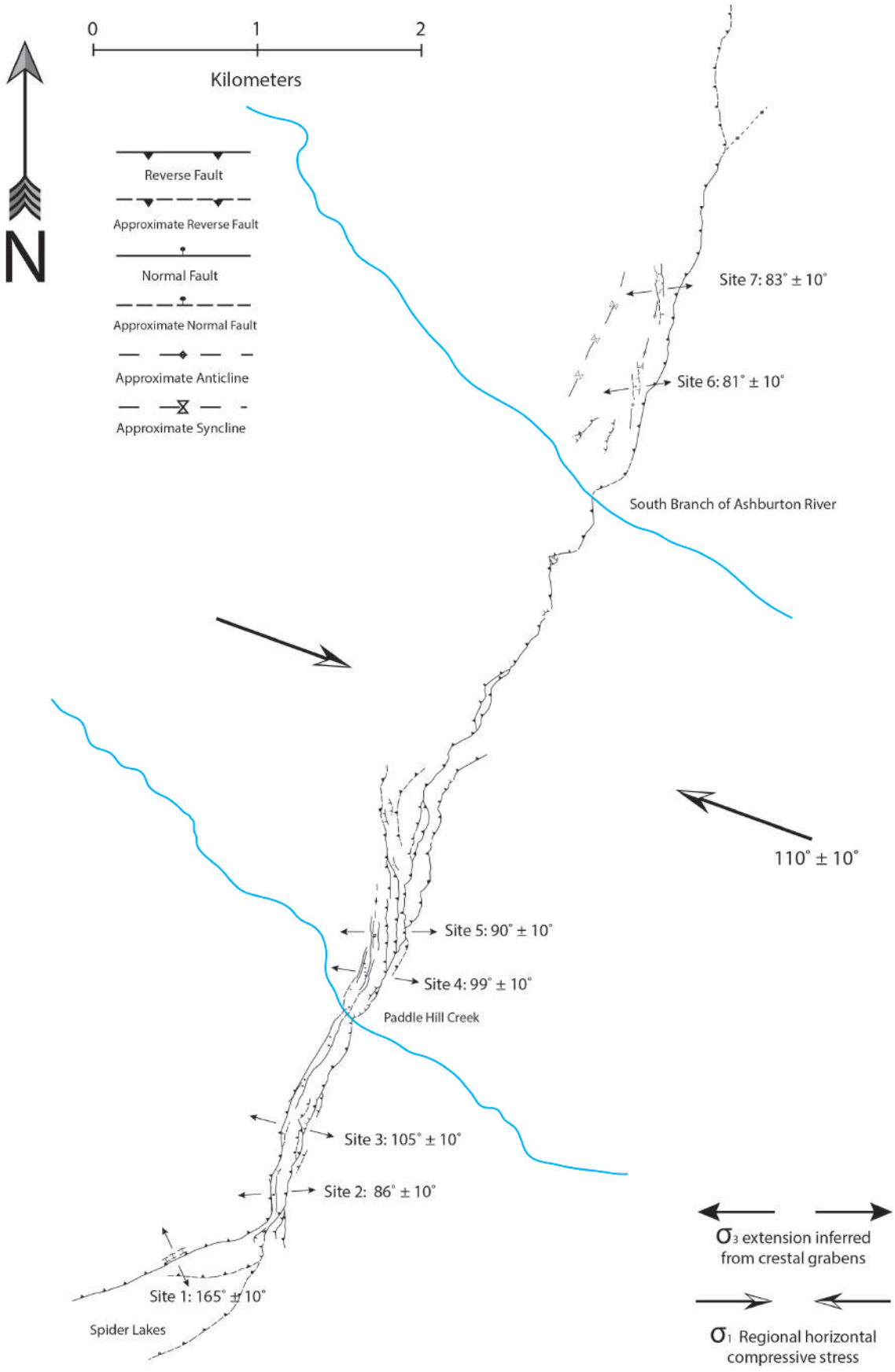

Figure 2.6: Seismotectonic framework of the Lake Heron Basin.

Site	Orientation of Graben	Principle Tensional Stress
1	75°± 10°	165°± 10°
2	176°± 10°	86°± 10°
3	15°± 10°	105°± 10°
4	9°± 10°	99°± 10°
5	0°± 10°	90°± 10°
6	171°± 10°	81°± 10°
7	173°± 10°	83°± 10°

Table 2.1: Orientation of each crestal graben, and the required instantaneous principle horizontal tensional stress

As the instantaneous tensional and compressional stress components required to produce each graben are on a microtectonic scale (i.e. 10s to 100s of meters), they can also be compared to the regional stress field. By using various geodetic models (Pettinga et al. (1998, 2001); Beavan et al. (2002); Wallace et al. (2007)), regional compression is assumed to have an orientation of $110^\circ \pm 10^\circ$. Though there is some variability in published orientations, which is dependent on geodetic sites used, $110^\circ \pm 10^\circ$ can be assumed to be the maximum principle compressive stress direction for western Canterbury.

By comparing the regional maximum compressive stress with that required to produce each crestal graben, conclusions can be made about their tectonic origin. By comparing measurements, it is likely that all graben other than the one at Site 1 formed due to a localized deep compressive stress either parallel or subparallel to the regional compressive regime. However, the localized stresses required to produce the graben at Site 1 require orientations significantly different to the regional stress. Such difference indicates that even within a small area, localized stress can vary significantly.

Regardless of whether the difference is small or large, these measurements indicate that at the time each graben formed, there was an alternative (relative to the regional component) stress acting upon that specific site. Whether this was due to basement rock features, overlying sediment characteristics, or the nature of seismic events, cannot be determined. However, what can be stated is that while there is a regional stress, insight into the instantaneous principle stress along a single fault trace can be noted through tensional fractures such as crestal graben.

Another feature noted through structural mapping was an apparent stepover near the South Branch of the Ashburton River (Figure 2.7). Initially, there were two reasons why a stepover was considered. First, a horizontal distance of approximately 150 m was measured between the main strands of the Lake Heron Fault (Localities A and B in Figure 2.7). These traces are then connected by a fault oriented roughly E-W. Such a abrupt discontinuity was initially

believed to represent a stepover based on tectonic geomorphology seen on other reverse faults (e.g. McCalpin, 2009). Additionally, the scarp on the the southern limb (Locality A in Figure 2.7) begins to diminish in size as it reached the terrace riser, possibly representing a fault terminus. This location was also deemed important because of the apparent dip of the fault along the riser from the Paddle Hill Creek Fan to the South Branch of the Ashburton River. Because the Lake Heron Fault dips to the west, this trace should trend in that direction. However, here it is oriented east, with the dip of a normal fault. As localized tectonic inversion was not considered likely on this scale, additional reasons had to be postulated.

One of the key characteristics of this location is a 70 m change in elevation between localities A and B, likely accommodated by alluvial gravels and glacial till. Additionally, Locality B is significantly closer to bedrock, as in situ greywacke was discovered at the South Branch of the Ashburton River 350 m away. Because such a difference in loading and lithologic variability has been seen to cause variation in fault propagation on other thrust systems (e.g. Lin, 2004), the same was considered possible here. From the sketch in Figure 2.7, this apparent stepover is instead believed to represent various thrust sheets originating from a larger structure. This sketch shows that at depth, the Lake Heron Fault branches, and that depending on the material through which it propagates, different thrusts dominate. This concept has also been shown in models and can be seen in Figure 2.14, letter "I" (McCalpin, 2009).

This explanation also helps describe the structure which appears to dip like a normal fault, and connects the traces. When examined, this feature showed no evidence of discrete lateral motion (Though a small amount could not be discounted), and instead appeared purely dip-slip. Because of these characteristics, it is assumed to be a "tear" fault, which formed as the area periodically uplifted. Though tear faults frequently show a component of strike-slip motion, they are often found at fault stepovers (McCalpin, 2009). Therefore, while this stepover and associated tear fault appears to be caused by imbricate thrust sheets, it cannot be considered anomalous, and instead sheds light on subsurface structures.

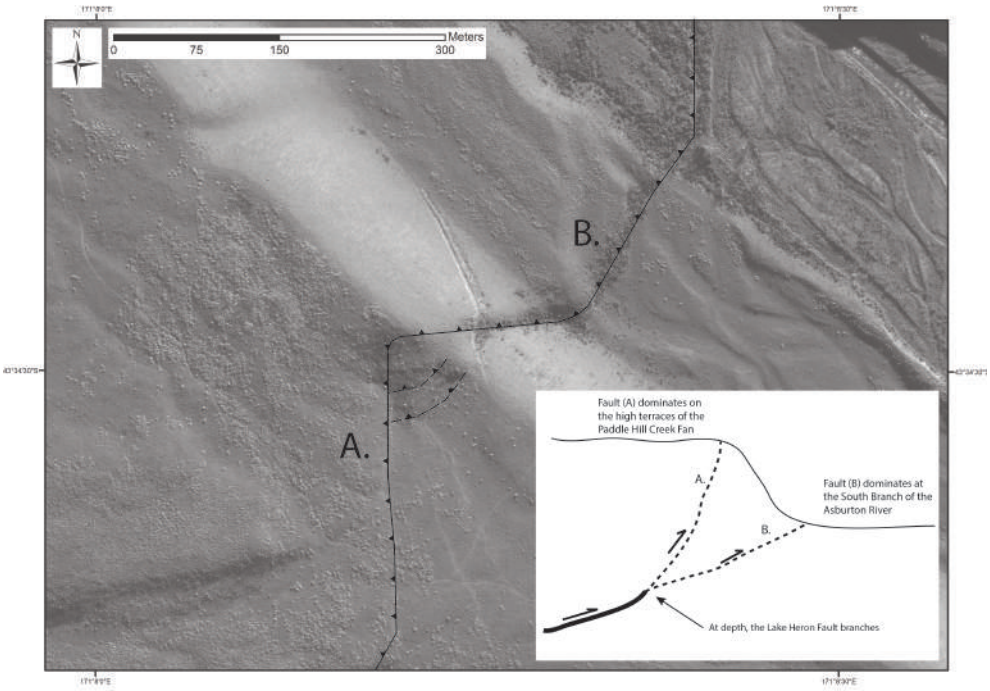

Figure 2.7: Apparent stepover near the South Branch of the Ashburton River.

The third notable feature observed during field mapping was an apparent fault discontinuity in the Castle Ridge Section. Approximately 2.6 km north of the South Branch of the Ashburton River, the Lake Heron Fault appears to disappear, and is only projected further north as "approximate." Though aerial imagery indicates it continues further north, which several authors (Cox et al. (2007); Barrell and Strong (2009); Barrell et al. (2011)) have done, detailed field examination suggests otherwise. For example, scarps, which south of this location were discrete and steep, become gentle and subtle (Figure 2.8). Additionally, differentiation in this area is difficult as geomorphic features (i.e. moraines and terrace risers) begin to trend parallel with the fault, bringing up the possibility that they were believed to be tectonic in origin.

Another key feature at this location is the disappearance of a paleochannel along the basin floor (Figure 2.9). The channel is absent over a length of 125 m, and it is suspicious as the last known strike of the Lake Heron Fault projects through this location. Therefore, it is likely that fault-related folding is the reason for the paleochannel disappearance. This suggests that the Lake Heron Fault may deviate away from the mountains, to instead track along the basin floor. Because of these factors, and because field investigation failed to uncover unambiguous evidence indicating the linear features at the base of the mountains are fault scarps rather than terrace risers, further projection north is only conjectural, with the more likely scenario of a NE-SW projection.

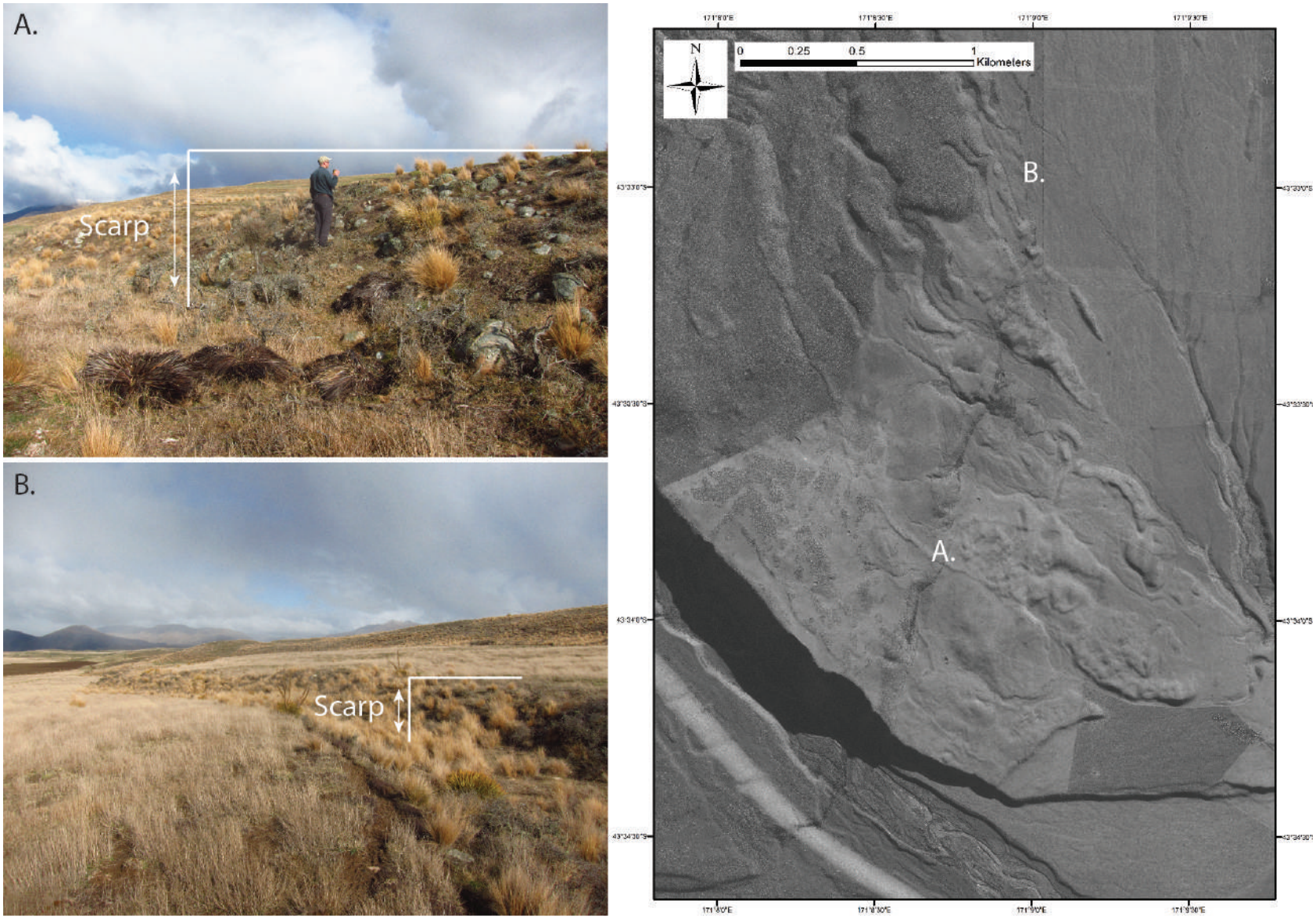

Figure 2.8: Example of a (A) steep, very discrete scarp and (B) gently-sloped scarp within the Castle Ridge Section.

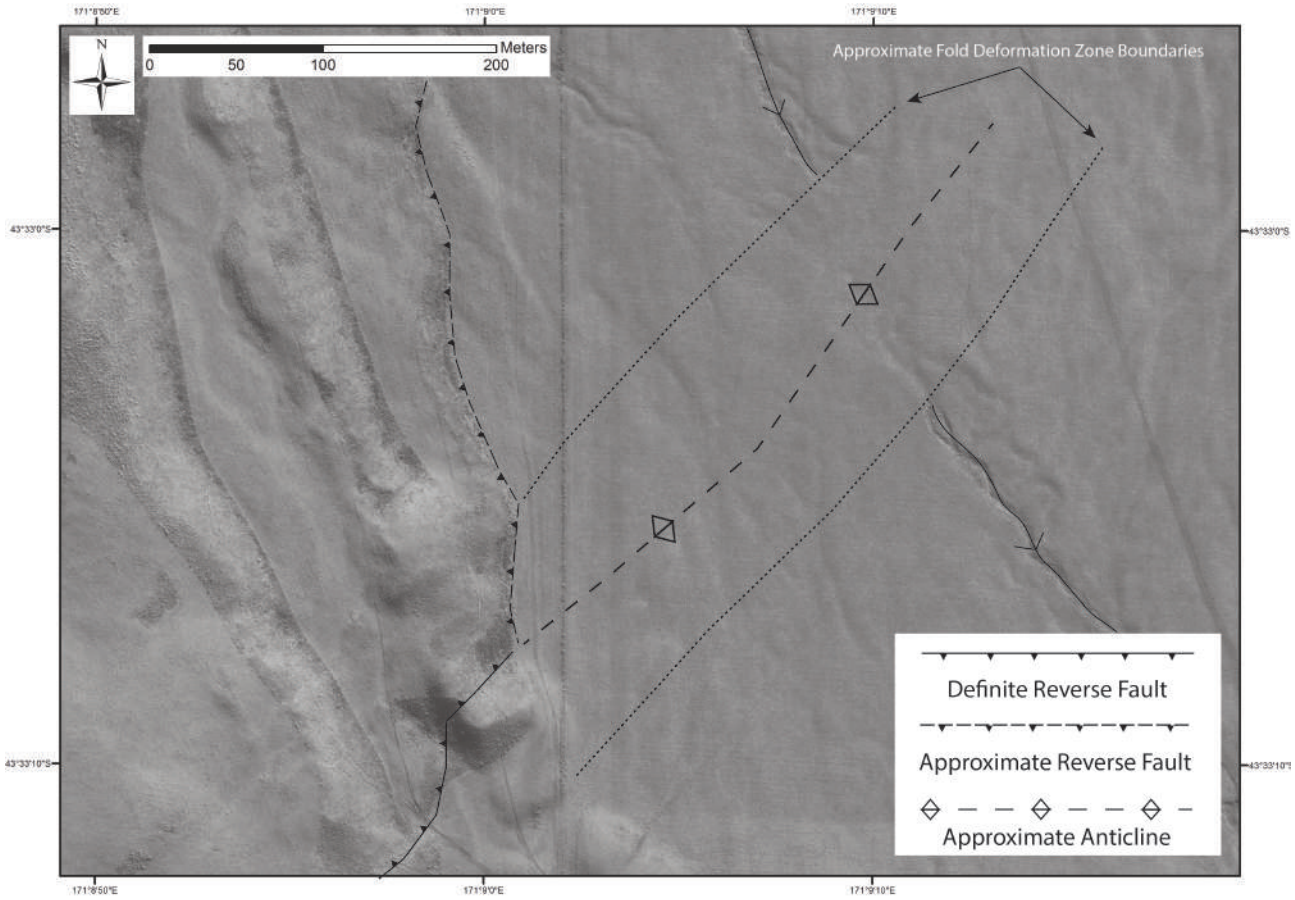

Figure 2.9: Location of possible fault deviation away from the base of the mountains, and along the basin floor

A final structural characteristic noted through mapping was a significant alteration in the number and type of faults exposed along a single surface, in this case, the Paddle Hill Creek Fan (Figure 2.10). In this figure, which shows the lowest surface of the fan, there is clear variation in how faults propagated the surface. In the southern portion, there are only two reverse faults, with four large normal faults making up a crestal graben system. However, further north, there are no normal faults, and reverse faults become numerous.

In the interpretation of this area, elevation was immediately discounted as all faults lie on the same surface. As it is unlikely multiple independent thrust faults caused this surface expression, it is likely an imbricate fan of thrust faults are responsible, similar to what was seen at the South Branch of the Ashburton River (Figure 2.7). While near the Ashburton River, changing elevation likely played a significant role, in this location, it could be heterogeneous sediment. As the fan is made up of alluvial gravels, there is likely heterogeneity throughout, which could influence fault propagation (Lin, 2004). For example, variable confining pressure and preexisting weaknesses within strata can play a role in how a fault propagates, including

near-surface branching. Regardless of what the exact reason is, this site suggests that in the near surface, the Lake Heron Fault is an imbricate thrust system, affected by factors such as topography and sediment type.

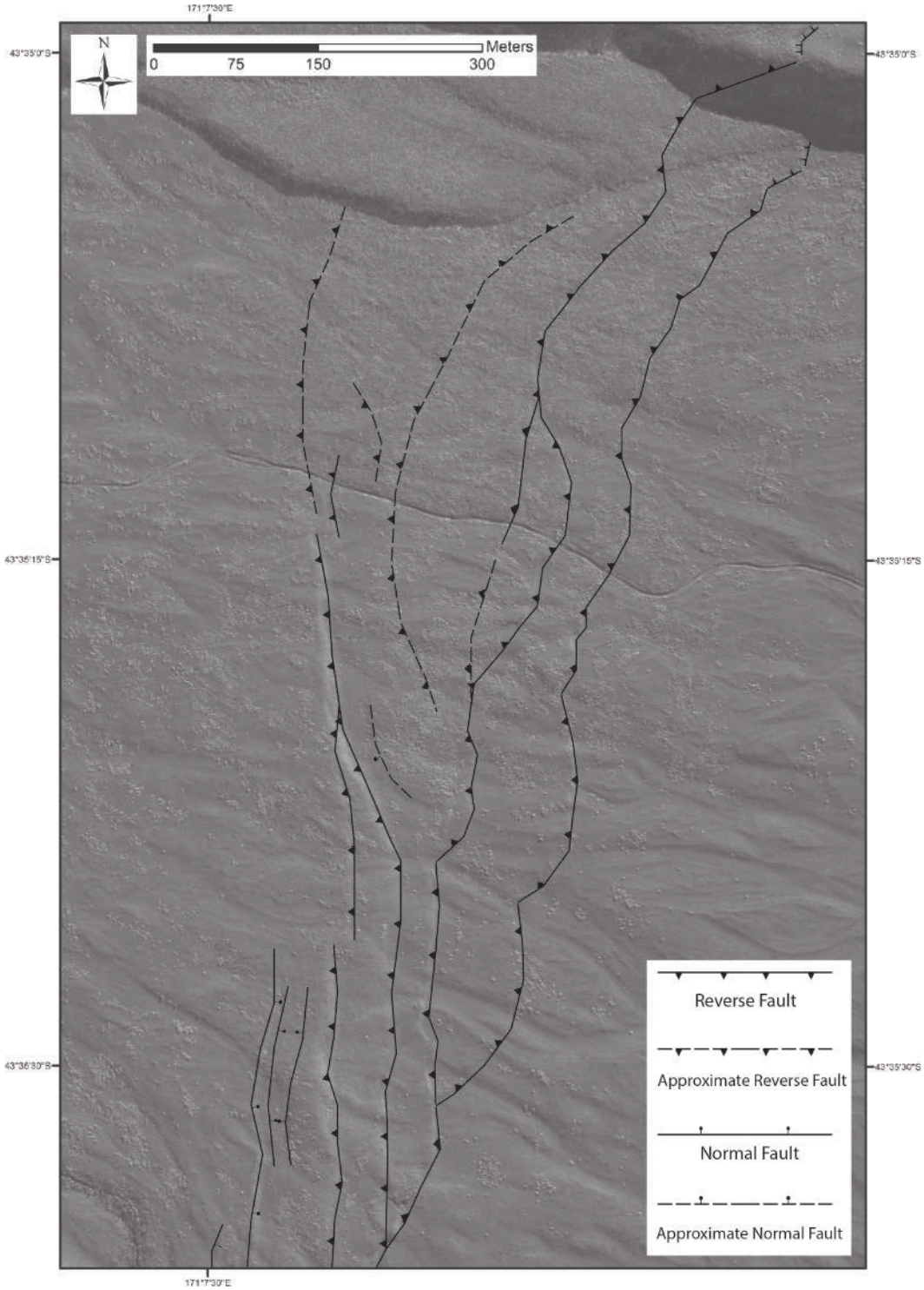

Figure 2.10: Region of significant alteration in the number and type of faults exposed at the surface

2.2.1.2 Topographic Contouring

Another method used to determine structural characteristics is topographic contouring. This involves using a differential GPS (dGPS), to take thousands of GPS points to create a 3D surface. Topographic contouring proved valuable as it allowed for an accurate representation of piercing points, which in turn, made it possible to determine the sense(s) of motion of the Lake Heron Fault. This was vital, as without it, the only 3D model would have been the 15 m DEM, which, because of large spacing, does not pick up subtle variation. Though topographic contouring was valuable, for reasons such as the time to take and process the points, it was only done at a single site in the Castle Ridge Section. The location chosen was a prominent moraine trending perpendicular to the fault, that is perfectly cross-cut (Figure 2.11).

At the moraine, 61 survey lines were taken at 1.5-2 m intervals. Care was taken to not overlap lines as this would have resulted in multiple points with varying accuracy in a single location, decreasing the reliability of the model. The 3000+ points were then transformed into a grid file, and imported into the program Surfer. In this program, 3D surfaces, wireframe models, and contour maps were made (Figure 2.12). From these, measurements from piercing points could be used to analyze fault motion. The most representative piercing points were the moraine crest and lateral extents, based on the ease of differentiating them from other geomorphological features.

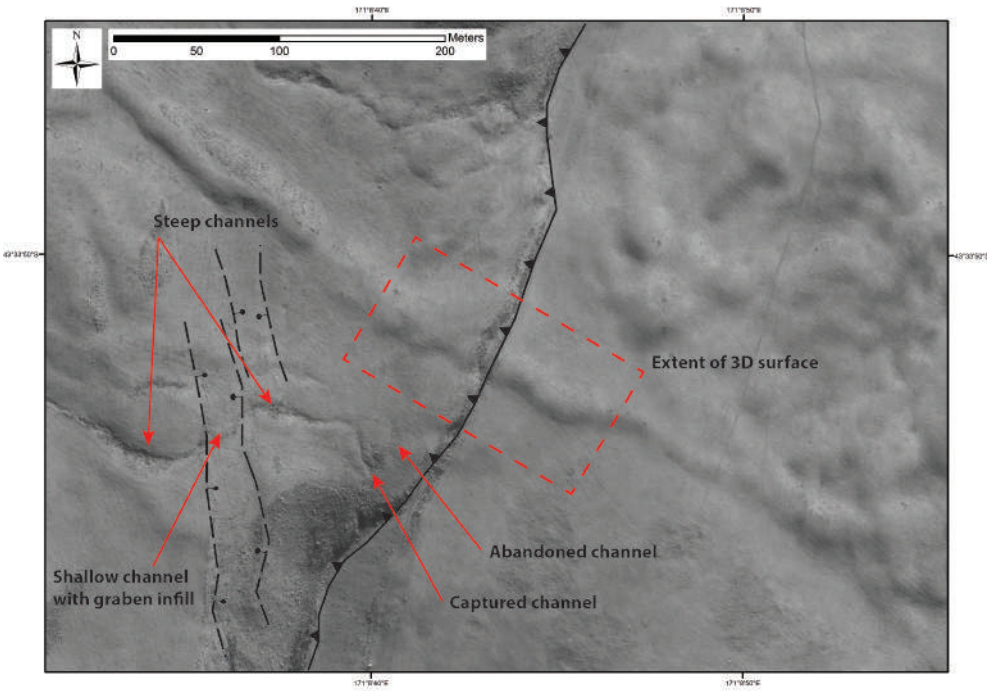

Figure 2.11: Satellite imagery of the Castle Ridge moraine being cross-cut by the Lake Heron Fault. Note the absence of any discernible lateral displacement across the main fault trace.

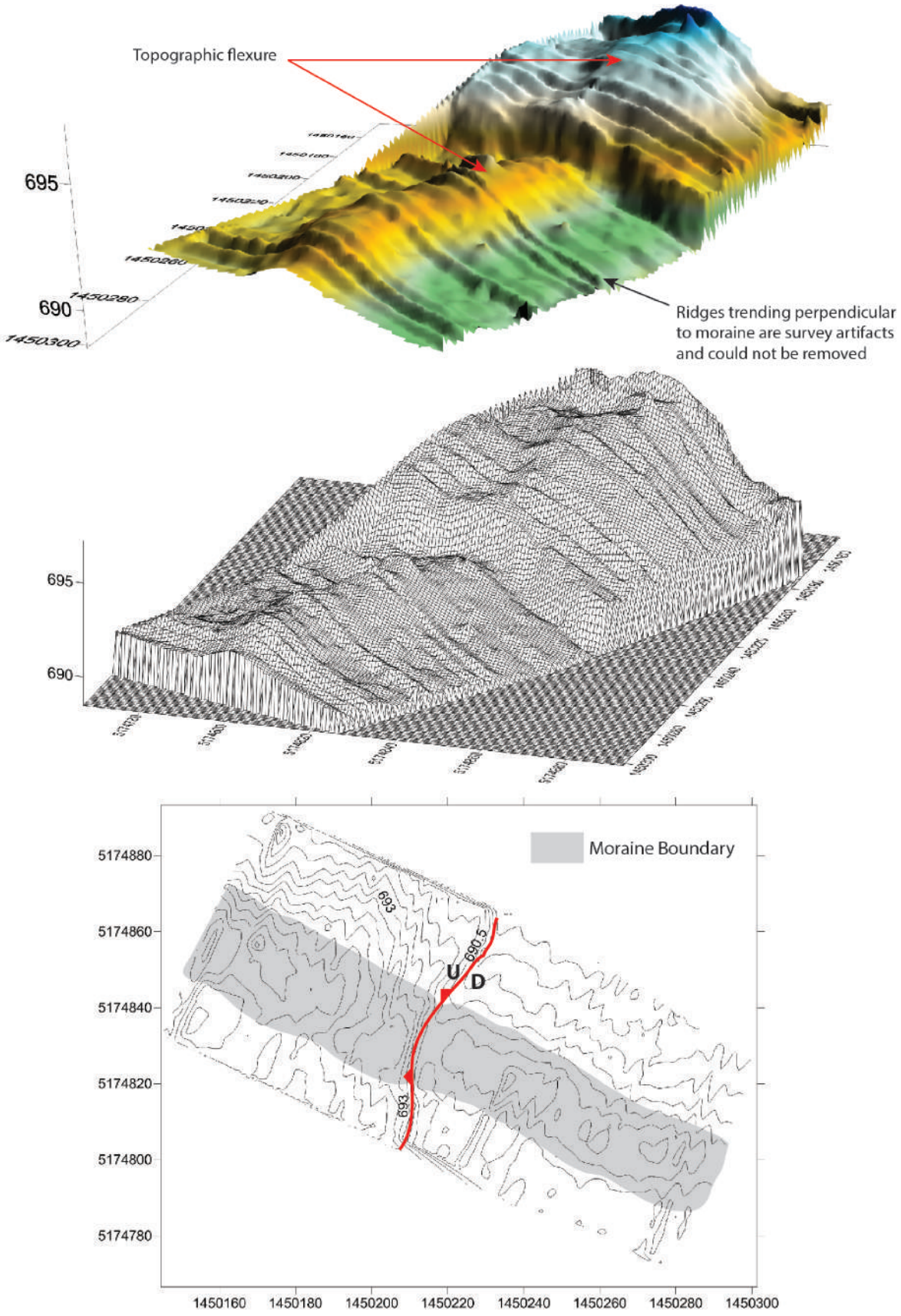

Figure 2.12: Topographic contouring surfaces, with associated annotations. For the top two images, the view is towards the southwest.

From Figure 2.12, one primary characteristic of the Lake Heron Fault becomes apparent, there is no discernible lateral displacement across the discrete surface rupture. This was determined as no lateral movement is required to connect piercing points. Instead, there is only a 2.3 m high fault scarp. It must be emphasized though, that on a smaller scale, lateral motion is possible, but given the uncertainty in the model (most GPS points had error of less than 0.5 m), small-scale movement would not be visible. Therefore, while the small component of sinistral motion Litchfield et al. (2013) and Berryman et al. (2002) suggest is possible cannot be discounted, it can be concluded that on discrete rupture traces, there is no large component of strike-slip motion.

Another observation is that on both the footwall and hanging wall, there is topographic flexure. On the footwall this takes the form of back-tilting, while on the hanging wall, there is pronounced buckling. Though back-tilting is more often seen on the footwall of normal faults, its presence indicates structural characteristics noted by McCalpin (2009), including changing near-surface fault plane geometry. Here back-tilting is restricted to within 200 m of the fault scarp. Back-tilting of the footwall is an indication of block rotation and/or drag folding. In either case, a folded depression is created, in which compression occurs, and reverse faulting can result.

In contrast, the flexure on the hanging wall has the opposite effect. While in the footwall, the bending of strata results in increased contraction, on the hanging wall it causes extension. Over time, as buckling of the hanging wall increases, fractures form, which can turn into artifacts including crestal graben, which are seen throughout the basin. Though a crestal graben is not present here, similar flexure is present. Therefore, flexure at the moraine suggests that along the Lake Heron Fault, there are components of folding and rotation.

A principle compressive stress direction required to produce this scarp can also be determined. Though a regional compressive stress orientation of $110^\circ \pm 10^\circ$ is given by various authors (Pettinga et al. (1998, 2001); Beavan et al. (2007); Wallace et al. (2007)) at the moraine, one can be interpreted and compared with the published value. Because there is no apparent strike-slip motion, it is likely the instantaneous principle compressive stress which produced this scarp was perpendicular to the strike of the fault. As the strike here is 202°, a compressive stress of 112° was calculated, which is almost identical to published values.

2.2.1.3 Discussion

Overall, from the data presented within this section, several structural characteristics become clear. First, evidence of topographic flexure in the form of crestal graben development

indicates that while the region as a whole undergoes deformation in response to a regional maximum compressive stress oriented $110^\circ \pm 10^\circ$, along a single fault, localized, near-surface instantaneous stress during faulting can differ by up to 80°. This shows that fault surface deformation zones are complex structures, which cannot be constrained by regional measurements, and that in order to fully understand the complex array of features exposed at the surface, microtectonic measurements must be made.

The likely reason behind the variation is that in the shallow subsurface, the Lake Heron Fault is an imbricate thrust system. From structural mapping and schematic diagrams, it becomes clear that in order to create the visible surface expression, the Lake Heron Fault must branch at depth. When this happens, splays likely propagate through the strata in varying ways due to factors such as heterogeneity of the material and fault dip, creating differing fault strikes, resulting in a complex array of surface features.

These observations and interpretations suggest that the mechanism of fault rupture along the Lake Heron Fault is quite complex. While in some areas fault rupture produces significant folding, in others it is predominantly discrete rupture. This variation is why this thrust system is a textbook example of how in a single earthquake event or along a single fault, superficial stress and localized surface rupture does not have to be representative of the structure at depth or regional stress.

2.2.2 Geophysics

2.2.2.1 Introduction

In addition to mapping and topographic contouring, shallow geophysical investigations were also undertaken in an attempt to determine additional fault characteristics. For this study, this was restricted to ground penetrating radar (GPR), which was chosen not only for its ease of use, but because it has been used in the area before, and with success on alluvial gravels. GPR relies on the reflection of electromagnetic energy to illustrate shallow subsurface features (Milsom, 2003). In this study, two electromagnetic frequencies were used: 100 MHz and 200 MHz. The 100 MHz GPR used a pulsEKKO system, during which each burst of energy was manually stepped and transmitted every 0.25 m. The 200 MHz GPR on the other hand was a GSSI shielded system, which used continuous bursts of energy to image the subsurface. Each one of these systems has their advantages and disadvantages. While the 100 MHz GPR reaches greater depths, it will not give the near-surface resolution the 200 MHz system can produce. Therefore, both systems were used to compare data.

For this study, GPR was undertaken at three different sites, all on the Paddle Hill Creek Fan (Figure 2.2). These sites were the trench location, which will be further discussed in Chapter 3, the large crestal graben, and a 4WD track running perpendicular to the fault. The pulsEKKO system was run across the trench site and the crestal graben, while the GSSI system was used at the trench site and 4WD track. Prior to running GPR lines, areas were cleared of vegetation and rocks in an attempt to reduce the interference the system would encounter. Despite this, there was significant interference in the crestal graben as there were large rocks and matagouri bushes which could not be moved, and impeded the ability of the sensors to touch the ground.

2.2.2.2 Geophysical Analysis

Due to time constraints, not all GPR lines were processed, though all raw files are available in the digital supplementary file. Instead, a single line was used to see if through GPR, the position of the fault could be determined. Calculating true dip would not be possible because velocity is not consistent, meaning the exact orientation of structural anomalies is not shown. Nonetheless, an estimate could be made and compared to other values from throughout the field site.

The only location which was fully processed and analyzed was the trench location. This was done for multiple reasons. First, because it was the trench location, gathering as much information from this spot is extremely useful, as subsurface structures and material was known. Additionally, because the fault scarp was clear, and the approximate location of the fault was known, it yielded an ideal location to use GPR to examine the subsurface.

Following processing undertaken by Dr. David Nobes, the single GPR line provided insight into shallow subsurface geometry of the Lake Heron Fault (Figure 2.13). One dominant structure is apparent, while a second is more subtle in appearance. Additionally, and possibly more importantly, the fault dips very shallowly, approximately 10°. Other data extracted from this profile include implications of the initial velocity, and the depth of the water table. Near the surface, the velocity was 1.7×10^{-10} m·s^{-1}, suggesting loose, sandy gravel material. This was expected given the profile was run along an alluvial fan, though it could only be confirmed through trenching. Additionally, based on changing velocities, the water table was determined to be 15 m below the surface.

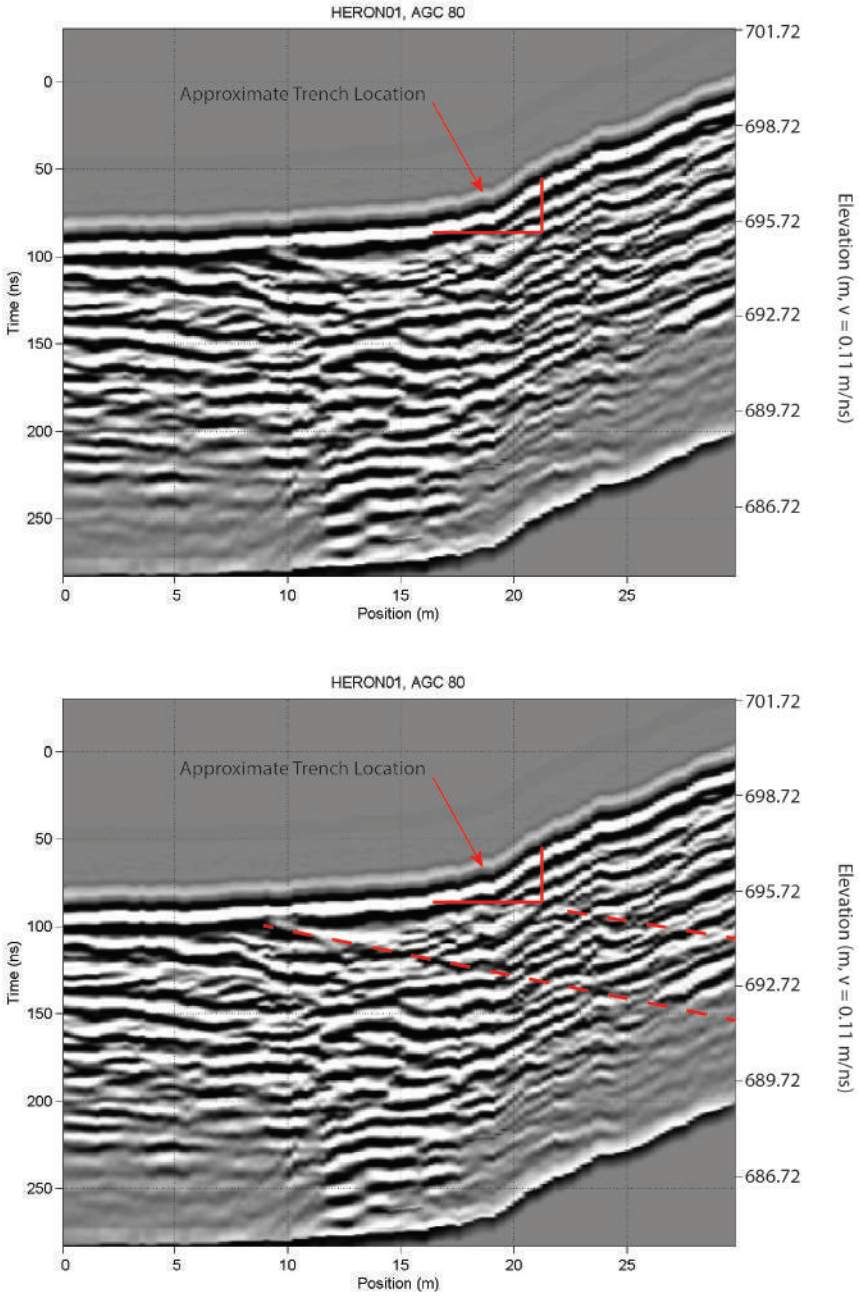

Figure 2.13: Processed GPR survey across the main trace of the Lake Heron Fault at the trench location. The top image shows the processed line without interpretation, while the bottom one shows the subsurface structures dipping at approximately 10°. It is important to note that both the mapped outboard thrust fault and main trace are visible in this GPR line.

2.2.2.3 Discussion

From geophysical analysis one point must be examined, the shallow ramping of the Lake Heron Fault near the surface. Though the measured value (10°) is low, it could be that as the Lake Heron Fault passes through unconsolidated gravels, the complex network of low angle thrusts can shallow so dramatically that in some areas dip becomes nearly horizontal.

Another possibility is that during episodic ruptures through unconsolidated sediment, "bulldozing" occurs (Figure 2.14). As this happens through periodic ruptures, the deformation migrates progressively outward to shallower imbricate thrusts. This process has been noted extensively in reverse faults through paleoseismic research (McCalpin, 2009). McCalpin (2009) noted that as a reverse fault system evolved, faults would "refract" to a lower angle, resulting in an increased deformation zone size. Additionally, this bulldozed material often resembled colluvial wedge sediments and/or fault breccia. And, as will be seen in Chapter 3, significant deposits were found in the trench resembling wedge deposits.

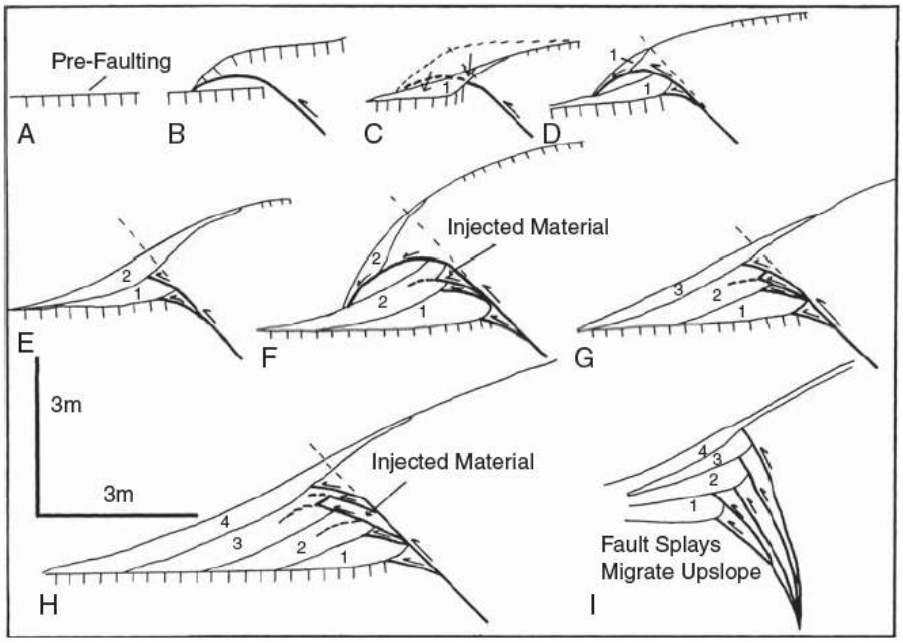

Figure 2.14: Idealized model of reverse fault evolution. Note in B and C the progressive shallowing of the fault near the surface from the bulldozing of material. Figure from McCalpin (2009).

2.2.3 Near Surface and Bedrock Measurements of Fault Dip

2.2.3.1 Fault Dip Measurements

Prior to this study, limited work was done to calculate the dip of the Lake Heron Fault. Additionally, most recently published dips were compiled from previous work rather than undertaking new research, and include estimates based on regional stress. Nonetheless, they do give a reference point. It is important to note that while published work is focused on dips to seismogenic depth, this work deals predominantly with near-surface complexities.

The first of the modern studies suggested that the fault, on average, dipped 45° to the NW, shallowing to 12° in some locations (Pettinga et al., 1998). Later studies indicated however, that it could be much steeper, possibly averaging dips in excess of 60°, with it reaching 70° in some places (Litchfield et al., 2013; Stahl, 2014).

The best locations for fault dip measurements were terrace risers. To measure fault dip here, paired GPS points were used. To do this, points were taken where the fault outcropped at the top and bottom of a terrace riser (Figure 2.16). From here, fault strike could be projected, a right triangle could be extrapolated, with trigonometry used to calculate dip. This was done at four locations in the Spider Lakes and Paddle Hill Creek Sections. Unfortunately, it could not be done in the Castle Ridge Section, as there were no large terrace risers. Lastly, it must be stressed that these measurements represent the near surface fault dip after it propagated through strata overlying Torlesse greywacke.

The other way fault dip was determined was through direct measurement at the South Branch of the Ashburton River, the only location along the entire trace where it is visible in bedrock. From this, a rough estimation of how the fault dips within bedrock could be made.

At this bedrock exposure, both the active fault plane and secondary fractures were visible (Figure 2.15). Five measurements were taken for this study, while an additional five were done in Stahl (2014)(Table 2.2). While strike varies in these measurements, because of the number of fractures, it is not unexpected. Despite this variation, dip remains relatively consistent (Around 60°), and it is therefore assumed, that once bedrock is reached, fault dip is approximately 60°.

Figure 2.15: Lake Heron Fault exposure in bedrock at the South Branch of the Ashburton River. This is interpreted as the active fault plane as it projects into displaced young sediment.

This Study	Stahl (2014)
208/65	145/70
207/53	075/80 with striae at a rake of 8°
212/42	182/82
215/65	168/65
202/68	348/33; Striae plunging 42° toward 052°

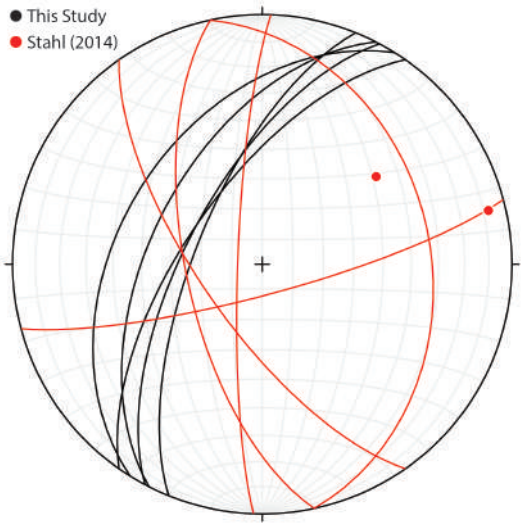

Table 2.2: Measurements from in situ greywacke at the South Branch of the Ashburton River, with accompanying stereonet showing poles of fault planes.

Following direct fault dip measurements within bedrock, the exact GPS points (Table 2.3) following differential correction, were used to calculate near surface fault dip (Table 2.4). From the paired GPS points, right triangles were created to determine fault dip (Figure 2.16). Because strike is incorporated into the measurement, the values represent true dip rather than apparent dip.

Location	Easting (m)	Northing (m)	Elevation (m asl.)
1	2359320.119	-5734664.817	730.855
	2359313.18	-5734648.18	725.591
2	2359135.486	-5734327.327	725.009
	2359045.208	-5734296.025	710.372
3	2358505.676	-5732601.939	694.539
	2358482.307	-5732570.838	685.926
4	2358487.871	-5732607.656	696.587
	2358471.97	-5732574.179	685.827

Table 2.3: GPS points used to calculate near surface fault dip.

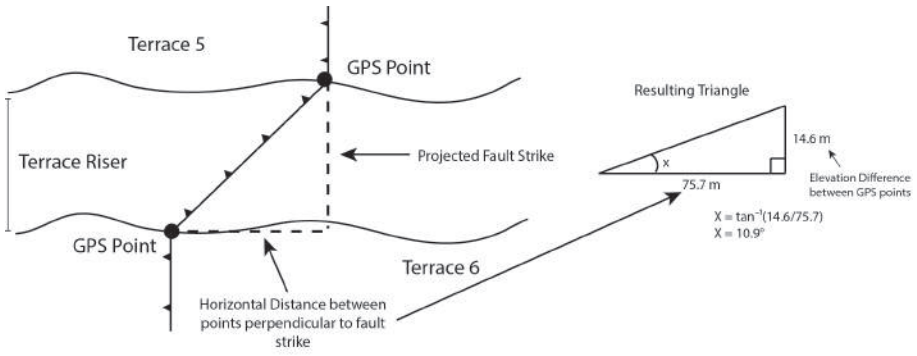

Figure 2.16: Method used to calculate near surface fault dip. This figure shows the fault in plan view.

Location	Dip
(1) Between Terrace 3 & 5 on Paddle Hill Creek Fan	20.6°
(2) Between Terrace 5 & 6 on Paddle Hill Creek Fan	10.9°
(3) Stream Channel near Spider Lakes	33.5°
(4) Stream Channel near Spider Lakes	56.8°

Table 2.4: Near surface fault dip measurements from river terraces.

Based on these measurements, one thing becomes clear, the near surface dip of the Lake Heron Fault fluctuates significantly. The fact that it halves in only 400 m (the distance between the two measurements on the Paddle Hill Creek Fan), and that there is a 46° difference in dips suggests a quite intricate near-surface system.

Additionally, from all measurements, it is clear that when the fault propagates through sedimentary strata, dip can shallow significantly, in some places by up to 80% (Figure 2.17). This was expected, as during field work it was observed that on the high terraces, where elevation remains relatively consistent, the fault trace was greatly affected by subtle changes in topography.

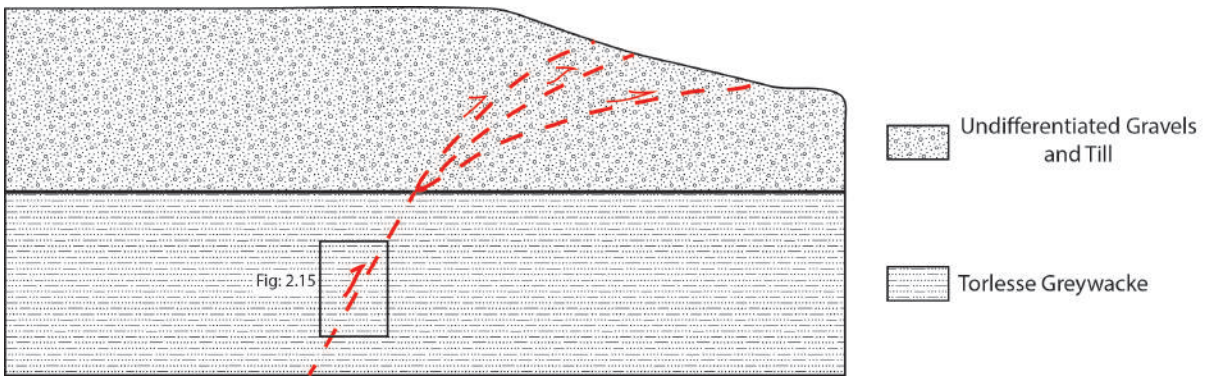

Figure 2.17: Schematic diagram illustrating fault deflection at the Torlesse greywacke-Quaternary sediment boundary.

2.2.3.2 Discussion

From the various measurements taken in the field, it is clear that the Lake Heron Fault has variable dip near the surface. While not unexpected, it does have certain ramifications. Through investigation of other faults both within New Zealand and worldwide, studies have shown that faults expressing a multitude of dips often indicates significant subsurface variation, both structurally and lithologically (e.g. Knuepfer (1989); Lin (2004); Amos et al. (2010); Campbell et al. (2010b,a)). For example, along the Ostler Fault, Campbell et al. (2010a) noted through geophysical analysis, that variation in fault dip could be attributed to shallow changes in the principle fault. Furthermore, the high degree of complexity seen towards the surface only extended to 300 m depth, at which point structures became significantly "simpler." A highly complex near surface system seems likely for the Lake Heron Fault, as there are single locations where different dips were found on large fault strands.

While the variation in fault dip could be due to a shallow imbricate thrust system, lithologic variability could also be responsible. Lin (2004) found that sedimentary strata could, in some instances inhibit propagation of thrust faults, resulting in differing dips expressed at the surface. As a fault propagates upward through sedimentary strata or bedrock it will often follow preexisting weaknesses, or in some cases be deflected due to a decrease in confining pressure.

Such a case seems possible at the location where a 9° dip was measured along the Paddle Hill Creek Fan (Locality 2 - Between terraces 5 & 6). This measurement appeared suspicious as it was less than any other measured dip. However, under further examination, the dip seems entirely possible, as this location is where an additional 10-12 m of gravel overlies the fault. In turn, this additional sediment could have caused dip deflection, resulting in a shallowly-dipping fault to be expressed.

2.3 Surface Deformation of the Lake Heron Fault

2.3.1 Introduction

Within the basin, there is a 7 km stretch where the Lake Heron Fault exhibits dramatic differences in surface deformation. While some (Pettinga et al., 1998, 2001; Barrell and Strong, 2009; Upton et al., 2009) suggest the fault is at least 40 km long, convincing surface deformation is confined to this shorter length from just north of Lake Emily to 2.7 km north of the Paddle Hill Creek Fan. Within this section, the strike of the fault averages 200°, though to the southwest, it deviates to 250°. It is also this section where the active trace begins to be obscured by Quaternary fan and flood deposits sourced from the Balmacaan Saddle and Lake Emily respectively. Though the strike of the fault is on average 200°, because of numerous surface ruptures and associated features, it does vary greatly in small areas, which effects the extent of the resulting deformation zone. Understanding this surface deformation is vital to this study as it can reveal key aspects related to the nature of the faulting, and even subtle differences in subsurface bedrock characteristics (Burbank and Anderson, 2012).

One of the ways in which surface deformation can be calculated is through matching of geomorphic markers (Burbank and Anderson, 2012). Across faulted surfaces throughout the Lake Heron Basin, several geomorphic features can be correlated, from which measurements can be taken to analyze the amount and type of expressed surface deformation.

Within this study site, the most useful features for analyzing surface deformation are river terraces and glacial moraines. When addressing the surface deformation, there were several factors that had to be understood. First, some of the deformation could have occurred during each earthquake (coseismically), while the rest may have formed during periods of relative quiescence (aseismically). Additionally, the amount of deformation at the surface does not necessarily need to remain consistent over the course of the entire surface trace due to factors such as fault segmentation, fault growth, variations in slip, and changes in geometry and dip (Cartwright et al., 1995; Burbank and Anderson, 2012). Lastly, in an earthquake, deformation can be distributed amongst hundreds of small ruptures, meaning the resulting deformation can be quite complex.

2.3.2 Methodology

In order to determine the extent of surface deformation throughout the Lake Heron Basin, surveying using a Trimble differential GPS was combined with the extensive structural mapping. GPS points obtained in the field were then corrected using the base stations at Mt. John

(68 km away) and Mt. Somers (25 km away), often yielding errors less than 0.5 m, though in areas where satellite signal lacked, it exceeded 1 m. Such error was always incorporated into calculations and interpretations.

When surveying was conducted, the dGPS unit was held at approximately 1.4 m height (Chest level) (Figure 2.18). All lines were run as close to perpendicular with the fault as possible, in an attempt to show an accurate representation of both the fault scarp width and deformation zone. A chosen setting was for points to be taken based on distance travelled rather than time. This was done as there were instances where walking through matagouri and Spaniard Grass was slow, which would have resulted in numerous points in similar locations.

Once surveying was completed and points had been corrected, they were imported into ArcGIS where point profiles were created. These profiles were then exported to Golden Software's Grapher, in which slope and height data could be calculated. In order to determine the approximate amount of vertical of surface deformation, slopes from the hanging and footwalls were matched. Once these slopes, which tended to fluctuate around 3°, were matched, a line perpendicular to them was measured to calculate vertical surface deformation using methodology in Thompson (2002), Amos et al. (2010), and Stahl (2014) (Figure 2.19).

Once this was completed, the width of the deformation zone could be determined. This was done by examining surface features such as fault scarps and folded topography. When fault-associated features were deemed to have disappeared, the distance between them, along the line of slope was measured. All of this data was then stored, and used to produce tables and graphs, illustrating the deformation variation seen along the Lake Heron Fault.

While measurements were taken to calculate the total deformation seen, they were further broken down into fault and fold components, aided by the use of structural maps completed in this study. Within this thesis, fault deformation was limited to reverse fault scarps, while all other deformation was considered folding, including normal faults. This was done as they were only found within crestal graben, which formed due to the presence of folding.

Figure 2.18: Technique used when operating a differential GPS (dGPS). This image was taken while surveying the southern portion of the Paddle Hill Creek Fan

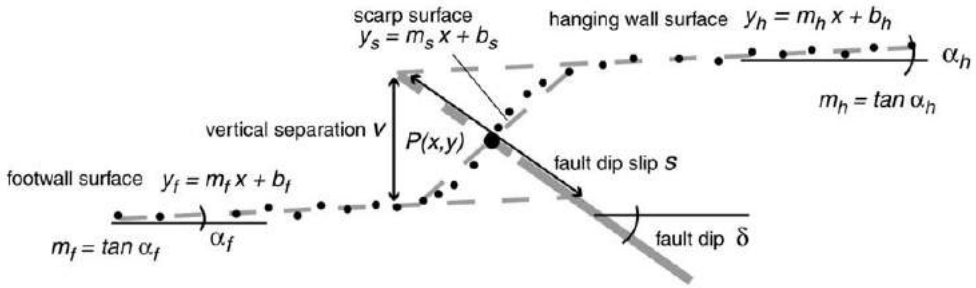

Figure 2.19: Methodology followed for survey line calculations. Figure from Thompson (2002)

2.3.3 Spider Lakes Section

2.3.3.1 Introduction

The Spider Lakes Section of the Lake Heron Fault is the southernmost portion where the strike remains 200°. This section extends from just north of Lake Roundabout to the Paddle Hill Creek Fan (Figure 2.20). This 4 km stretch represents a vital location in the larger interpretation of the region, and is also a section where cosmogenic isotope ages were acquired in earlier research (Evans, 2008; Rother et al., 2014). The extent of surface deformation within this area will be examined, and then be compared to the other two, Paddle Hill Creek and

Castle Ridge, in an attempt to interpret the reasons behind the varying deformation size and how it illustrates a complex history.

Within the Spider Lakes Section, 26 survey lines were run, most in a 1 km section where the strike of the fault fluctuates around 200° (Figure 2.22). This section was prioritized because the strike is consistent with the Paddle Hill Creek and Castle Ridge Sections. The deviation in strike to the south, while important, results in vastly different surface deformation, likely due to a changing orientation relative to the compressive regime. This section is also compromised, as the geomorphology has resulted in steep slopes leading to Spider Lakes, a series of tarns. Because of these differences, and for the purposes of maintaining consistency, this section is noted though not compared to the sections where the strike of the fault remains 200°.

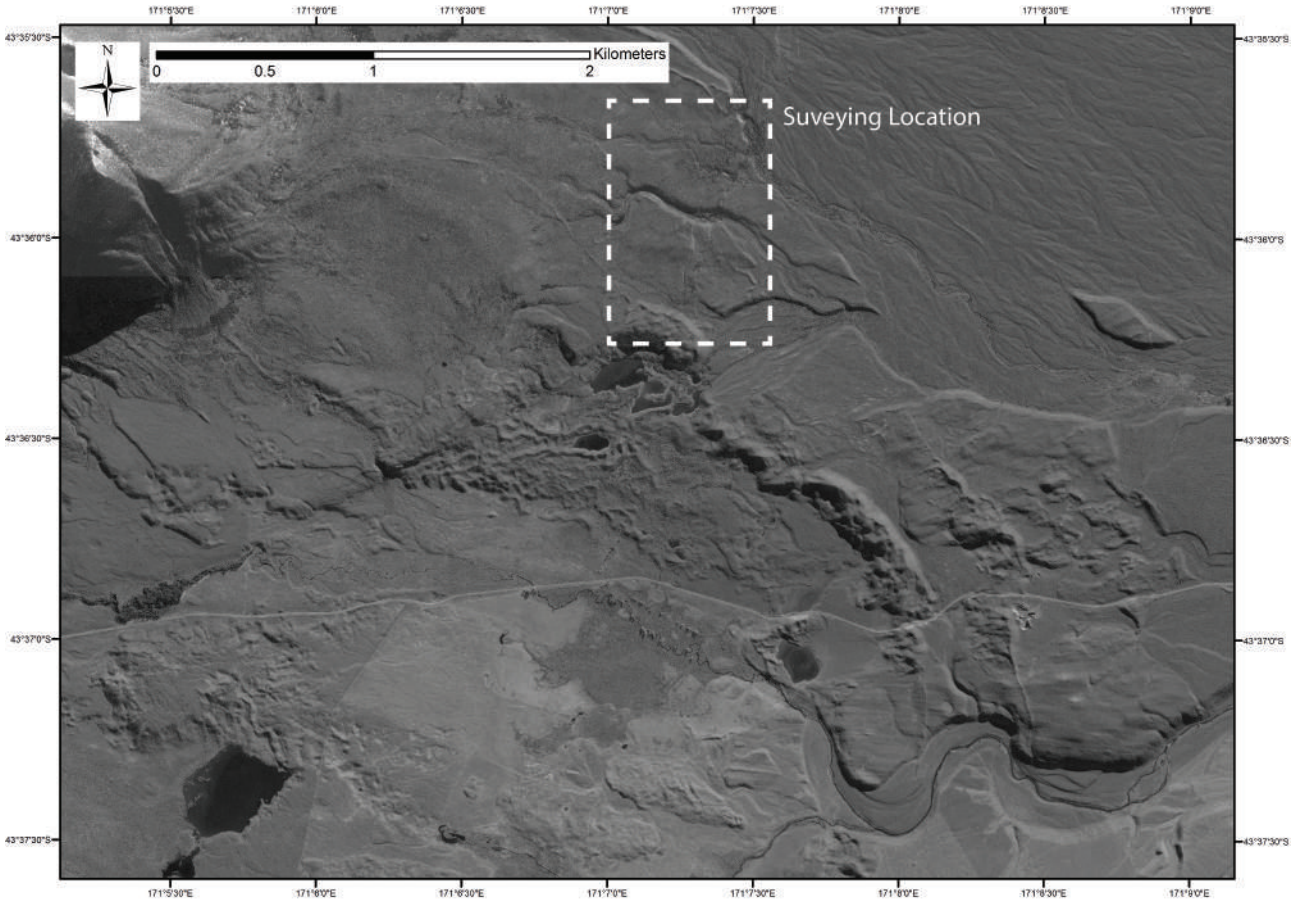

Figure 2.20: Overview map of the Spider Lakes study site with surveying location. Lake Roundabout is in the southwest portion of the figure.

2.3.3.2 Deformation

Within the northern 1 km of the Spider Lakes Section, the zone of deformation remains relatively consistent. However, the way in which deformation is distributed, in addition to surface rupture traces and features, changes dramatically. In this northern section, 18 survey lines were used to analyze the deformation seen (Figure 2.22). While more were taken, they were omitted from this analysis for factors such as limited accuracy, and/or their focus on smaller features.

Throughout the Spider Lakes Section, there is significant deformation, of which the vertical component is accommodated by discrete displacement across fault scarps, and distributed folding and buckling. Some of these fault scarps are large (8 m), while others are subtle (0.5 m). Similarly, the folding within this section has created associated features such as bulging of the hanging wall, and the crestal graben described in 2.2.1.

Starting at the southern extent of the analyzed area, survey lines pick up both discrete and distributed components of deformation (Figure 2.21). This line, run within a channel just north of Spider Lakes, illustrates not only the entire vertical and horizontal components of the deformation zone, but subtle and obvious examples of how deformation is distributed. Using the methodology in 2.3.2, it was determined that the deformation zone is approximately 213 m wide, and 21 m high. This 21 m is accommodated on four fault splays, and associated folding. The fault scarps make up approximately 6.5 m (30-35%), of the vertical displacement, meaning that at the southernmost extent, around $^2/_3$ of the vertical deformation is accommodated by folding. Though this is a significant amount given the number of fault traces, the trend is not maintained, as only 300 m north, 70% of the deformation is fault-associated (Figure 2.23). An increase of approximately 40% over such a short distance is attributed to the presence of a single 8 m high scarp, which diminishes both north and south. However, this percentage drops off quickly, as in the northern portion of the Spider Lakes Section, around 20% of the total vertical displacement is taken up by faulting. These stark differences tend to coincide with features such as crestal graben and/or large river channels.

Extreme variation in trends such as this have been seen on other reverse faults in New Zealand. Along the Ostler Fault to the SW, they noted that the amount of fault-associated deformation fluctuated between 33% and 95% (Davis et al., 2005; Burbank and Anderson, 2012). Therefore, calculated values for the Lake Heron Fault are not believed to be anomalous.

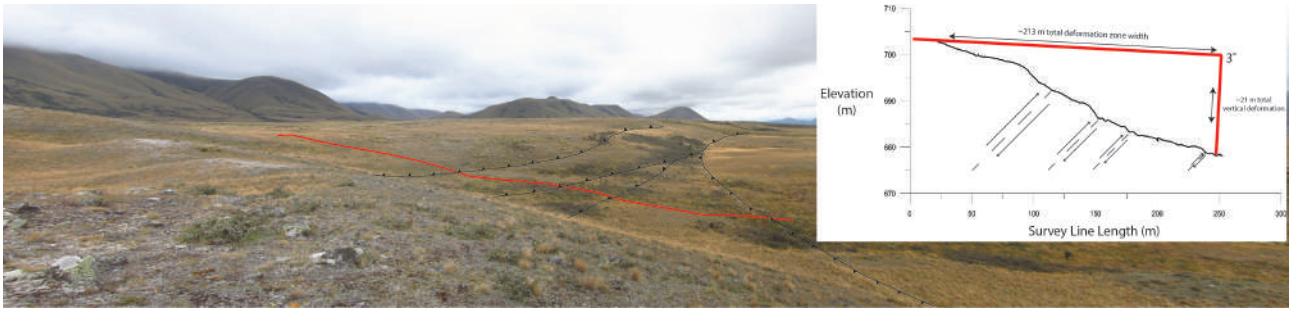

Figure 2.21: Annotated photograph of southern end of Spider Lakes section, with location and profile of accompanying survey line.

While the ratio of fault vs. fold deformation changes dramatically from south to north, many aspects of the deformation zone remain consistent. One of these is the total vertical deformation, which fluctuates between 17.3-24.5 m. When error is considered, all values fall within a similar range, and variation can be attributed to minor differences in surface geomorphology and/or where slope projections were taken from. This indicates that the entire section has experienced the same amount of vertical displacement, and that the only difference is how it has been accommodated. It also suggests, though it cannot be confirmed, that the entire faulted surface is of roughly similar age. However, as will be seen later, other sections of the Lake Heron Fault have undergone the same amount of vertical deformation despite having vastly differently-aged surfaces.

Another characteristic which remains consistent is the fracture zone width. The fracture zone is defined as the distance between the easternmost and westernmost faults within the deformation zone. In order to maintain consistency, a bearing perpendicular to the average strike of the fault was used (290°), and all fault locations were based on field mapping compiled for this study. What becomes apparent is that outside one location, 800 m south of Paddle Hill Creek, all fracture zone widths fluctuate within a 20 m range. This is understandable as minor fluctuations in fault strike, or additional fault splays can easily alter the size of the zone.

While the fracture zone width remains relatively consistent, the related deformation zone width does not illustrate the same trend. As is apparent from the deformation and fracture zone width graph, the Spider Lakes deformation zone ranges from 122-233 m wide (Figure 2.23). While a 100 m difference is quite large, where the deformation zone is widest corresponds to areas of greatest fold deformation. This could be due to the fact that folding is often gradual, meaning its extent will be spread out over great distances. This is in contrast to regions where faulting dominates, and buckling on the hanging wall is limited.

Another metic calculated for all sections of the Lake Heron Fault was fault density. This was

broken up into three categories; fault density, reverse fault density, and normal fault density, each of which is based on the number of faults per 100 m. This was done in an attempt to show subtle variations, for by limiting the y-axis, those small changes are clearly visible. Had this not been done, an apparent inverse relationship to the true one would have been seen.

Survey Line	Deformation Zone Width (m)	Total Number of Faults
A	160	6
B	213	4

Table 2.5: Example survey lines for fault density calculations

Calculation Showing Fault Density by Meters/Fault:

$160/6 = 26.67$ meters/fault

$213/4 = 53.25$ meters/fault

Calculation Showing Fault Density by Faults per 100 m

$(6/160) * 100 = 3.75$ faults/100 m

$(4/213) * 100 = 1.87$ faults/100 m

By looking at the fault density graph, it is clear the density changes dramatically throughout the section, often due to the increased presence of normal faults in crestal graben structures (Figure 2.23). However, just because there are more normal faults, does not always translate to a higher fault density, as the number of reverse faults also changes.

A final metric is the percentage of the total width of the deformation zone which accommodates 50% of the vertical deformation. This study found that on average, 50% of the vertical deformation occurs over approximately 30% of the deformation zone, though values ranged from 23-44%. While possible relationships were examined, there did not seem to be any correlation between this metric and others calculated. Possible links investigated included a relationship to the amount of fault vs. fold deformation as well as the number of faults. However, values fluctuated significantly and did not appear to correlate. While the values acquired display a large range, the upper limit is similar to those found on the Greendale Fault study in Canterbury (Van Dissen et al., 2011, 2013; Quigley et al., 2012). While the Greendale Fault is predominantly strike-slip in nature, this work found that 50% of the deformation on average occurred over 40% of the deformation zone. Therefore, while the Lake Heron Fault values are slightly lower, they remain within the range of what has been found on other faults rupturing through late Quaternary gravel sequences.

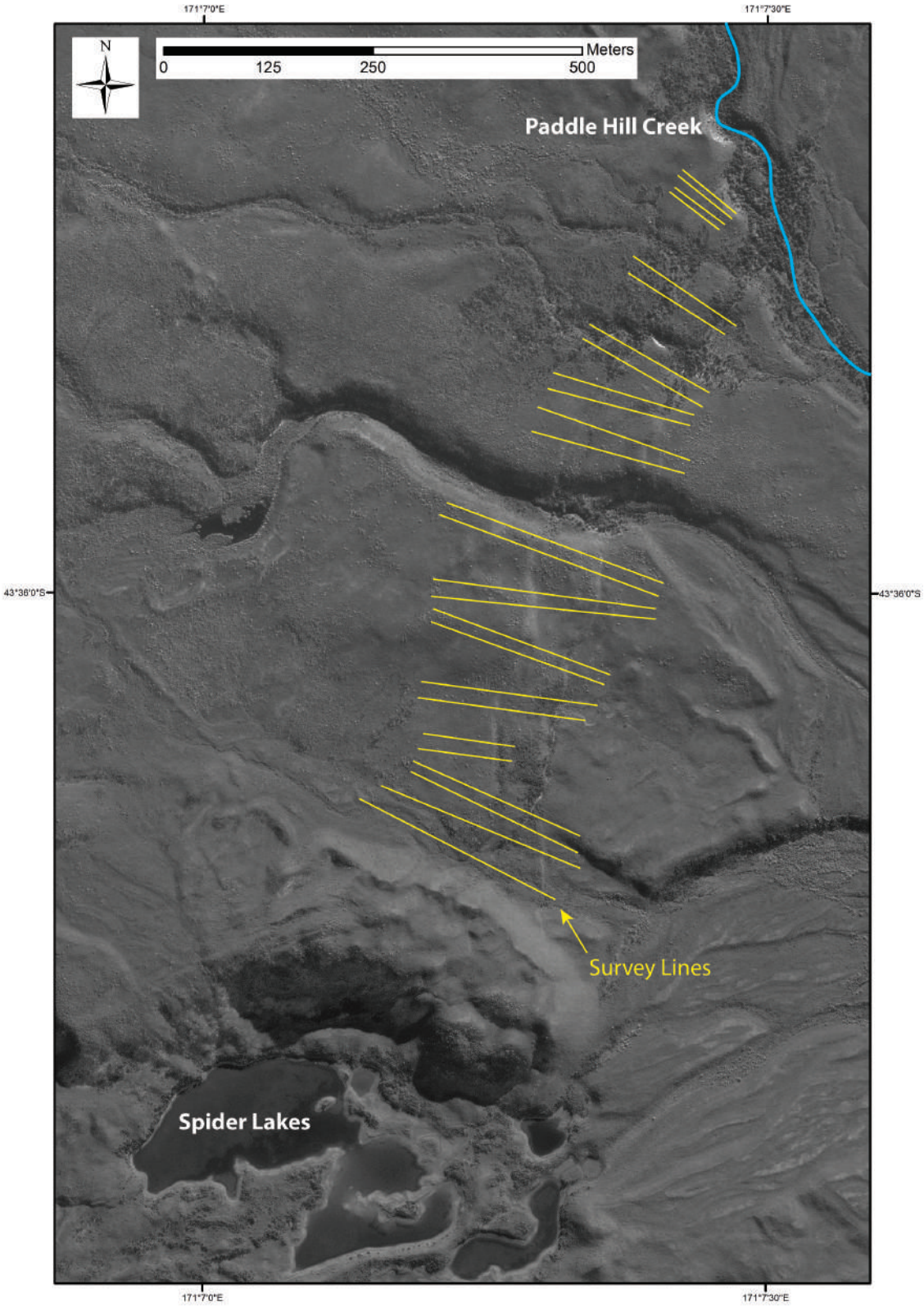

Figure 2.22: Enlarged portion of Spider Lakes Section showing location of survey lines. This shows all survey lines taken, though only 18 were used to create the deformation and fault charts.

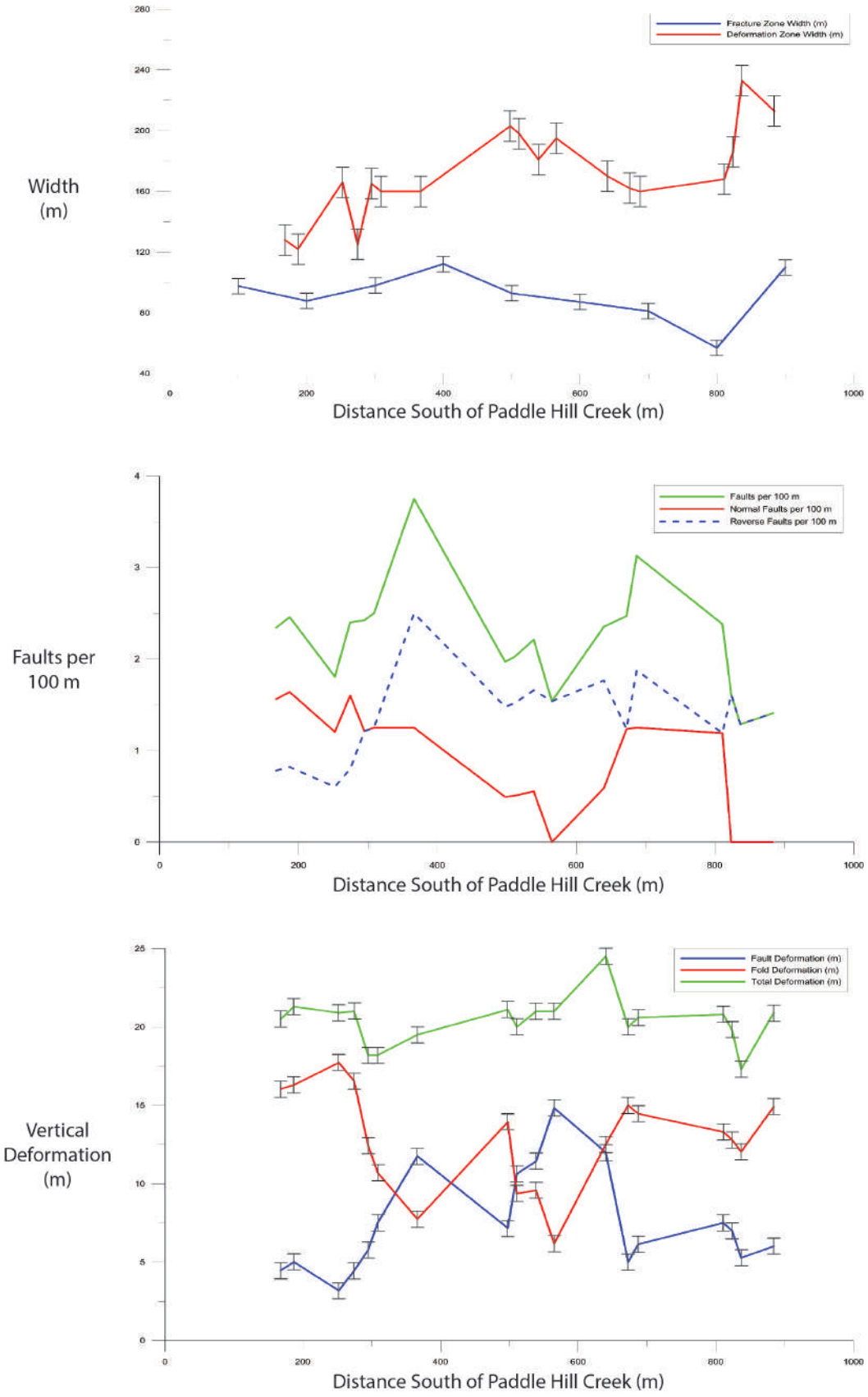

Figure 2.23: Spider Lakes Deformation Characteristics. From top to bottom, they are: fracture and deformation zone widths, fault density, and vertical deformation.

2.3.4 Paddle Hill Creek Section

2.3.4.1 Introduction

The Paddle Hill Creek Fan is the middle section of the Lake Heron Fault, between Spider Lakes to the south, and Castle Ridge to the north (Figure 2.4). Just as was the case for the Spider Lakes Section, the strike of the fault remains approximately 200°. This fan, which was originally categorized as 17-28 ka outwash and glacial moraine, with approximately 20 m of total vertical deformation, is 2.5 km long and 5 km wide (Barrell et al., 2011). However, this dating was not conducted using absolute dating methods, and was done instead through surface correlation and knowledge of New Zealand glacial advances.

The Paddle Hill Creek Fan represents an immaculately-preserved landscape which allowed for an in-depth analysis of fault behavior. Because of the preservation, geomorphic features such as fault scarps are clearly visible not only on the ground but in aerial imagery. This was useful as it allowed for identification of key sections, and fault mapping. By comparing the amount of surface deformation on the fan's terraces, a greater understanding of the Lake Heron Fault's behavior could be derived.

Prior to this study, limited work had been done on the Paddle Hill Creek Fan. The fault was mapped several times, though not in great detail by Gair (1967), Mabin (1980), and Oliver et al. (1990). Stahl (2014) also mapped the fan, but for this study, a more comprehensive dataset was compiled. This was done because of the fan's importance to understanding how the Lake Heron Fault ruptures, the surface features created, and how frequently earthquakes occur. Additional research in the area, (Evans, 2008; Pugh, 2008) also produced geomorphic maps, though neither dated the main terrace surfaces.

Along the Paddle Hill Creek Fan, 25 survey lines were run, each with varying length, which depended on how extensive the deformation zone was deemed to be and/or if features such as rivers effected the ability to continue them (Figure 2.24). Where there were gaps in the dataset, the 15 m DEM was used. This proved reliable for confirming vertical deformation, as it is very abrupt and clear on the DEM. This technique, though valuable, was limited to the total vertical deformation, as individual scarps were not visible.

2.3.4.2 Deformation

Within the Paddle Hill Creek Section, dramatic differences are seen in the deformation zone width, fault density, and fault vs. fold deformation. However, while aspects of it change,

total vertical deformation remains relatively consistent. Across the entire stretch of the fan, the vertical deformation remains around 19 m, roughly the same that was seen in the Spider Lakes Section.

Along the fan, evidence of deformation is clearly visible, both through fault scarps, and distributed folding. In some sections, fault scarps are numerous and reach individual heights of 8 m, while in others, folding dominates, with only a solitary fault scarp. In the southern section of the fan, a large crestal graben dominates, and is the same one seen in the northern part of the Spider Lakes Section. Regardless of the type of deformation, surveying allowed for each individual fault scarp and fold to be clearly defined and measured.

Beginning just north of Paddle Hill Creek, the first of the survey lines runs straight through the large crestal graben. In this area, total vertical deformation, calculated using the method in 2.3.2, was 17.5 m, spread out over a distance of 141 m. Of this 17.5 m, approximately 12 m (65-70%) is taken up by distributed folding, while the rest (30-35%) is accommodated by reverse faults. This is a significant amount of folding, though the classification of a crestal graben as fold deformation is likely a contributing factor.

While much of the deformation in the southern portion of the fan is taken up by folding, the trend is not maintained. Approximately 450 m north, the opposite relationship is seen, where of 19.2 m of vertical deformation, 75-80% is accommodated by fault scarps, while only 20-25% is folding. This is due to two large fault scarps, each exceeding 5 m in height. However, 600 m to the north, the fault-associated portion drops to 25% (Figure 2.25).

The decrease in the amount of fault deformation tends to coincide with a decrease in the number of fault splays (As many as 7, down to 4), as well as a change in elevation due to large (15 m high) terrace risers. Nonetheless, the changes in fault vs. fold deformation are ones that while their respective percentages fall within the range found on the Ostler Fault, indicate important characteristics of the Lake Heron Fault (Davis et al., 2005; Burbank and Anderson, 2012).

While there are stark changes in how deformation is accommodated, the total vertical deformation remains relatively similar (14.6 to 22.7 m). Although the range is quite large, the majority of measurements are quite similar, with only a single survey line illustrating significantly less (14.6 m) vertical deformation (Figure 2.25). This value is believed to be anomalous and is instead believed to highlight the uncertainty involved in measurements. The similar amount of total vertical deformation on the fan is peculiar as the terraces have different ages (Section 3.2.4).

Although the total vertical deformation remains consistent, two other metrics (Deformation and fracture zone width) change significantly. While at the crestal graben, the deformation

zone is approximately 150 m wide, it quickly (300 m north) increases to over 300 m wide. This trend is mimicked by the fracture zone, as at the crestal graben, it is about 100 m wide, while 500 m north, it doubles to 200 m. Up to the 1 km mark north of Paddle Hill Creek, the deformation and fracture zone widths gradually increase to 369 m and 291 m respectively. However, after this point, the deformation zone decreases in width slightly (down to 270 m), while the fracture zone width diminishes to 5 m. This dramatic difference in fracture zone width can be attributed to a solitary fault splay on the high terraces. The deformation zone however appears to be unaffected by factors such as elevation and number of fault splays.

Fault density also displays significant changes from south to north. Within the crestal graben, fault density is 4-4.5 faults/100 m, 500 m north, it drops to 1.5 faults/100 m, and on the high terraces it is less than 0.5 faults/100 m. This can be attributed to the fact that on the high terraces, there are only 1-2 fault traces though the deformation zone width remains relatively consistent. Because of this, a strong correlation is seen between the total number of faults and the fault density. Lastly, it is important to note that north of the crestal graben, the total fault and reverse fault densities are the same.

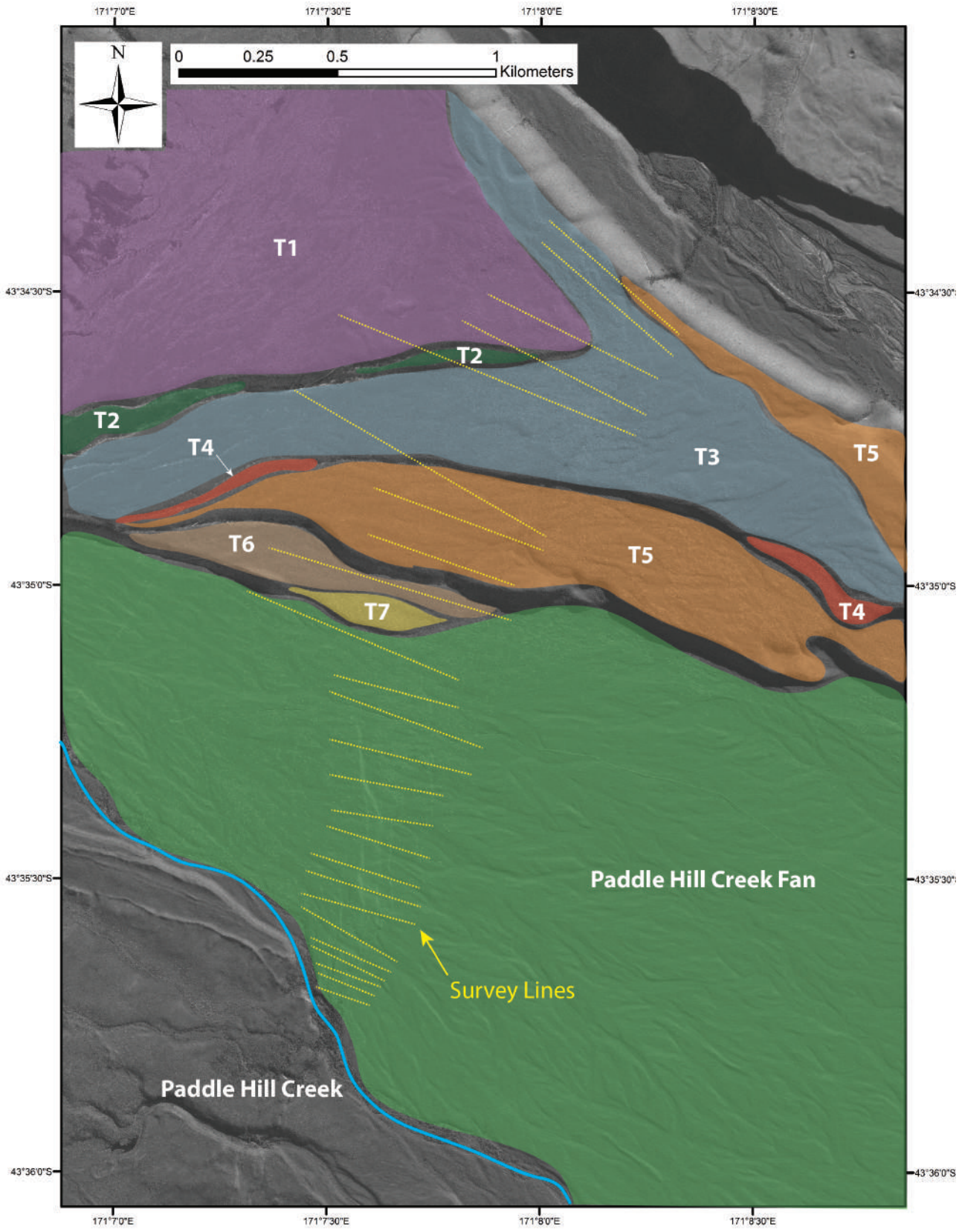

Figure 2.24: Terrace map and location of survey lines on the Paddle Hill Creek Fan. These lines were used to create the deformation and fault charts. When survey lines were not long enough to pick out the entire deformation zone, the 15 m DEM was used.

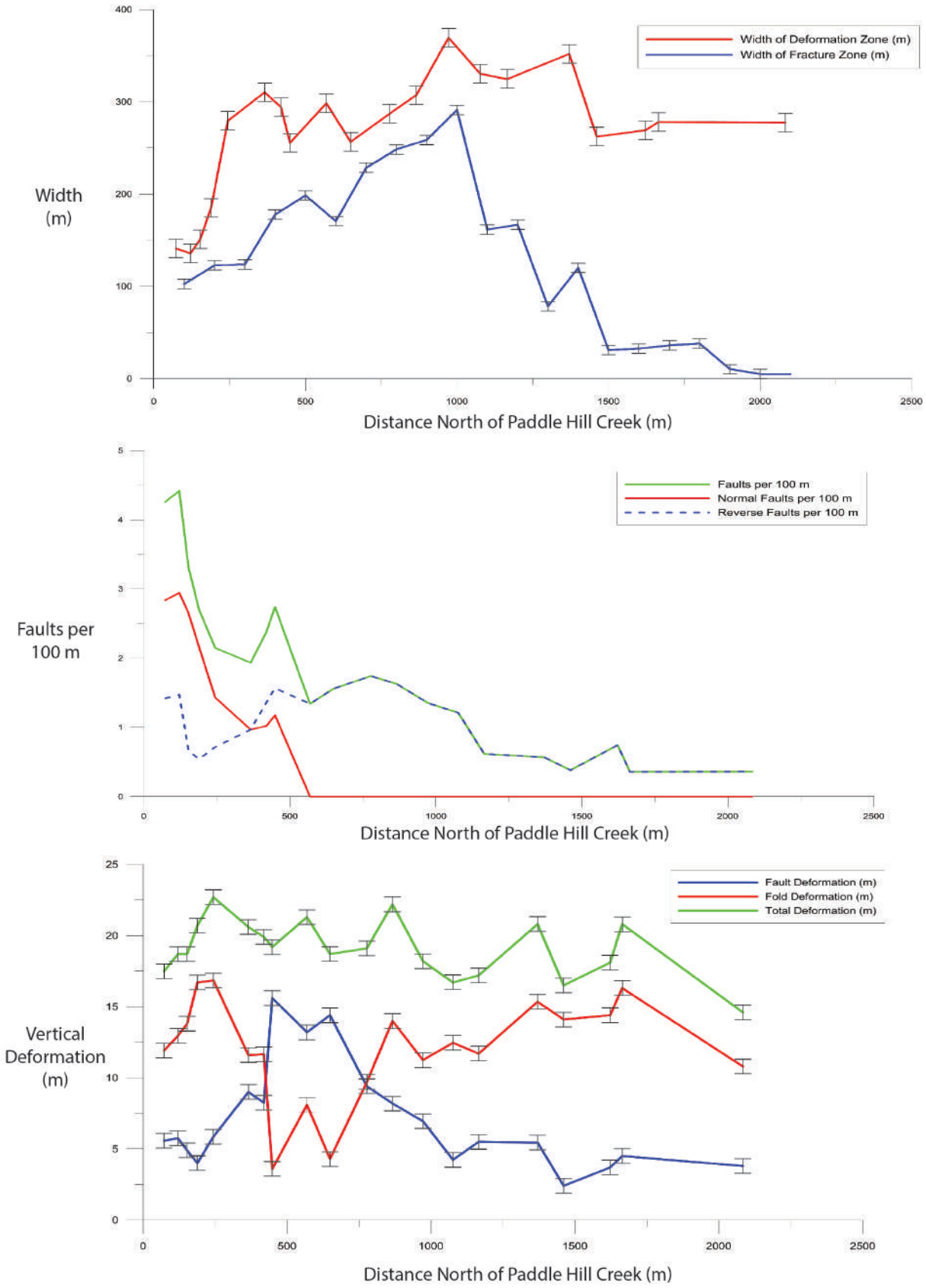

Figure 2.25: Deformation characteristics for the Paddle Hill Creek Fan. From top to bottom, they are: fracture and deformation zone widths, fault density, and vertical deformation.

2.3.5 Castle Ridge Section

2.3.5.1 Introduction

The Castle Ridge Section is the northernmost portion of the Lake Heron Fault, and includes all structures north of the Paddle Hill Creek Fan. While the other two sections contain numerous large fault scarps, this region is much more subtle, with folding dominating deformation (Figure 2.26). Though previous work has been done here (Pugh (2008); Barrell et al. (2011)), like the previous two sections, no active fault research has taken place, and the focus was primarily on glacial geomorphology.

Within the Castle Ridge Section, approximately 50 survey lines were run in an attempt to analyze the surface deformation. In addition to these lines, 61 were taken to complete the topographic contouring discussed earlier. Though significant surveying was done, this section proved difficult to analyze as the area has been heavily cultivated, resulting in both removal and addition of surface deposits. The geomorphology also plays a significant role in complicating analysis. Due to the orientation and proximity of the mountains to the west, the resulting pediment is much closer to the fault than in other sections. Additionally, geomorphological features such as moraines and terrace risers are nearly parallel to the strike of the fault, making differentiation difficult.

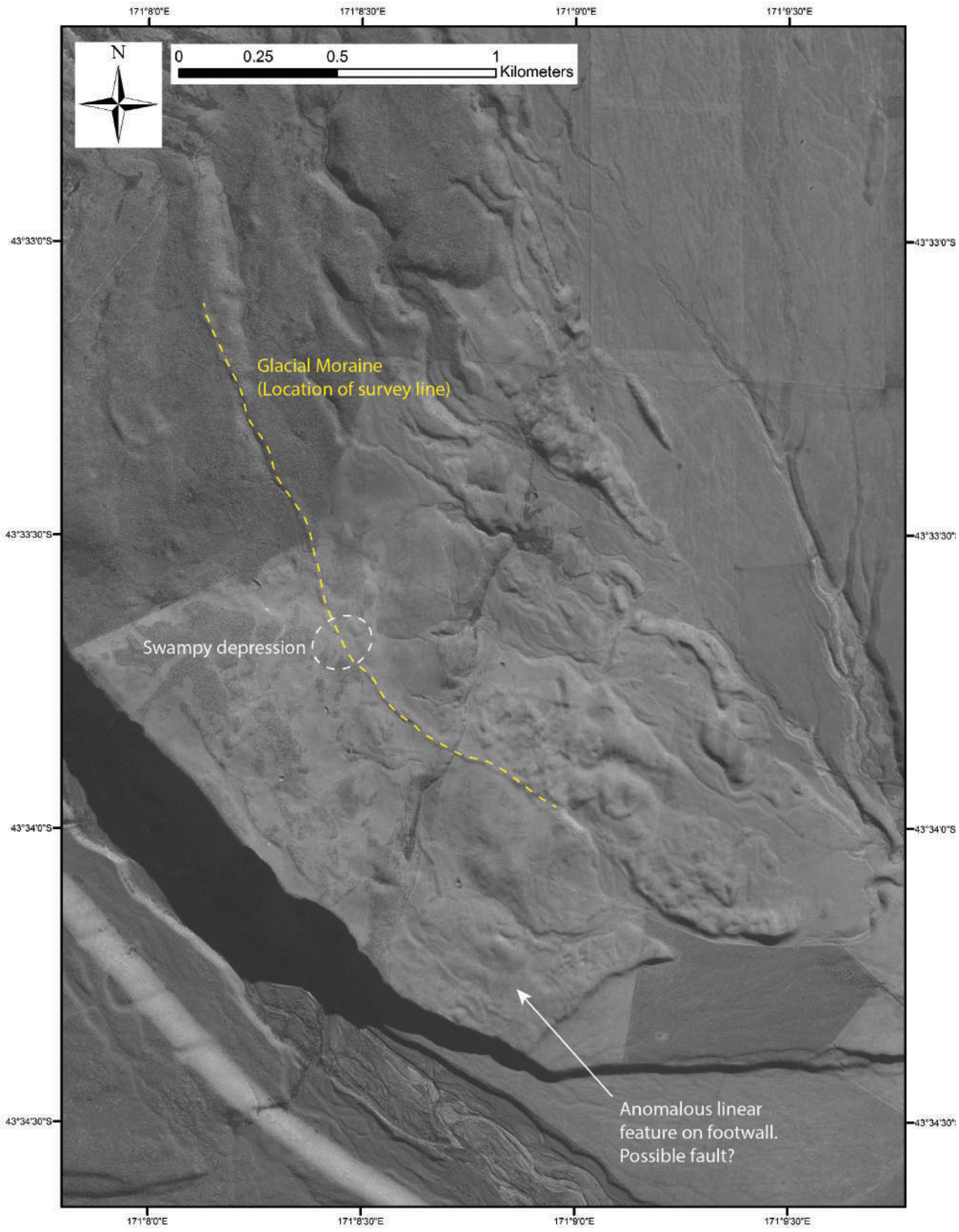

Figure 2.26: Castle Ridge study site

2.3.5.2 Deformation

In this northernmost section, almost all deformation is accommodated by folding. In most places, there is only a single 2.3 m high scarp. However, differentiating tectonic scarps from other geomorphic features was complicated as terrace risers and moraines run parallel with the strike of the fault. Therefore, following initial analysis, it was determined only a few survey lines were suitable to use.

Prior to analysis, aerial imagery suggested the deformation zone in the Castle Ridge Section may be significantly wider than was seen in the Paddle Hill Creek Section. In this section, there is a prominent moraine trending roughly E-W. On the hanging wall of the fault, this moraine disappears for approximately 150 m. (Figure 2.27). Upon visiting this location, it was seen to be swampy, suggesting ponding could have taken place, covering or removing all moraine remnants. Such ponding could have resulted from backtilting in response to fault-related folding, indicating deformation is substantially wider than in other sections.

While the deformation zone appeared much wider on the hanging wall, the same was not the case on the footwall. Although there is a linear feature cutting across the surface, its existence as progressive outboard movement of the deformation zone was not deemed convincing enough to be deformation-related (Figure 2.26). However, a substantial increase in the size of the hanging wall deformation zone could indicate significant fault characteristics. Therefore, surveying the length of the moraine ridge was deemed to be the most suitable solution, as it was the most identifiable continuous feature, and likely old enough to accommodate all deformation (Figures 2.26 & 2.28).

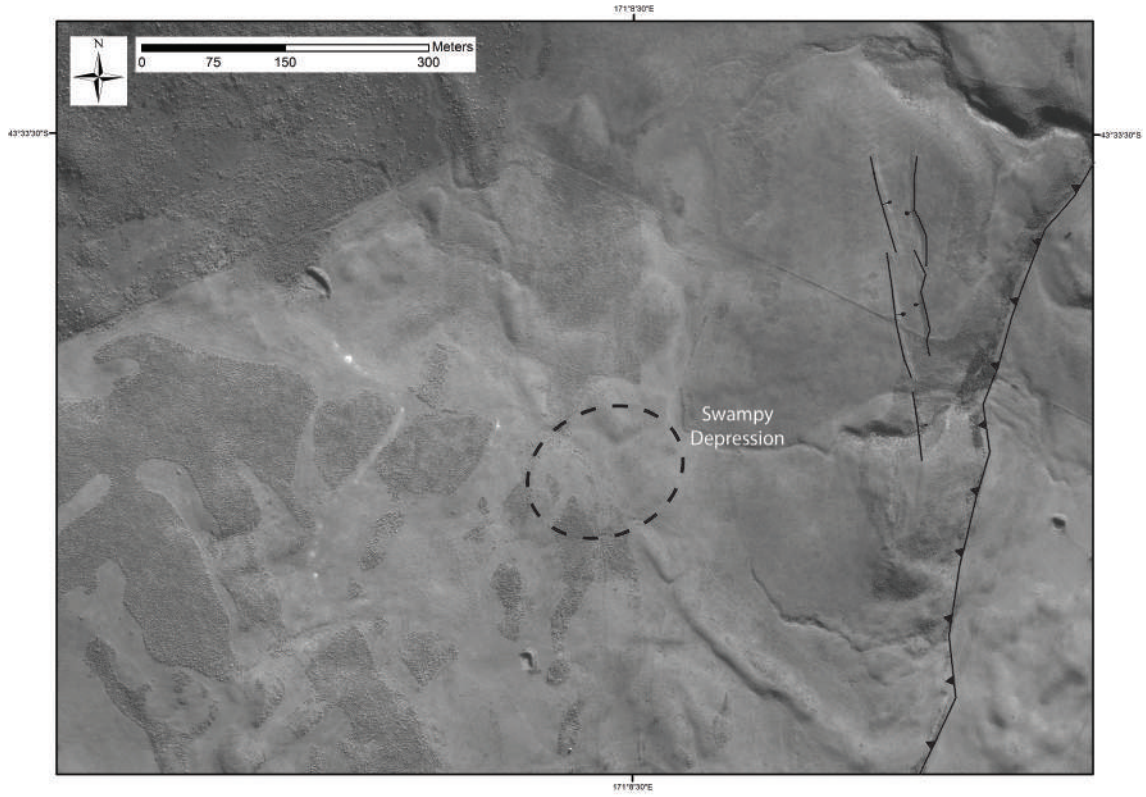

Figure 2.27: Zone of possible ponding where glacial moraine is covered before reappearing.

From the survey line run along the moraine crest (Up to 2.5 km), the entire deformation zone becomes clear (Figure 2.28). This survey indicates that the total vertical deformation is approximately 19 ± 3 m, while the deformation zone and associated backtilting extends for 734 ± 10 m. While there is error associated with these numbers, each value is significant for separate reasons. The 19 m of total vertical deformation is nearly equal to what is seen in the Spider Lakes and Paddle Hill Creek sections, suggesting that surfaces of varying age (Based on approximated ages in Barrell and Strong (2009) and Barrell et al. (2011) and cosmogenic ages in Rother et al. (2014)) display the same amount of vertical deformation. The other valuable piece of data at that in this location, the deformation zone is over 400 m wider than it was on the Paddle Hill Creek Fan. To more than double the width of a deformation zone in a little more than a kilometer is substantial, and could indicate variations in the subsurface geology, including fault dip, sedimentary strata, and preexisting structures.

Because of the width of the deformation zone, and the difficulty in differentiating the geomorphology, a comprehensive analysis like those done in the Spider Lakes and Paddle Hill Creek sections could not be done. Various analyses including the amount of deformation accommodated by faulting could be done from individual survey lines.

At the moraine, there is only one definite fault scarp, approximately 2.3 m high, meaning

10-15% (Given error) of the total vertical deformation is taken up by faulting. This trend appears to continue, as throughout the entire section, there is only a single definite reverse fault trace, with a few crestal graben and approximate reverse faults (Figure 2.5). The presence of at least three crestal graben supports the idea that very little deformation is taken up by faulting, as similar numbers were seen at locations of crestal graben in other sections.

While the deformation zone at the moraine is approximately 734 m wide, and 19 m high, these trends do not remain. In order for that deformation zone width to be maintained further north, it would either extend deep into the foothills, or across the flat basin floor. This is unlikely as it is not picked up by either the 15 m DEM, or survey lines. For example, 350 m south of where the active fault trace becomes obscure, the deformation zone appears to be less than 100 m wide (Figure 2.29). A decrease this substantial likely indicates dramatic subsurface structural variation.

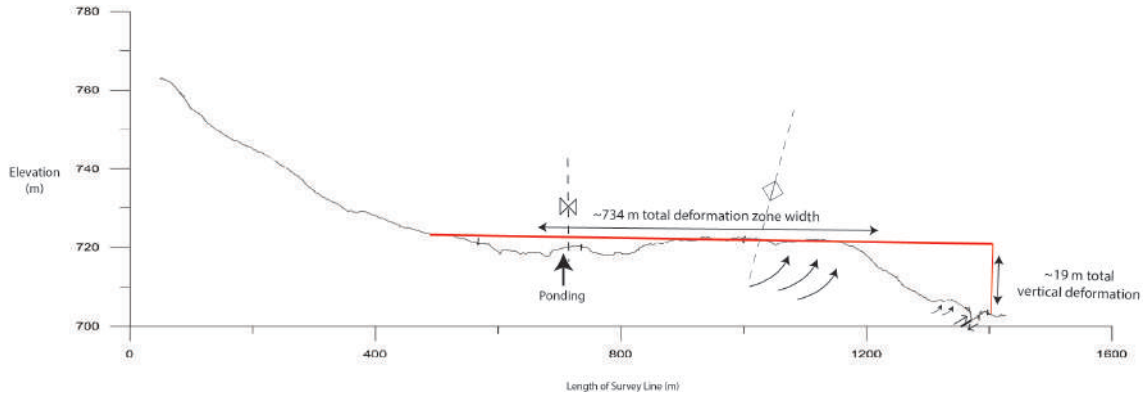

Figure 2.28: Castle Ridge Moraine Survey Line. From this survey line, both the entire extent (width) of the deformation zone becomes evident, as does the total vertical deformation. The total vertical deformation (19 m) matches up nicely with that found within the other two sections of the Lake Heron Fault.

At the northernmost point of the definite fault trace, before its projection further north becomes approximate, there is a 2.3 m high fault scarp. While a survey line was not run in this location, no other visible deformation was noted. Additionally, because survey lines were run just to the south of this location, a decrease in vertical deformation could also be confirmed (Figure 2.29). From this line, it is clear that the vertical portion of deformation has lessened significantly (10.4 m), to almost half what was seen seen a kilometer south. Therefore, just like the southern portion of the Spider Lakes Section, the northern extent of the Castle Ridge Section shows a dramatic decrease in the overall size of the deformation zone.

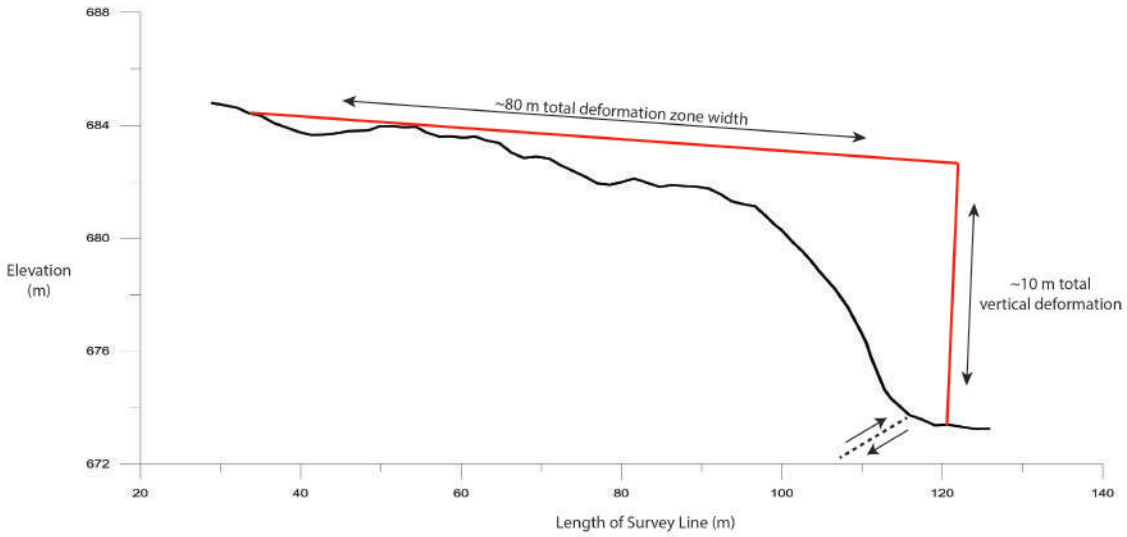

Figure 2.29: Survey line illustrating rapid decrease in both total deformation zone width and height.

2.3.6 Discussion

Within each of the three study areas, characteristics must be further examined. Within the Spider Lakes Section it is why, when the total vertical deformation remains fairly consistent does the way it is distributed change so dramatically? Testable hypotheses include strain partitioning, changes in fault plane curvature including subtle changes in fault strike, changes in the basement rock rheology, and thickness of sediment cover. Strain partitioning is often defined as the variation in strain due to heterogeneity found in rocks, in addition to gradual alterations in material properties (Axen et al., 1998). This process, which is well-documented, can take place for a variety of reasons, such as a heterogeneous fault plane (Burbank and Anderson, 2012). One possible explanation is that over the course of the fault, patches fail to rupture completely. If this were to happen, differential deformation would be expressed in the surface geomorphology. While this phenomenon is often used to explain large-scale changes, it is possible that small, more rigid sections experiencing different types of slip may exist along the Lake Heron Fault. Another possible explanation is changs in fault plane curvature (Amos et al., 2007). In this study, it was found that by changing the radius of curvature along a fault plane, different types of folds were produced at the surface (e.g. detachment folds, simple-shear fault-bend folds, listric/planar folds) (Figure 2.30). Additionally, it is possible that small changes in bedrock characteristics (i.e. fracture density), which for the most part are unknown in this area, result in changes in fault surface expression. In turn, these changes may be accentuated by surface deposits. These sediments, which are likely unsorted and unstratified, may behave differently to folding, causing them to be predisposed to forming features such as crestal graben.

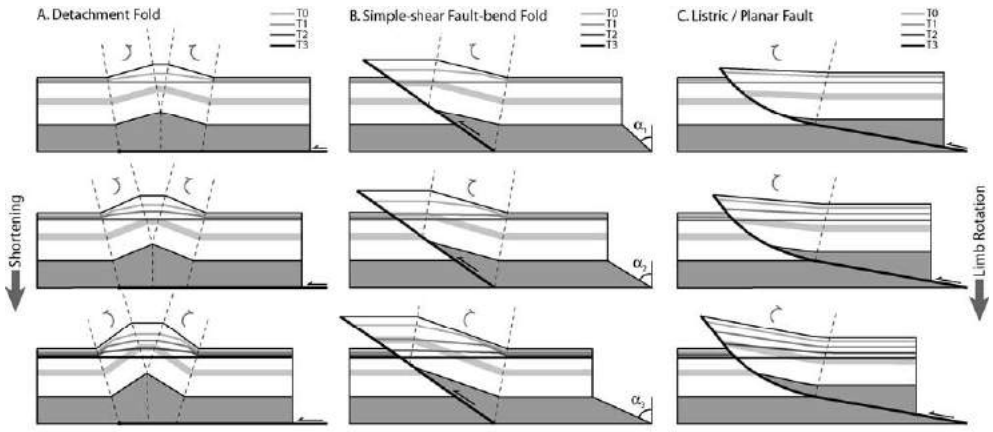

Figure 2.30: Examples of various types of surface folding caused by reverse faults. Figure from Amos et al. (2007)

Of relevance to the surface deposits are surface complexities at large features such as drainages. Along the Ostler Fault, Amos et al. (2011) noted that at major drainages, most notably the Ohau River, there were complex patterns in surface faulting. This trend is mimicked along the Lake Heron Fault. At the two main drainages within the Spider Lakes Section, crestal graben form. Because features such as these are considered elements of folding, it is quite possible that some of the variation visible in the deformation graph is due to this characterization.

When it comes to bedrock characteristics, authors (e.g. Ghisetti et al. 2007a; Amos et al. 2011) have repeatedly noted that variation can dramatically change a fault's surface expression. These changes include fracture density, type of bedrock, and preexisting faults that formed prior to New Zealand's compressive regime. Many of the reverse faults found throughout the Southern Alps, are examples of inversion tectonics, where Cretaceous normals faults became reverse in the Miocene due to changing principle stress directions (Ghisetti and Sibson, 2006; Ghisetti, 2006; Ghisetti et al., 2007a). Therefore, their orientation and structure could vastly impact surface morphology when reactivated.

Along the Paddle Hill Creek Fan, the main question was why, on the high terraces, is almost all the vertical deformation accommodated by folding? A possible answer to this question, is that the presence of significantly thicker gravel deposits. For example, Pettinga and Nicol (Personal Communication, 2015) observed that on terraces near the Rangitata River, those near the fault tip, with almost no gravel veneer, expressed surface deformation predominantly through faulting. However, for higher (10-15 m) terraces, with thicker sediment cover, the same deformation was accommodated almost entirely through folding.

Observations such as these led them to believe that it could be that once a certain threshold is reached, in this case, in excess of 10 m of gravel, resulting deformation is seen in the form of

folding (Jarg Pettinga, Personal communication, 2015). While factors such as fault geometry, slip, and the type of gravels likely effects this, a similar development is possible on the Paddle Hill Creek Fan. Additionally, as the Rangitata River is located just south of this field area, and has undergone similar geomorphic processes, similar thresholds could be expected.

While this is one explanation, there is a potential problem. As was explained, there is only a single location where bedrock exposure exists. This site, at the South Branch of the Ashburton River, just north of the fan, is approximately 60 m beneath the highest terrace (735 m to 676 m). When this terrace is compared to the lowest fan surface, it is 20 m higher, meaning that if the bedrock depth remains consistent, there would still be 40 m of gravel overlying bedrock on the lowest surface. However, bedrock is likely to have a highly variable paleotopography, and its depth cannot be assumed to remain consistent. Nonetheless, because fault geometry, variable slip, and the type of gravels likely affects how deformation is accommodated at the surface, there is still a possible correlation between gravel veneer thickness and surface deformation.

Lastly, in the Castle Ridge Section, two attributes must be examined in greater detail: the change in the width of the deformation zone just north of the South Branch of the Ashburton River, and the decrease in the total deformation zone in the northern part of the section. The possible reasons for these occurrences are significant in the greater understanding of the Lake Heron Fault, as they potentially shed light on behavioral tendencies.

While the sudden change in the width of the deformation zone is dramatic, it is not surprising. Given the difference in the nature of surface deposits from the Paddle Hill Creek Fan to the Castle Ridge Section (fluvial to glacial), a changing deformation zone could be expected. Because the deposits on the fan are fluvial in nature, they are likely sorted, stratified, and have a more cohesive matrix. Castle Ridge deposits however, are predominantly till, meaning they will be unsorted and unstratified. It is possible that this difference has resulted in variable fault propagation. Such variation has been seen on faults as they begin to encounter stepovers, structural variability, and/or rheologic differences (Knuepfer, 1989; Lin, 2004; Ghisetti et al., 2007b; Elliott et al., 2009; Amos et al., 2010; Campbell et al., 2010b,a; Stahl, 2014). In fact, Lin (2004) suggests that existing bedding planes within sedimentary strata can deflect thrust faults, resulting in stress transfer. It is also possible that for the reasons described earlier, structural characteristics have caused the variability seen.

The rapid decrease in both the total deformation zone width and vertical deformation in the northern part of the section sheds light on potential structural implications. As was explained earlier, deformation at the southern and northern extents of the fault decrease significantly. A possible reason for this is fault segmentation (Figure 2.31)(Amos et al., 2010; Burbank and Anderson, 2012). What can be seen from this figure is that while there are various segments

of the Ostler Fault, collectively, the slip rate remains roughly the same, though at the tips, it decreases substantially, in one instance, to zero. This trend appears to be mimicked on the Lake Heron Fault, suggesting it may have similar attributes to the Ostler Fault. This would not be unexpected as they are both within zones of almost exclusively thrust faulting (e.g. Pettinga et al. (1998)), and it lies within the South Canterbury Fault Zone outlined in Stahl (2014). While the Ostler Fault plot illustrates 50 km of fault, the Lake Heron Fault plot only shows 10 km. Therefore, what may be the case is that only a single segment of a larger structure has been examined.

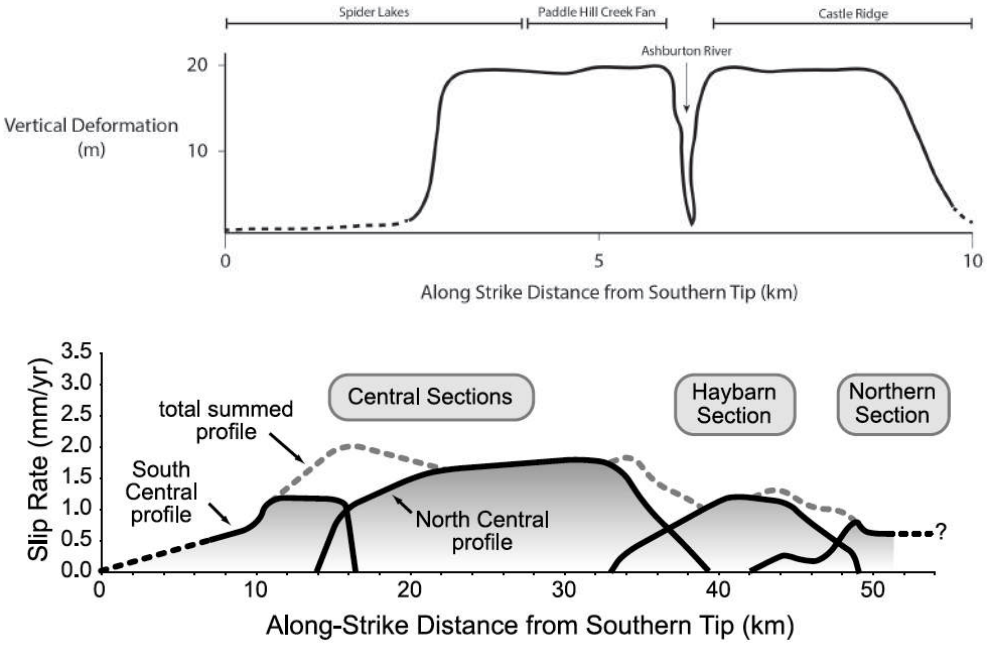

Figure 2.31: Variation in total vertical deformation along the course of the Lake Heron and Ostler faults. The top diagram shows the consistent 20 m of vertical deformation along much of the Lake Heron Fault, with large decreases towards the tips of the definitively-mapped trace in this study. While this figure appears to show a decrease in vertical slip at the Ashburton River, this is just a product of erosion. Figure from Amos et al. (2010).

2.4 Discussion

2.4.1 Cross Sectional Analysis

Numerous cross sections were used in deformation analysis and these can also be combined with the near-surface structural analysis and regional interpretations. To do this, a block model of the field site was created in an attempt to show near surface subtleties, and large structures at depth (Figures 2.32 & 2.33). To allow near-surface subtleties to be highlighted, three sections were enlarged from survey data. While there is error in projecting structures

from survey lines, because of how dramatic fault scarps and associated folding are, it remained limited, and was often constrained to fault dip and error in elevation data.

While most near surface structures can be shown with great detail, deeper features must be extrapolated through additional information from the surrounding region. Such information includes seismic and magneto-telluric surveys, which have significant error and interpretations can be ambiguous (Wannamaker et al., 2002; Long et al., 2003; Beavan et al., 2007; Campbell et al., 2010b,a; Stahl, 2014). However, for analysis of deep structures, it is the best there is. While no seismic or magneto-telluric surveys have been done within the Lake Heron Basin, some have been done to the south, imaging faults of similar nature, which is why they were used to makes conclusions of how the Lake Heron Fault behaves at depth.

From magneto-telluric surveys and seismic lines run across New Zealand's South Island, including one through the Rangitata River 12 km south of the Lake Heron Fault, most thrust faults within the rangefront zone are seen to shallow into a decollement at approximately 10-20 km depth (Beavan et al., 2007) (Figure 4.3). One of these faults is the Forest Creek Fault, which is believed to be of similar origin to the Lake Heron Fault (Beavan et al., 2007; Upton et al., 2004). The Torlesse greywacke-Quaternary sediment boundary is also shown on the model. From measurements presented in Section 2.2.3, it was seen that within basement greywacke, fault dip was much steeper than in Quaternary sediments. Therefore, while the exact depth of greywacke throughout the basin is unknown, the change in dip is highlighted. Other than these features, no deep structures could be interpreted without encountering significant error.

The survey data on the other hand shows near surface variation in fault scarps and folding along the Lake Heron Fault. Therefore, the level of accuracy increases significantly. From the three survey lines analyzed, a wide range of deformational features are seen, ranging from narrow deformation zones with significant fault scarps, to wide deformation zones with the majority of the vertical deformation accommodated by folding. Lastly, the numerous fault scarps exposed at the surface support the theory that the Lake Heron Fault has a network of near surface imbricate thrusts, which is subtly shown on the block model.

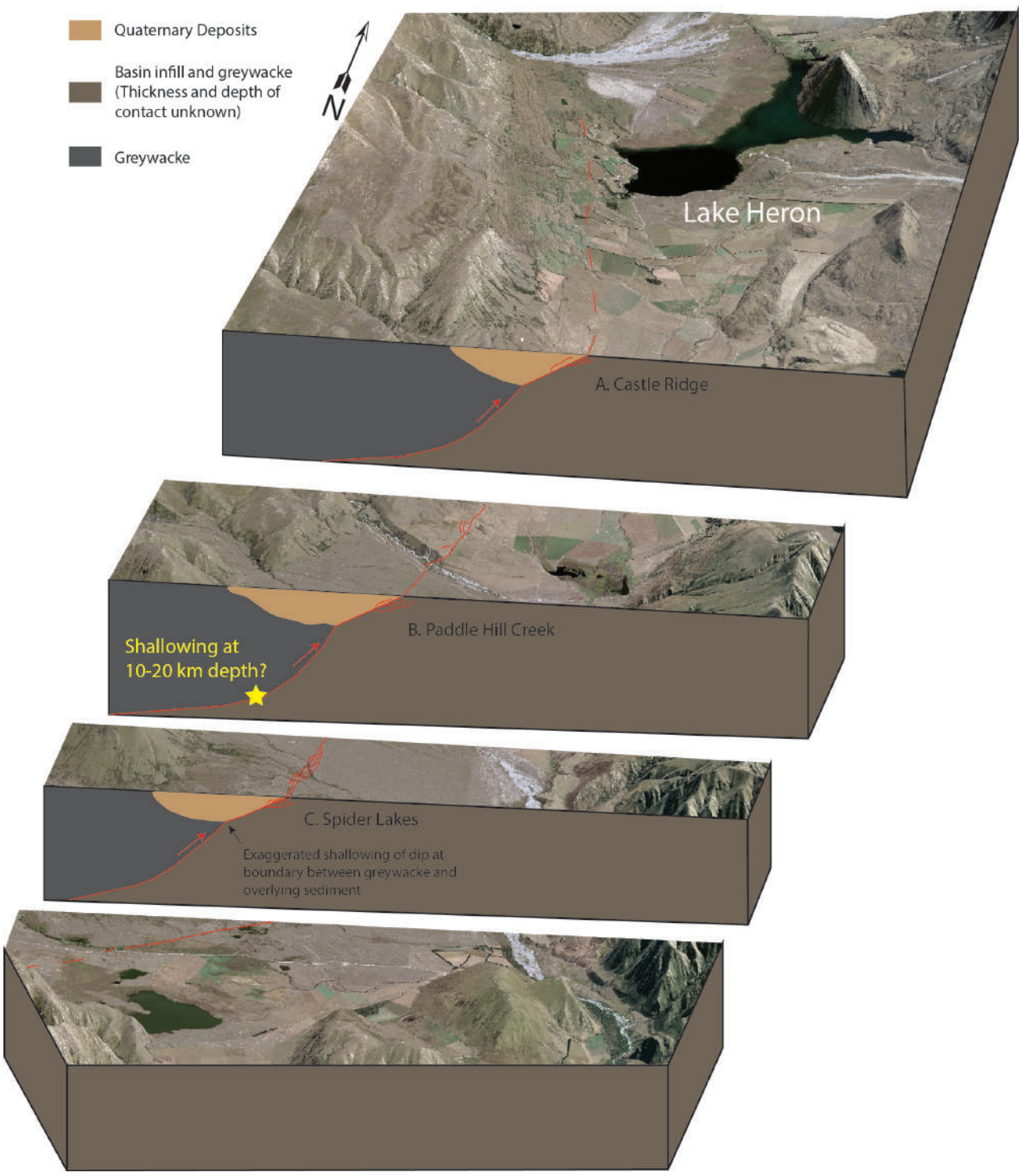

Figure 2.32: 3D block model of the Lake Heron Fault. This model shows the shallowing of the fault into a decollement at 10-20 km depth as proposed by Beavan et al. (2007). This model also shows some near surface structural tendencies, including the inbricate thrust network, and a shallowing dip near the greywacke-sediment boundary (This change in dip is exaggerated to highlight the change).

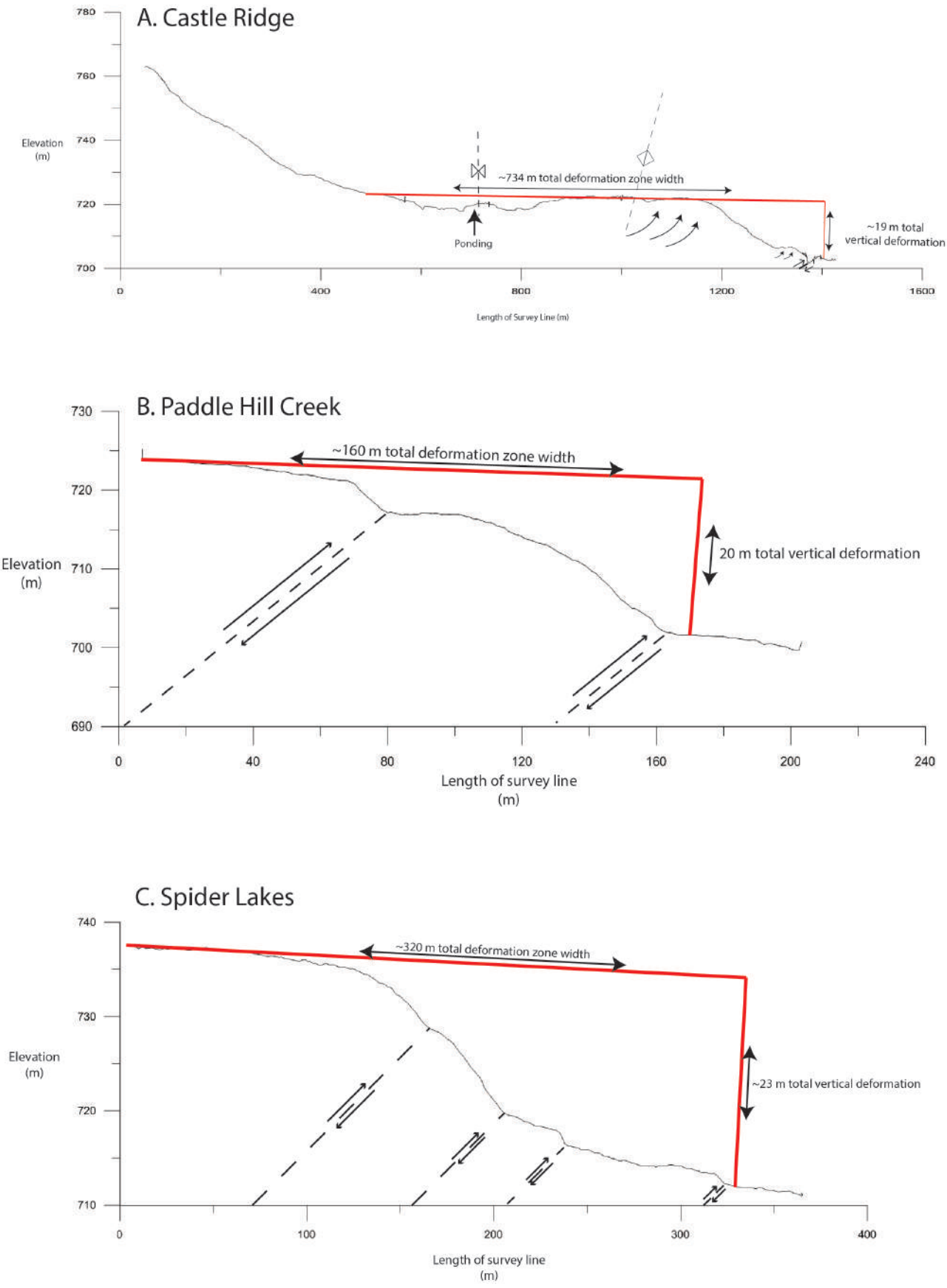

Figure 2.33: Near-Surface Variation of the Lake Heron Fault

3 Chronologic History of the Lake Heron Fault

3.1 Introduction

In order to develop a greater understanding of the Lake Heron Fault, the timing of events, and surface ages had to be known. Therefore, both alternative dating techniques such as Schmidt hammer exposure age dating (SHD), and traditional methods (e.g. radiocarbon dating) were used to constrain the timing of earthquake rupture along the Lake Heron Fault.

By using these techniques, and coupling the ages with structural and deformation characteristics, a clearer history of paleoseismic activity could be developed for the Lake Heron Fault, including calculation of slip rates, recurrence intervals, and single event displacements.

3.2 Schmidt Hammer Exposure Age Dating of Greywacke Boulders and Surface Correlation

3.2.1 Geomorphology

The Lake Heron and neighboring Lake Clearwater basins were both extensively glaciated 28-15.8 ka (Rother et al., 2014). Therefore, the majority of surface geomorphology consists of ground moraine, moraine ridges, and Quaternary alluvial and outwash deposits. Much of this geomorphology has been extensively mapped, and the timing of individual glacial advances has been proposed (Evans, 2008; Pugh, 2008; Barrell et al., 2011; Rother et al., 2014)(Figure 3.1). These authors identified and mapped four phases of glacial fluctuation within the Rangitata catchment in the last 30 ka (Figure 3.3). Many of these studies used cosmogenic isotope dating to constrain the timing of events (e.g. Evans (2008); Rother et al. (2014)). This method, while valuable, is expensive and has long turnaround times. However, the fact that ages were calculated with minimal error, allowed for other regions within the Lake Heron Basin to be dated and calibrated using alternative techniques.

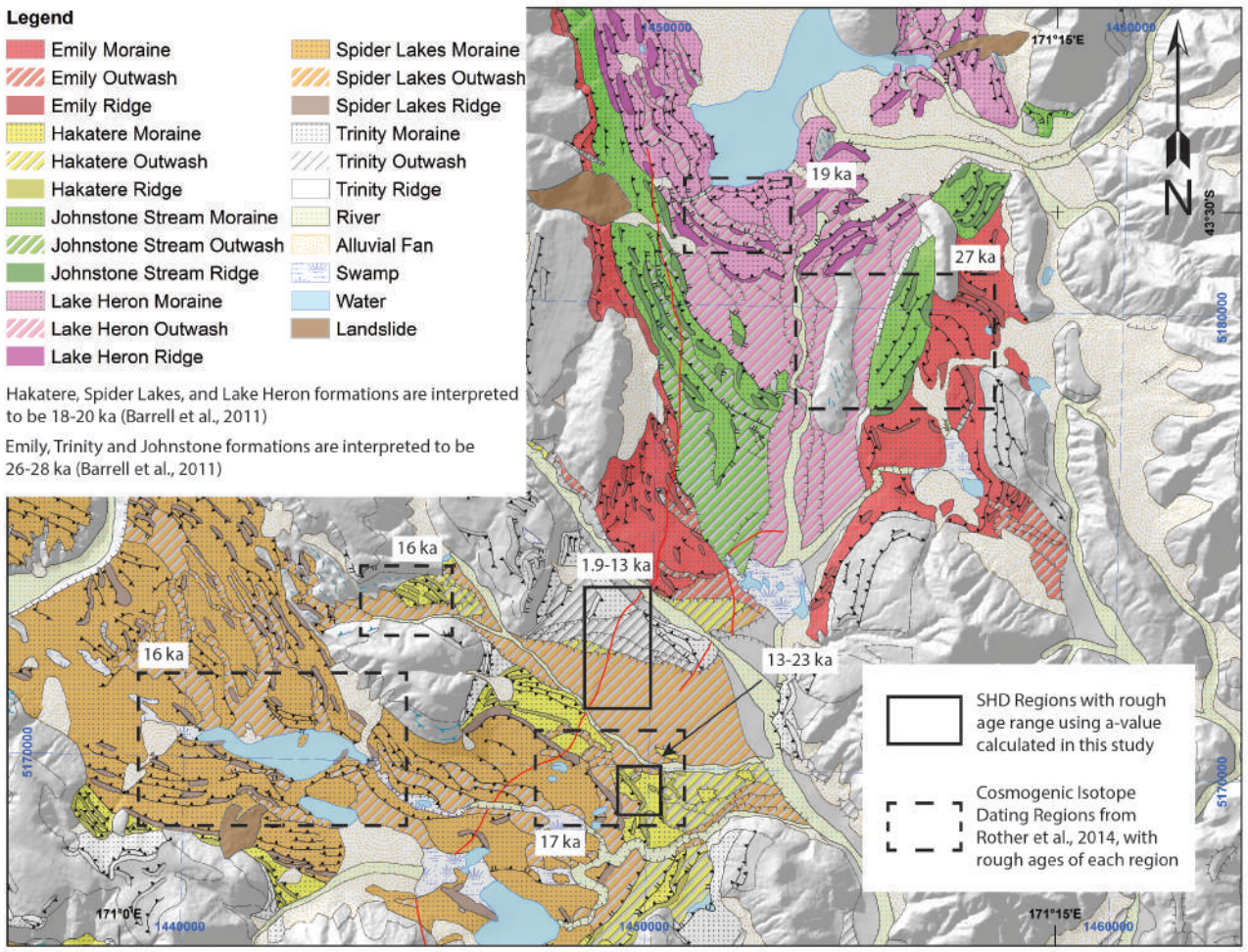

Figure 3.1: Geomorphic age map of the Lake Heron and Lake Clearwater basins. The geomorphology was further differentiated from the Barrell et al. (2011) published version in order to show all mapped glacial advances and associated deposits. The ages shown on this map include those from previous studies (e.g. Barrell et al. (2011); Rother et al. (2014)) as well as those generated in this study. For the cosmogenic ages, rough regions rather than individual locations are shown due to error of GPS coordinates. In this figure, red lines correspond to structural features, while black lines refer to risers of varying origin.

Within the Lake Heron Fault field site, there are several locations, such as the Paddle Hill Creek Fan, which do not have published absolute ages. Areas such as this are of vital importance as knowing their age has the potential to significantly constrain the timing of faulting, resulting in better slip rates and recurrence intervals. Changing metrics such as these could also go a long way to interpreting not only the basin history itself, but the greater range-front region. Therefore, being able to use alternative dating techniques such as SHD has great advantages.

Although the Schmidt hammer was originally developed for concrete testing, it is now also used as a relative-dating technique of inorganic deposits (Schmidt, 1951; Shakesby et al., 2006). SHD relies on rebound values (R-values) testing a rock's hardness, which are then used to interpret its exposure time. In theory, as a rock ages, its mechanical strength decreases, resulting in lowering R-values, which numerous studies have shown (Winkler, 2005; Shakesby et al., 2006; Stahl et al., 2013)(Figure 3.2). Once acquired, these R-values can be used in conjunction with calculated a-values to produce chronofunctions, which can then be used to generate ages for new test sites.

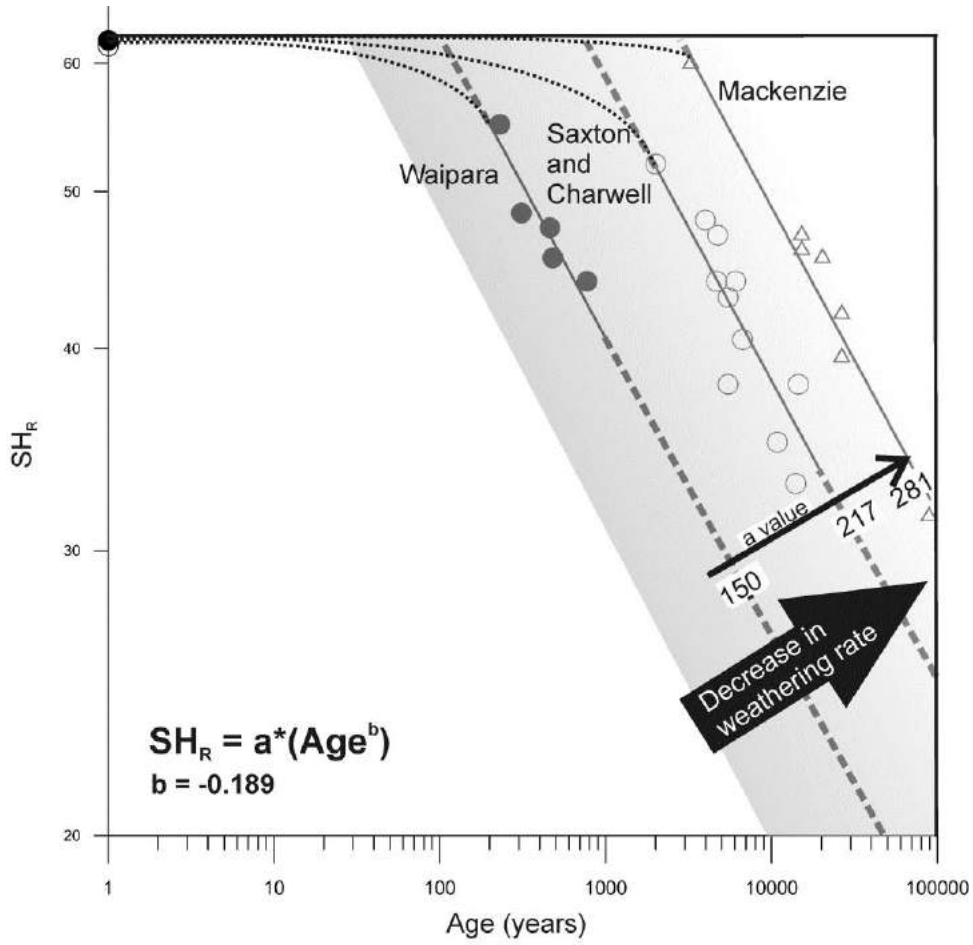

Figure 3.2: Example of Schmidt hammer R-values from Stahl (2014) showing decreasing a-values with increasing exposure time.

In this chapter, SHD is done on fluvial terraces and glacial moraines. While application on fluvial terraces is new, and was done for the first time by Stahl et al. (2013), in his study, it proved reliable, which is why it was conducted for this thesis. More commonly SHD has been successfully conducted on moraines throughout New Zealand (e.g. Winkler (2005)).

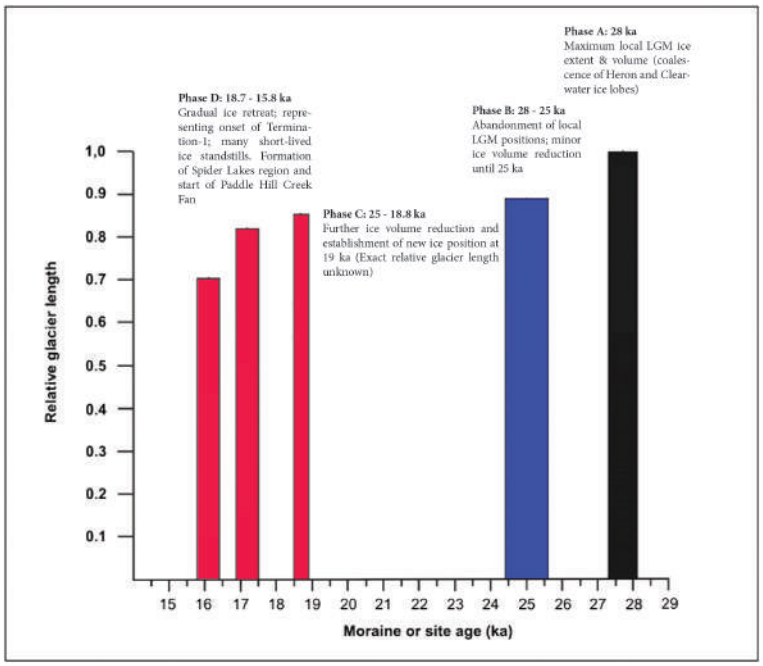

Figure 3.3: Proposed glacial fluctuations within the Rangitata Catchment. The ages associated with each period was acquired through cosmogenic isotope dating by Rother et al. (2014).

3.2.2 Methodology

In order to date fluvial terraces, two methods were used. One applies the calculated a-value (268) from Stahl (2014) to determine ages. A-values are related to the weathering rate, and are known as a scaling constant, which influences the location of the Schmidt hammer rebound (SH_R)-age line on a logarithmic scale. Undertaking this method only required the acquisition of a mean R-value from sites of unknown age. While valuable, this method had its limitations as the a-value was calculated using climate station data and weathering information from outside the Lake Heron Basin.

The other technique involved acquiring Schmidt hammer R-values from greywacke boulders at sites of known age. This was done by visiting locations where cosmogenic isotope dating had been done (Evans, 2008; Rother et al., 2014). By taking measurements here, R-values could be calibrated by generating a new a-value and regression curves. In turn, R-values from areas of unknown ages, such as terrace surfaces, could be more accurately dated.

At each SHD site, one Schmidt hammer R-value was taken for 50 individual boulders. While more measurements can be taken, this study was often limited by the number of suitable boulders exposed at the surface. Nonetheless, 50 measurements actually provides similar

results to data calculated from significantly larger sample sizes (Niedzielski et al., 2009). For these reasons, it was considered suitable.

In addition to the number of individual boulders sampled, many other factors were considered. First, all sampling was conducted in dry conditions, as wet conditions would not only damage the Schmidt hammer, but alter each rock's hardness (Sumner and Nel, 2002). During wet periods, porous rocks absorb a small portion of water, which, if tested with a Schmidt hammer would result in lower R-values, skewing the data. Therefore, dry conditions were required. Next, the Schmidt hammer was held perpendicular to the rock surface, and as vertical as possible to maintain consistency and to avoid biased R-values being effected by impact angles (Figure 3.4). Physical characteristics of the rock itself were also considered. First, rocks were not altered in any way prior to sampling, including cleaning or smoothing them. Additionally, lichen covered surfaces, mineral veins, and any structural anomalies were always avoided as these would produce unreliable values. In the process of sampling, if the rock moved, it was immediately discounted. If pieces chipped off, or the sound of the Schmidt hammer was not resonant, an additional location would be tested. If the same problems persisted the rock would not be considered. The sound the Schmidt hammer impact made was extremely important to consider as a non-resonant sound could indicate cracking beneath the rock's surface. Lastly, a rock would not be used if the exposed surface diameter was less than 15 cm. This size was not set by this sampler, but was considered a criteria in Stahl (2014), which this study is based off on. Therefore, similar care was taken to maintain consistency.

Figure 3.4: Technique used while Schmidt hammering on the Paddle Hill Creek Fan. All boulders chosen for Schmidt hammering were required to meet a certain set of criteria in order for them to be counted. (Photo Credit: Alec Wild)

3.2.3 Spider Lakes Section

Throughout the Spider Lakes Section, surface deposits are predominantly glacial, including ground moraine, moraine ridges, and outwash. The presence of these deposits allowed for SHD of the exposed boulders. This field study built upon previous geomorphic mapping by Evans (2008) and Barrell et al. (2011).

Initial work in the valley suggested that at least three stadials resulted in glacial advances, deemed Spider Lakes 1-3 (Mabin, 1980). This was based primarily on geographic positioning of glacial moraines, and other geomorphic features. However, no absolute dating was done to verify any of these findings, meaning the study's reliability was considered questionable. It was only in 2008 when reliable ages for the Spider Lakes region were obtained, by means of

cosmogenic isotope dating of large greywacke boulders (Evans, 2008). These results indicated that the Spider Lakes region of the Lake Clearwater Basin, is a maximum of 15.3 ka, with a weighted mean closer to 14.6 ka. Rother et al. (2014) reanalyzed much of this work and came out with an age closer to 17 ka. The age of sediments in this area is important for multiple reasons. First, age control allows for the timing of faulting to be constrained, as all deformation must have occurred following the deposition of the moraines. Additionally, known ages allowed for Schmidt hammer R-values to be calibrated for the entire Lake Heron Fault study area.

As there were areas of known ages (with associated error), Schmidt hammering at these locations was done, allowing for R-values to be linked with available ages. Using this calibration, Schmidt hammering could then be done at sites of unknown ages to determine how old they are. Additionally, the calculated a-value could be compared to those in other studies (e.g. Stahl (2014)), which could indicate characteristics of the Lake Heron Basin. While this technique does have significant error, even being able to slightly constrain faulting has the potential to significantly alter the interpretation of the Lake Heron Fault. This technique was also deemed reliable as nearly the entire area has been glaciated, and all rocks tested were greywacke, for which Schmidt hammers have been calibrated.

Therefore, while not much additional research was done on specific aspects of the geomorphology of the Spider Lakes section, previous work allowed for alternative dating techniques to be used. In turn, this made it possible to calibrate ages for the entire field site.

In order to Schmidt hammer locations of known age, sites chosen by Evans (2008) and Rother et al. (2014) had to be identified (Figure 3.5). While GPS latitude and longitude coordinates for all cosmogenically sampled boulders were available, they were found to be incorrectly located (in some cases, over 1 km off), and boulders had to be identified from images and evidence of sampling. Because of this, only two sites (three samples) were located and tested. Nonetheless, they provided a means of generating an a-value different to the one calculated in Stahl (2014). The following tables and equations show the difference in ages calculated by using the Stahl (2014) a-value, and one from Schmidt hammering sites of known age.

Rother et al. (2014) Site	**Cosmogenic Age**	**SH Age using a-value from Stahl (2014)**
RAN-SPL-1-1, 1-2	15.7 ± 0.9 ka, 15.3 ± 1.2 ka	12.6 (+ 2.3)(- 2.0) ka
RAN-SPL-1-3	20.1 ± 1.0 ka	15.5 (+ 2.9)(- 2.4) ka

Table 3.1: Cosmogenic ages and Schmidt hammer ages using a-value (268) calculated in Stahl (2014).

In order to calculate a SH age using the a-value from Stahl (2014), the following equation was used:

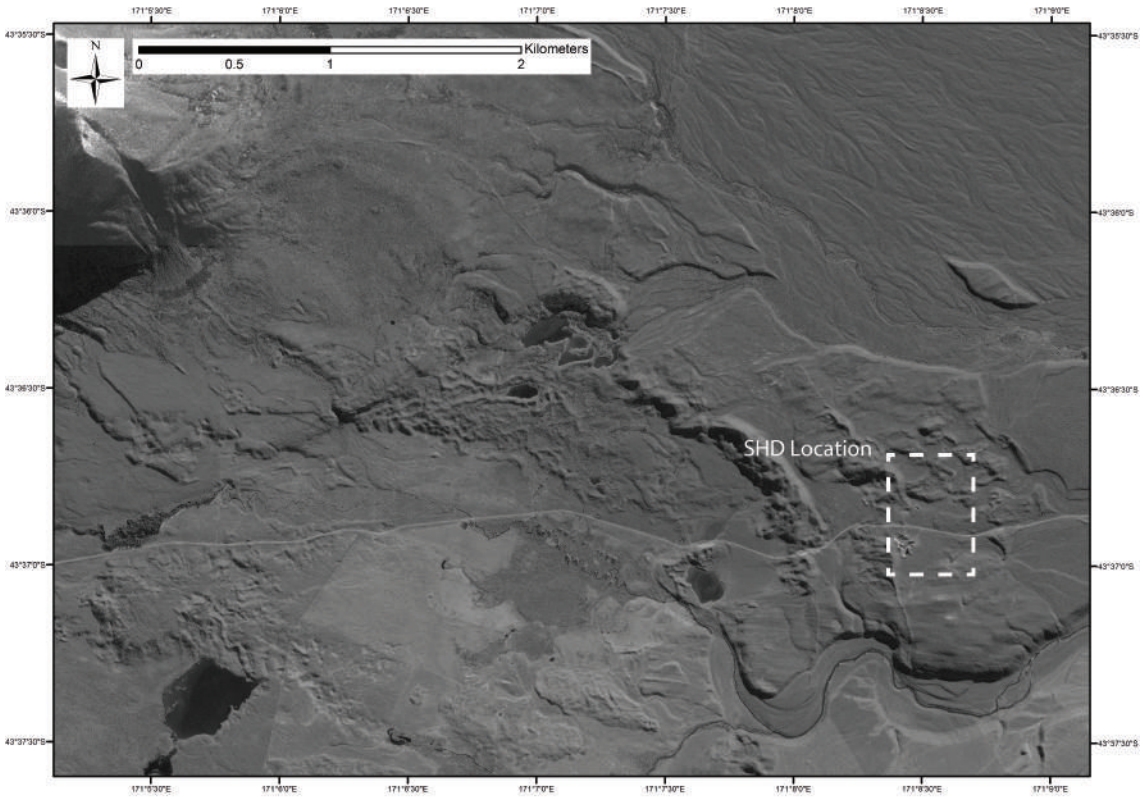

Figure 3.5: Location of Schmidt hammer exposure age dating in Spider Lakes Study Area.

$(SHR/268)^{1/b} = Age$

SHR corresponds to the mean of 50 Schmidt hammer rebound values, 268 is the a-value from Stahl (2014), and the b-value remains constant as all sites tested were Torlesse greywacke. This b-value, or -0.189, is also known as the power law slope. An example calculation can be seen below:

$(43.24/268)^{1/-0.189} = 15523.83$

As is evident from these values, the SH ages calculated using the Stahl (2014) a-value are far too young when compared to the cosmogenic age (Table 3.1). While there is error, it appears too significant. As the b-value and mean cannot be changed, an incorrect a-value is likely the source of the inconsistency. Fortunately, a new one, calibrated from the sites of known age, was calculated. A differing a-value is entirely possible as the one computed in Stahl (2014) was generated using data from outside the Lake Heron Basin. And, as the a-value is inversely related to the weathering rate, an alternative one could be expected. In order to do this, the following equation was used:

$SHR = a * (age^b)$

By using this equation, a new a-value was calculated using the Rother et al. (2014) site

with two known ages. From the rebound values acquired at this site, an a-value of 279 was generated, an increase of 11 from the value in Stahl (2014). From this new a-value, ages could be calculated (Table 3.2).

Rother et al. (2014) Site	**Cosmogenic Age**	**SH Age using new a-value (279)**
RAN-SPL-1-1, 1-2	15.7 ± 0.9 ka, 15.3 ± 1.2 ka	15.7 (+ 2.8)(- 2.6) ka
RAN-SPL-1-3	20.1 ± 1.0 ka	19.2 ka (+ 3.6)(- 2.9) ka

Table 3.2: New SH ages for Spider Lakes moraines based on areas of known ages.

Based on the ages in Table 3.2, the a-value of 279 value seems robust, as the 19.2 ka age falls within the error of the cosmogenic age. This a-value suggests that rocks within the Lake Heron Basin weather slower than Stahl (2014) believed. However, all ages must be used with caution due to the error associated with them, and the reliability of using one or two ages to define the age of an entire geomorphic structure or region. Nonetheless, because all boulders from which Schmidt hammer R-values were collected from the same feature and were in close proximity to the cosmogenically-sampled boulders, it can at least be assumed that the ages are reliable.

3.2.4 Paddle Hill Creek Section

There are varying interpretations of the geomorphology of the Paddle Hill Creek Fan, including both what is at the surface, and the age of the deposits. In Barrell et al. (2011) the Paddle Hill Creek Fan is considered a combination of outwash and ground moraine, with the lowest surface having an age of 17-18 ka. This is assumed because "Paddle Hill Creek has been woefully underfit ever since it ceased to receive any Rangitata meltwater" (D. Barrell, Personal Communication, 2015). Therefore, it becomes coeval with his Spider Lakes formation, which is 17-18 ka. The high terraces on the other hand are interpreted to be 26-28 ka, as Barrell believes they are part of a moraine belt found throughout New Zealand.

In contrast, this author, and Stahl (2014) deem the entire fan outwash, as there are no features which are distinctly identifiable as moraine. Additionally, both break the Paddle Hill Creek Fan into eight different surfaces (including the modern fan), of varying age (Figure 3.6).

Prior to 2014, almost no dating had been done on the Paddle Hill Creek Fan. Cosmogenic isotope dating by Evans (2008) was done near the source of Paddle Hill Creek, yielding a maximum age of 16.5 ka, which was further analyzed by Rother et al. (2014), who obtained an age of 15.8 ka. Regardless of this slight alteration, on the basis of these results, it can be assumed that the lowest fan surface is younger than these deposits.

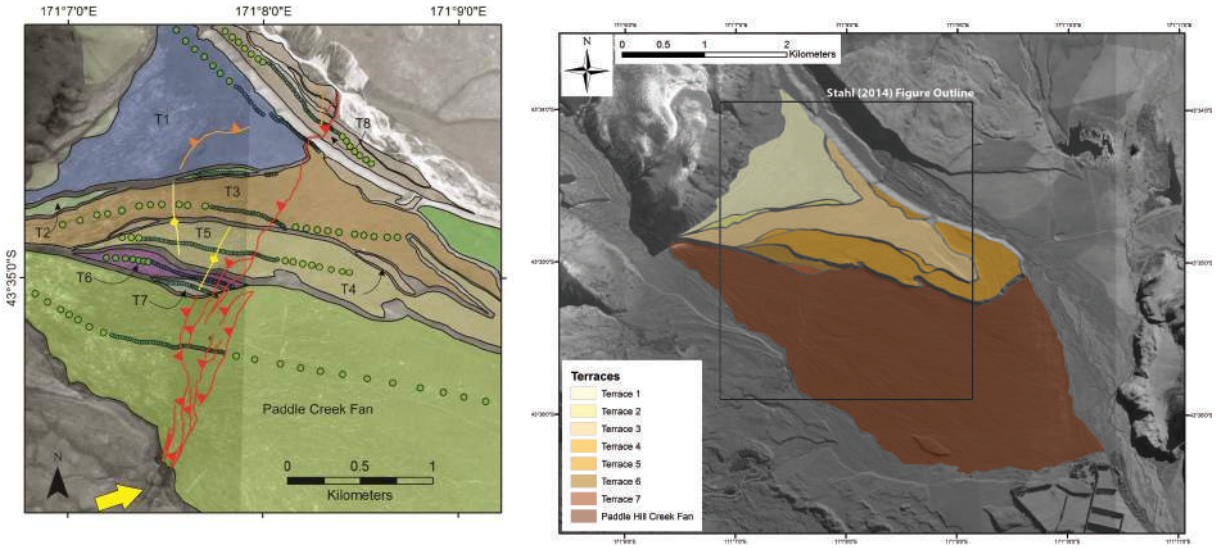

Figure 3.6: Terrace and fault map from Stahl (2014) (left) and terrace map compiled in this study.

While this limited dating is valuable, both this author and Stahl (2014) used SHD on the Paddle Hill Creek Fan to constrain the timing of faulting. While Stahl's analysis was preliminary, it did allow for results to be compared, and in some places expanded on. The difficultly of this technique is that at least 50 boulders meeting the criteria designated in 3.2.2 had to be found. On several terraces, this was not possible, although in total (combining both this study and Stahl (2014)) eight surfaces were dated, each of which helps constrain the window into which faulting must have occurred.

In order to show variation in the possible age of Paddle Hill Creek Fan terraces, the methods in 3.2.3 were used, involving both the 268 a-value from Stahl (2014), as well as the 279 value generated in this study (Figure 3.7). The following tables show the variation in age calibration using both techniques.

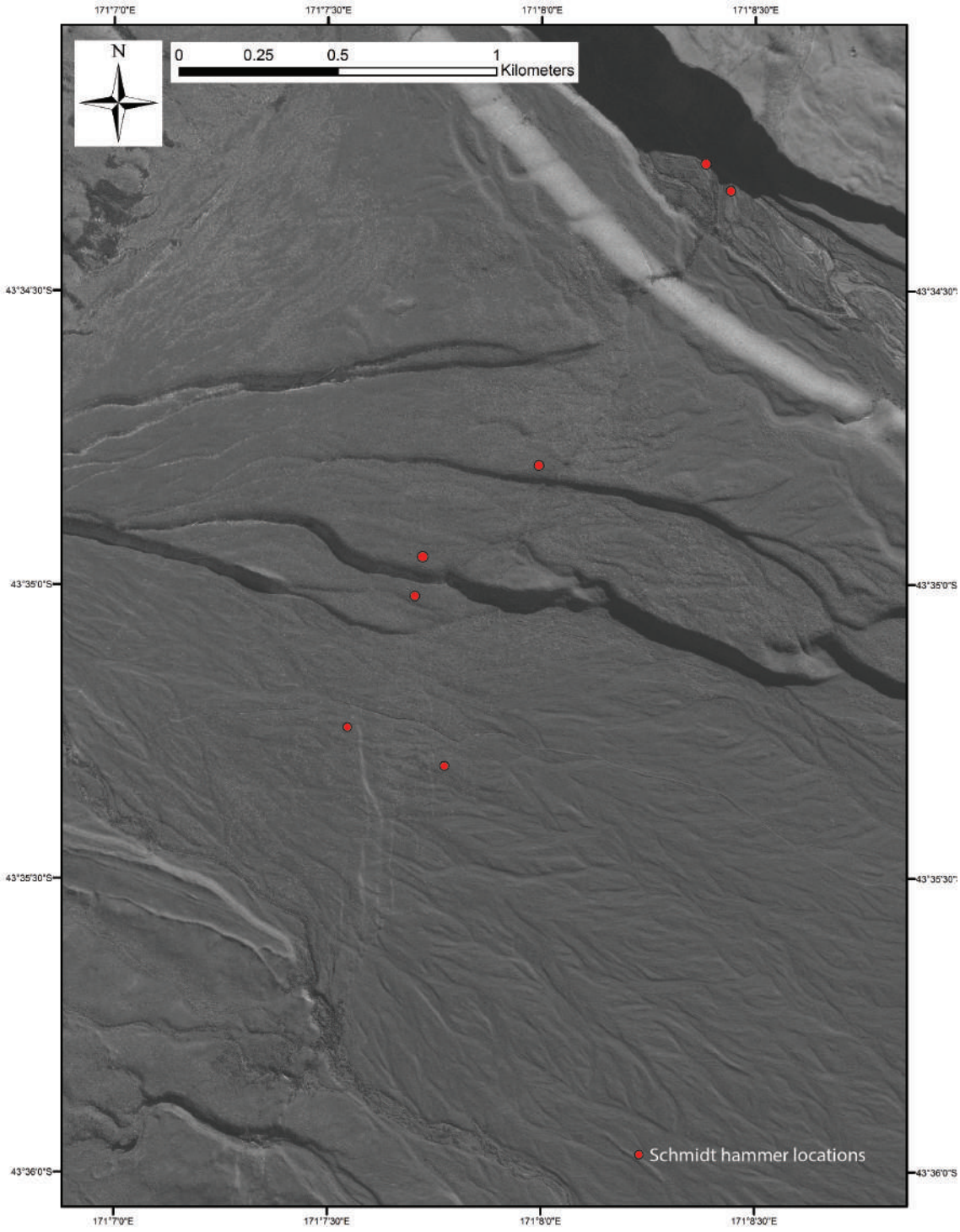

Figure 3.7: Location of Schmidt hammer exposure age dating on the Paddle Hill Creek Fan.

Study	Terrace Surface	SH Age (a-value = 268)
Stahl (2014)	T1	20.5 ± 6 ka
	T3	12.8 ± 5 ka
	T5	9.9 ± 4.5 ka
This Study	T3	13.3 (+ 4.6)(- 3.2) ka
	T5	11.4 (+ 4.6)(- 3.1) ka
	T6	11.0 (+ 3.2)(- 2.3) ka
	Paddle Hill Creek Fan (Upthrown)	8.9 (+ 1.7)(- 1.4) ka
	Paddle Hill Creek Fan (Downthrown)	7.0 (+ 1.4)(- 1.1) ka
	Modern Terrace at Ashburton River (Upthrown)	2.8 (+ 0.48)(- 0.27) ka
	Modern Terrace at Ashburton River (Downthrown)	1.6 (+ 0.09)(- 0.15) ka

Table 3.3: Calibrated Schmidt hammer ages for the Paddle Hill Creek Fan using an a-value of 268.

Study	Terrace Surface	SH Age (a-value = 279)
Stahl (2014)	T1	25.3 ka
	T3	15.8 ka
	T5	12.2 ka
This Study	T3	16.5 (+ 5.6)(- 4.1) ka
	T5	14.1 (+ 5.3)(- 3.9) ka
	T6	13.7 (+ 3.9)(- 3.0) ka
	Paddle Hill Creek Fan (Upthrown)	11.0 (+ 2.1)(- 1.7) ka
	Paddle Hill Creek Fan (Downthrown)	8.7 (+ 1.7)(- 1.5) ka
	Modern Terrace at Ashburton River (Upthrown)	3.6 (+ 0.45)(- 0.47) ka
	Modern Terrace at Ashburton River (Downthrown)	1.9 (+ 0.19)(- .10) ka

Note: Error for Stahl (2014) not calculated as not all raw data was available.

Table 3.4: Calibrated Schmidt hammer ages for the Paddle Hill Creek Fan using an a-value of 279

In order to calculate these ages, the same calculation in 2.3.3 was used (See below). Once completed, error could be determined using the standard error of each set of 50 Schmidt hammer R-values. While the error in some places is significant, at the very least terrace ages are constrained.

Example calculation:

$(SHR/268)^{1/b} = Age$

$(50.26/268)^{1/-0.189} = 7004.32$

This calculation was done for all surfaces on the Paddle Hill Creek Fan, indicating that as a whole, it has vastly differently-aged terraces. However, as was explained in 2.3.4, they all

have the same amount of vertical deformation. This means all deformation occurred after the abandonment of the lowest terrace of the fan, approximately 7.0-11 ka (dependent on which a-value is used) and that there was no vertical deformation between the abandonment of the oldest surface (20-25 ka) and 7-11 ka.

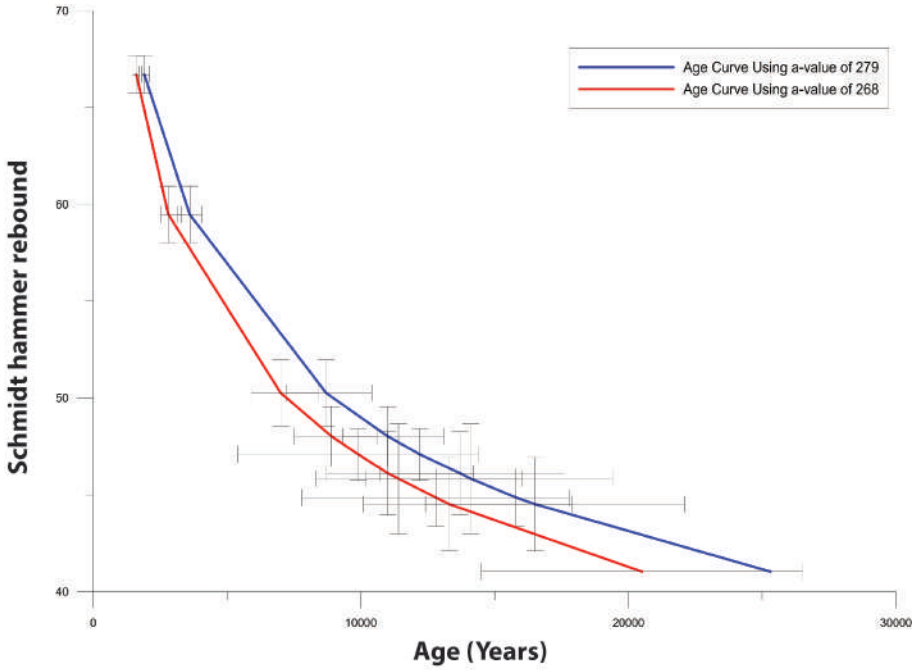

Figure 3.8: SH_R-age curves for the Lake Heron Study Site using the a-value found in Stahl (2014), and the a-value calculated in this study.

What can be seen from the tables and graphs, is that when the new a-value calculated from the Spider Lakes section is applied to the Paddle Hill Creek Fan, ages get older (Figure 3.8). As would be expected, a more dramatic change is seen on the older terraces. Nevertheless, calculating additional ages that are only slightly different only helps decipher the earthquake history of the Lake Heron Fault.

3.2.5 Castle Ridge Section

While significant work was done on the geomorphology in the other two sections, very little could be done in the Castle Ridge Section, due to factors such as limited surface exposure of rocks and the fact that cultivation has reworked the surface. Therefore, this study relied heavily on previous work in an attempt to understand how how faulting has effected the section.

Prior to this study, the majority of work involving the Castle Ridge Section focused on the geomorphology (Pugh, 2008; Barrell et al., 2011; Rother et al., 2014). However, within the

area in question, work was limited to mapping of surface deposits. Further north however, cosmogenic isotope dating was done, illustrating a complex glacial history. These studies suggested that the area experienced at least two major advances approximately 27 ka and 19 ka, with the younger deposits located further north, closer to the glacial source (Rother et al., 2014). This indicates that the most recent advance was not as extensive as earlier ones, for had it been, older deposits would have been destroyed.

While it would have been beneficial to date every surface within the Castle Ridge Section using SHD, this was not possible. The most prominent feature, the glacial moraine, did not have many boulders exposed at the surface, and those that were, either did not meet the specifications required, or had clearly been brought in by landowners for stabilization. Because of this, the landform and landscape could not be dated.

As no alternative dating techniques could be used, similar methods to those used in Barrell et al. (2011) (i.e. surface correlation) had to be implemented. To do this, surface features and associated elevations were compared. For example, at the southernmost portion of this area, just north of the Ashburton River, the elevation is approximately 740 m, similar to the highest terrace of the Paddle Hill Creek Fan. While the surface deposits appear slightly different, based on their proximity to one another, and similar elevations, the two sites are believed to be of similar age. If true, this would give the southernmost portion of the Castle Ridge Section an age of 20.5-25.3 ka (depending on which Schmidt hammer a-value is used, and error not included).

3.2.6 Discussion

By using this methodology, two important points must be further examined. The first of these, is that the Schmidt hammer a-value calculated by testing a site of known age is higher than the one calculated by Stahl (2014). This has significant implications as it can greatly effect the age of surfaces throughout the basin. As was explained in 3.2.3, Stahl (2014) calculated a Schmidt hammer a-value of 268 based on data from outside the basin and his chemical weathering empirical relationship (Stahl et al., 2013). However, even he notes that the relationship between a-value and chemical weathering rate contains many more variables than he uses. For example, site specific variations in rock geochemistry or climate can greatly effect resulting a-values. Because of these issues, calculating an a-value from sites with absolute ages was crucial. Based on the new a-value (279), it is apparent that rocks in the Lake Heron Basin appear to weather slower than Stahl believed. This could be due to factors such as seasonal rainfall and/or rock geochemistry. Additionally, this value corresponds to those computed by Stahl (2014) for the Mackenzie Basin. This seems entirely

plausible as both basins are intermontane, and display similar geomorphology (Amos and Burbank, 2007; Amos et al., 2007, 2010, 2011). Because of these factors, and those explained earlier, it is deemed suitable to believe that the new a-value calculated within this study generates more reliable ages for the Lake Heron Basin

Additionally, a crucial discovery came when SH ages were calculated for the Paddle Hill Creek Fan. Prior to this study, the most widely accepted ages were those in Barrell et al. (2011), suggesting the fan is 17-28 ka. However, Barrell agrees that these ages are more based on inference rather than absolute dating methods (Barrell, Personal Communication, 2015). Due to the fan's importance to the Lake Heron Fault's history, more reliable ages were needed. From Schmidt hammering the lowest surface, ages between 5.9-13 ka were calculated (Depending on which Schmidt hammer a-value is used). While there can be significant age error associated with Schmidt hammering (In some cases exceeding 5 ka), the ramifications of these ages are significant. These ages mean that all deformation would have had to have occurred within the last 13 ka, as the same amount of vertical deformation is seen on all surfaces. It also would mean that there was no deformation following the abandonment of the oldest surface (20-25 ka) and 5.9-13 ka. This observation has important ramifications for possible temporal variations in the slip rate of the Lake Heron Fault.

3.2.6.1 Slip Rate implications

Over a timescale of approximately 10 ka, there is good evidence to indicate that there has been significant activity on the Lake Heron Fault. This becomes apparent, as total vertical deformation remains consistent over surfaces of vastly different ages. This occurs despite the fact that the way in which the deformation is accommodated differs greatly (Figure 2.23 & 2.25).

While the exact reason for this phenomenon may not be known, it does lead to a discussion on the implications these findings have on the fault's slip rate. For example, Barrell et al. (2011), propose that the lowest terrace on the Paddle Hill Creek Fan is 17-18 ka, with approximately 20 m of vertical displacement, resulting in a vertical slip rate of 1.1 mm/yr. However, findings in this study reveal that the same surface could be 9.45 ± 3.55 ka, based on Schmidt hammer exposure age dating. Such an amendment would significantly revise the suggested slip rate.

From the data acquired during the course of this research, all evidence points towards increased activity following the abandonment of the lowest surface on the Paddle Hill Creek Fan. Despite there being surfaces of vastly different age (maximum 15 ka age difference), all display the same amount of vertical deformation (19.3 ± 3 m). The only way for this to

occur would be for there to have been a period of quiescence, followed by a period of increased seismicity. The ramifications of this on potential slip rates is significant as current estimates are based on ages not acquired through absolute dating. Instead, ages were done primarily through surface correlation (Barrell et al., 2011). For that reason, the estimated vertical slip rate of 1.1 mm/yr is considered a starting point (Barrell and Strong, 2009). Through the use of Monte Carlo simulations different slip rates were calculated using the methodology in (Thompson, 2002) coupled with the deformation and ages calculated in Chapter 2. In order to demonstrate the potential range in slip rates, four calculations were done from the four Schmidt hammer ages of the lowest surface on the Paddle Hill Creek Fan.

In order to complete these Monte Carlo simulations, total vertical deformation and age, with their associated distributions had to be input into the software program @Risk. For each simulation, the same vertical deformation (19 $\pm$ 3 m), with a normal distribution was used. This error was included in the 95% confidence window. Therefore, the only variation in the simulations was the age, with associated error. Because the positive and negative error for Schmidt hammer ages is not identical, a log-normal distribution was chosen, from which, deformation was divided by age to compute the vertical slip rate.

The first vertical slip rates calculated were those generated using the Stahl (2014) Schmidt hammer a-value (268). Because these potentially overestimate how quickly rocks weather, the slip rates tend to be on the higher side (Figure 3.9). From the normal distribution output, it becomes clear that depending on which age is used, the vertical slip rate varies greatly. If both ends of the spectrum of the 95% confidence range are taken, the vertical slip rate potentially doubles (1.7 - 3.4 mm/yr), though the modes are similar (2.7 and 2.3 mm/yr).

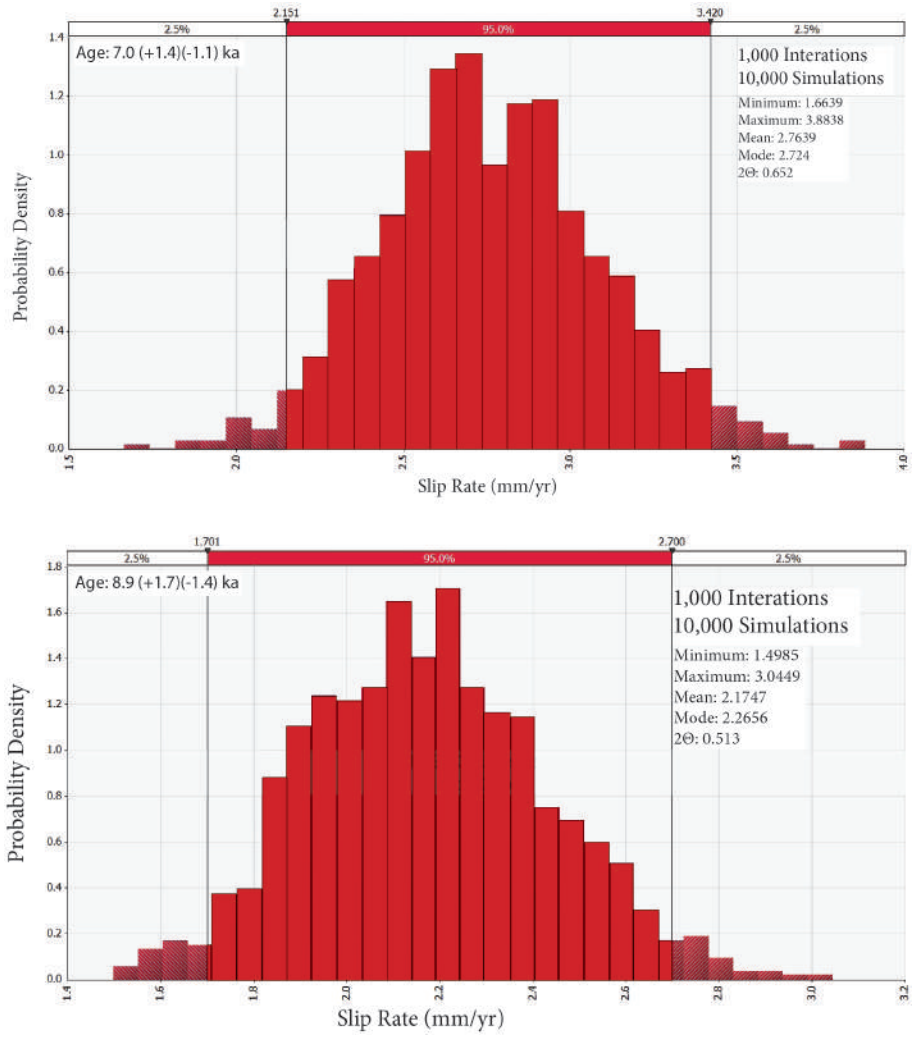

Figure 3.9: Monte Carlo simulations for slip rates using the Stahl (2014) Schmidt hammer a-value (268).

In addition to slip rates calculated using the Stahl (2014) Schmidt hammer a-value, rates were also computed using the a-value calculated in this study (279) (Figure 3.10). Because this a-value was calculated by Schmidt hammering boulders of known age, they are given a greater weight than those using the Stahl (2014) value. From these simulations, the 95% confidence range puts the estimated slip rate between 1.2-3.3 mm/yr, with modes of 1.8 and 2.2 mm/yr. What this shows is that even the lowest slip rate within the 95% confidence of this study is greater than the estimate by Barrell and Strong (2009), suggesting the Lake Heron Fault has been more active than previous studies indicate. While these slip rates are valuable, they fail to show that prior to the age used for each simulation, slip is assumed to be minimal based on comparable vertical deformation across differently-aged surface. This is because the ages used for each simulation were from the lowest surface of the Paddle Hill Creek Fan, which displays the maximum vertical deformation seen on any surface.

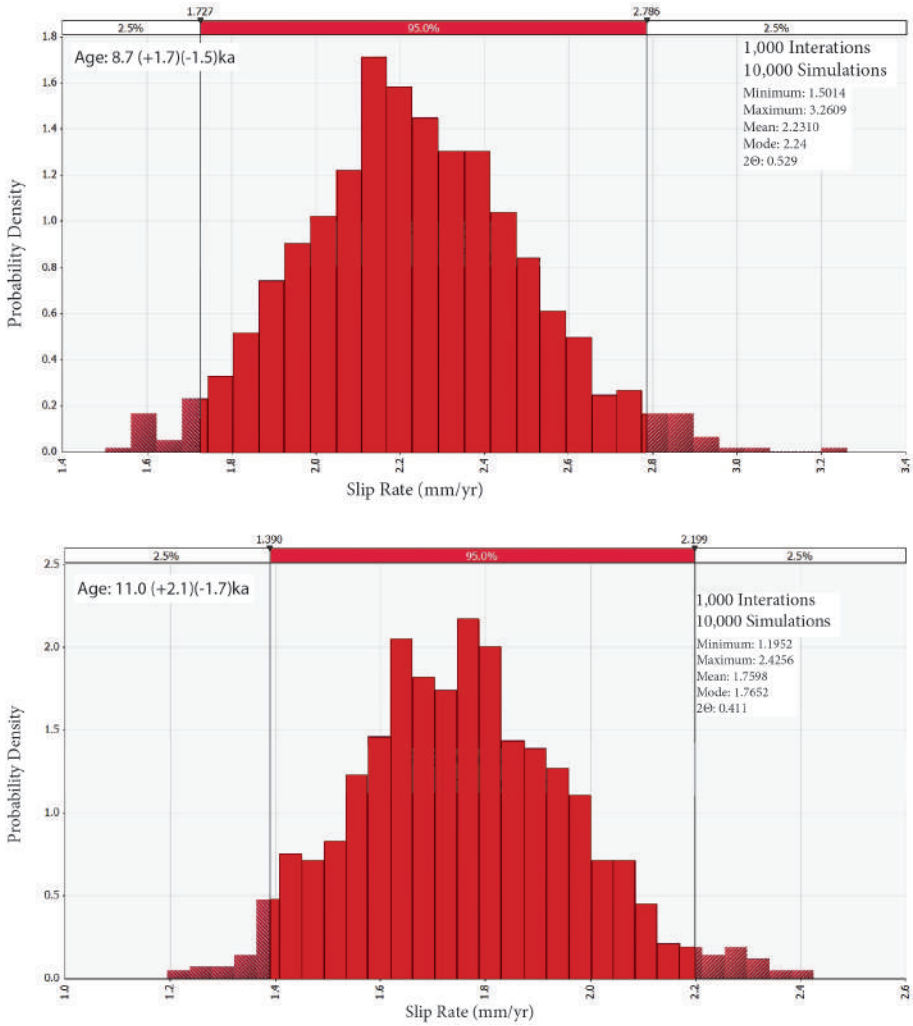

Figure 3.10: Monte Carlo simulations for slip rates using the a-value calculated in this study (279).

3.3 Paleoseismic Trenching of the Lake Heron Fault

3.3.1 Introduction

Prior to this study, no paleoseismic analysis had been done on the Lake Heron Fault. While there are published recurrence intervals and earthquake magnitudes, these are based on weathering rind data, scaling relationships, similarities with other faults, fault mapping, arbitrary assumptions, and approximate ages (Oliver et al., 1990; Pettinga et al., 1998, 2001; Barrell and Strong, 2009). For example, in Pettinga et al. (1998), weathering rind data and geomorphic expressions were used to estimate the last earthquake occurred 2.7 ka. Additionally, they note that along the fault, an 8 m high fault scarp could have formed in a single event, requiring an earthquake magnitude of 7.7-7.8, using scaling relationships. The author then used a characteristic earthquake model to assume that over the course of 30 ka (the estimated age of the alluvial terraces), three ruptures occurred, yielding a recurrence interval of 10 ka. However, because the Lake Heron Fault was at the time, believed to be 18-40 km in length, and due to large uncertainties associated with the data used, a more conservative estimate of Mw 7.4 ± 0.3 was given.

More recent research by Barrell and Strong (2009) significantly modified both the recurrence interval and single event displacement of the Lake Heron Fault. This study estimated a recurrence interval of 1,800 $\pm$ 1,206. The 1.8 ka value was calculated by estimating an age of 18 ka for the deformed landscape, and assuming 2 m of vertical deformation per event. Error was then calculated by taking 67% of the recurrence interval. While Barrell and Strong (2009) indicated that the best way to conduct this type of study is through individual site investigation, scaling relationships from Wells and Coppersmith (1994) were used to estimate the single event displacement. However, because the exact length of the Lake Heron Fault remains unknown, this method produces similar error. Using these relationships, 1.0-1.5 m of displacement per event would be expected. Nonetheless, Barrell and Strong (2009) chose a greater single event displacement for the purpose of defining a recurrence interval classification.

From the error and methodologies used in these studies, a more comprehensive approach was taken for the Lake Heron Fault to better constrain its recurrence interval, potential earthquake magnitude, and single event displacement. In order to do this, trenching was undertaken. Once this was done, results were used in conjunction with deformation, geomorphic, and structural data to better understand the paleoseismology of the Lake Heron Fault.

3.3.2 Trenching

During the initial phase of research, it was proposed to complete three paleoseismic trenches (Figure 3.11). Each location was chosen systematically based on factors such as the likelihood of finding datable material, and where other successful studies trenched across reverse faults (e.g. McCalpin, 2009). All locations were on the Paddle Hill Creek Fan, as it is immaculately-preserved, and displays excellent tectonic geomorphology, such as the crestal graben described in Chapter 2. Because of features like this, in addition to colluvial wedges and large fault scarps, potential variety in the type of preserved material could be found.

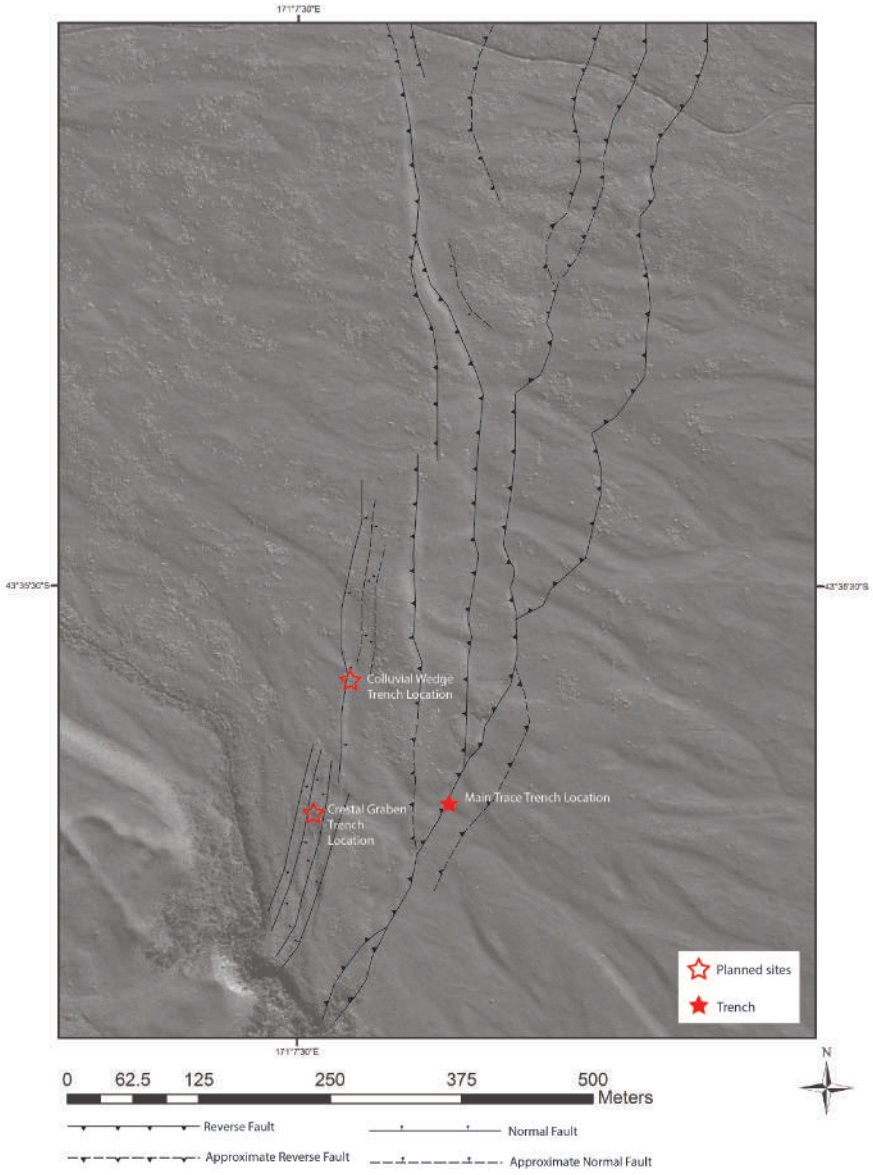

Figure 3.11: Initial locations of paleoseismic trenches.

However, in the steps leading up to trenching, permission was not given by the Department of Conservation to trench on the Paddle Hill Creek Fan, as they deemed the land would be damaged beyond repair. DOC was interested in the research however, and gave clearance to hand dig trenches, meaning the scope of the project was changed to put in two small trenches. This meant that trench locations had to be systematically chosen, taking into account what could be found, and the practicality of digging through fan material.

3.3.3 Trench Site Location

Following discussion, sites on the main trace, and colluvial wedge were chosen (Figure 3.12). The main trace was chosen in an attempt to determine a single event displacement, and the age of the most recent event. Because the fault scarp is abrupt (5-6 m high) and extremely well-preserved, it was believed that datable material such as organic matter or silt lenses could provide the timing of the last rupture. Additionally, because of the clear offset, the hope was that it would be possible to correlate units in the hanging wall and footwall to calculate a single event displacement. Vegetation at the proposed location was sparse, with only short grasses and occasional matagouri and tussock. Additionally, this site lies in an old paleochannel. While the channel is small, the location was chosen as it increased the likelihood of finding silt lenses datable using optically stimulated luminescence. Furthermore, as water once ran here, it would likely ensure the residence time of detrital charcoal would be low, yielding more accurate ages. Lastly, approximately $\frac{2}{3}$ of the way up the fault scarp, large greywacke boulders become more prevalent. These boulders were not in situ, and could easily be rolled down the scarp.

The colluvial wedge location was chosen to obtain datable material, and to identify at least a single "earthquake horizon." Because the colluvial wedge likely collapsed during an earthquake, it would have covered organic matter at the surface, preserving the timing of that event in the form of charcoal, or organic carbon. The possibility also existed of finding several "earthquake horizons," in which case, multiple events would be able to be constrained.

At each site, a small (4 m long, 2 m wide, and 1.5-2 m deep) slot was planned, both in an attempt to maximize the potential of finding useful material, while also understanding the limitations of hand-dug trenches. Prior to starting, augers were put in to determine the thickness of soil cover, gauge the possibility of finding organic matter, and to potentially see if an offset layer could be found. For each auger, soil characteristics were recorded at 15 cm intervals to note variation, with the possibility of unit correlation in the hanging wall and footwall. Because the locations were on an abandoned fan, it seemed likely a gravel unit would be encountered. Due to the likely ease of identifying this unit, it was hoped that its

location would be determined by augering. Lastly, using auger data in the planning stages gave a rough indication of both the type of material which would be encountered, and how deep each trench needed to be.

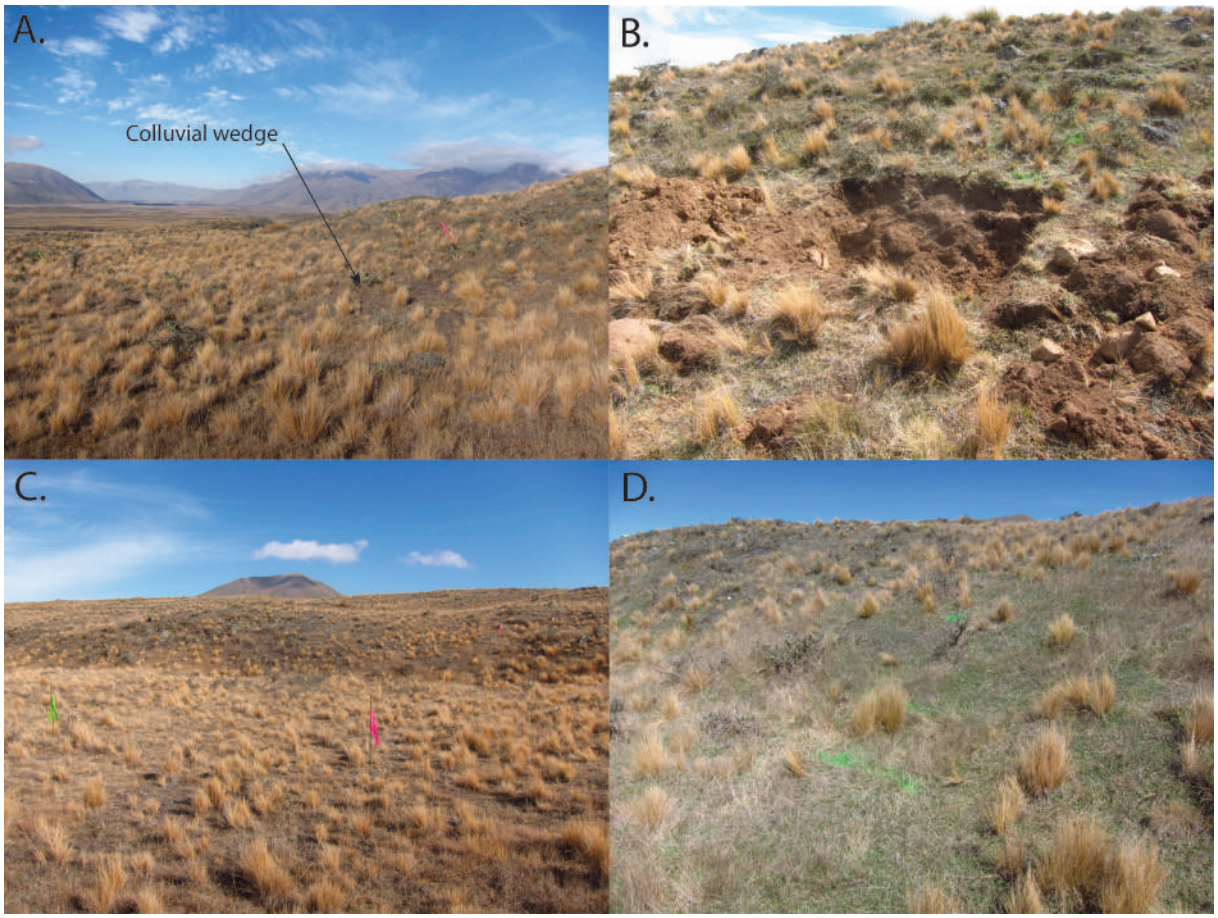

Figure 3.12: Initial two trench locations. The photos show the location of the colluvial wedge trench (A), the colluvial wedge trench after partial excavation (B), the location of the main trace trench (C), and the outline of the trench in green spray paint (D).

3.3.4 Trench Excavation and Logging

Preliminary augering of the colluvial wedge, suggested there was a homogenous soil cover 20-40 cm thick, as rocks were struck at this depth. This cover was dark brown to black in color, predominantly silt, and contained some greywacke pebbles. Even though a slot at this location was planned, it was cancelled and filled in almost immediately as at 20 cm depth, large boulders were encountered.

At the location along the main trace, augering indicated that the soil cover was 1.1-1.2 m thick on both the hanging wall and footwall. Just as was the case at the colluvial wedge, the soil was dark brown to black in color, silty, and showed little to no variability with increasing

depth. The initial trench outline spanned both the footwall and hanging wall so that layer correlation would be possible.

In order to excavate the trench, and to comply with DOC regulations, the soil cover was first removed in blocks and set aside. After this, all additional material was kept separate, to be filled in later. This trench was oriented perpendicular to the scarp, as no strike-slip motion was apparent, determined by examining piercing points of an offset gravel bar adjacent to the site, and to comply with methodology described in McCalpin (2009).

Following completion, the trench was 4 m long, 1.5 m wide, and 2 m deep at its deepest point, though it averaged 50-60 cm depth. While a deeper trench would have been preferred, it would have required making the trench significantly wider, which was not feasible. Additionally, the deeper the trench got, the more compacted the soil became, meaning excavation took longer.

Once excavation was complete, the walls were cleaned to remove both shovel and scraper marks (Figure 3.13), and an initial set of photographs were taken in order to document possible changes through time, and in case the trench collapsed. In these photos, very little was visible, and almost no unit boundaries were distinguishable (Figure 3.14). However, as the trench walls dried, features became visible, and interpretations could be made.

On the day of logging, the trench was further cleaned, and gridded into 1 m^2 squares so that it could be logged at a 1:10 scale. Initial observations noted several subvertical linear features, containing small root fragments (Figure 3.15). These features extended from the trench floor to approximately 15-30 cm below the surface. Because no offset was visible on either side of the features, they could not be confirmed as structural. Therefore, while they were noted in the original log, additional assistance was required.

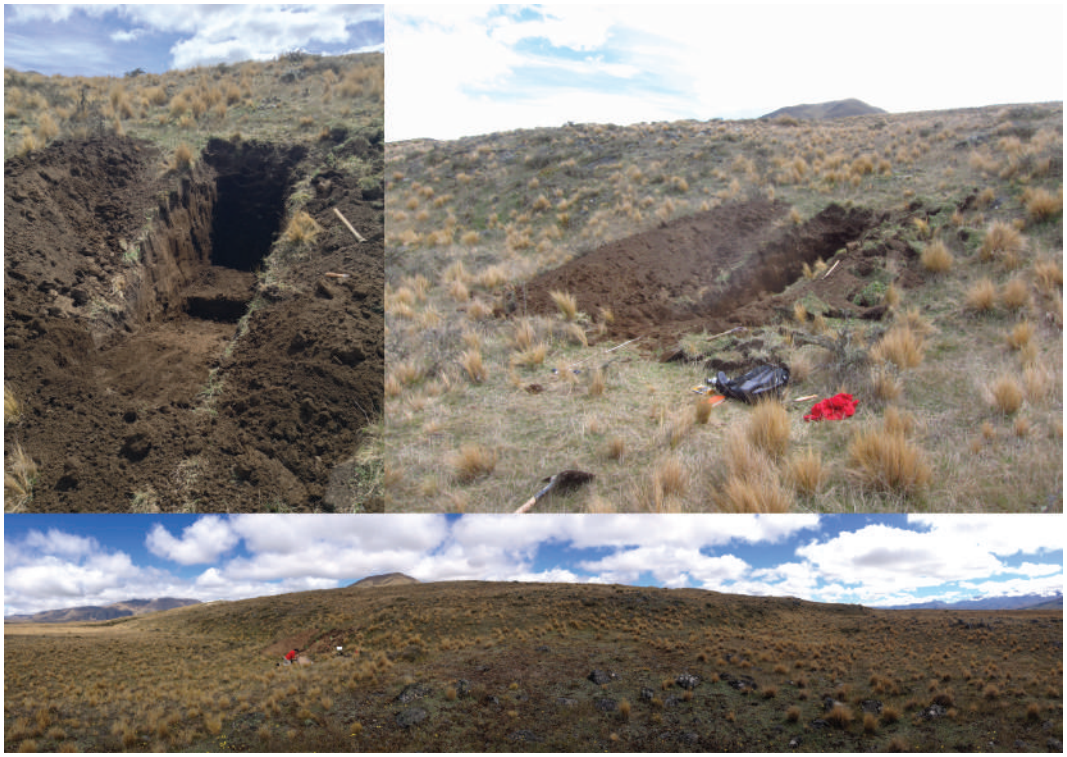

Figure 3.13: Completed trench photos.

Figure 3.14: Initial trench wall photos.

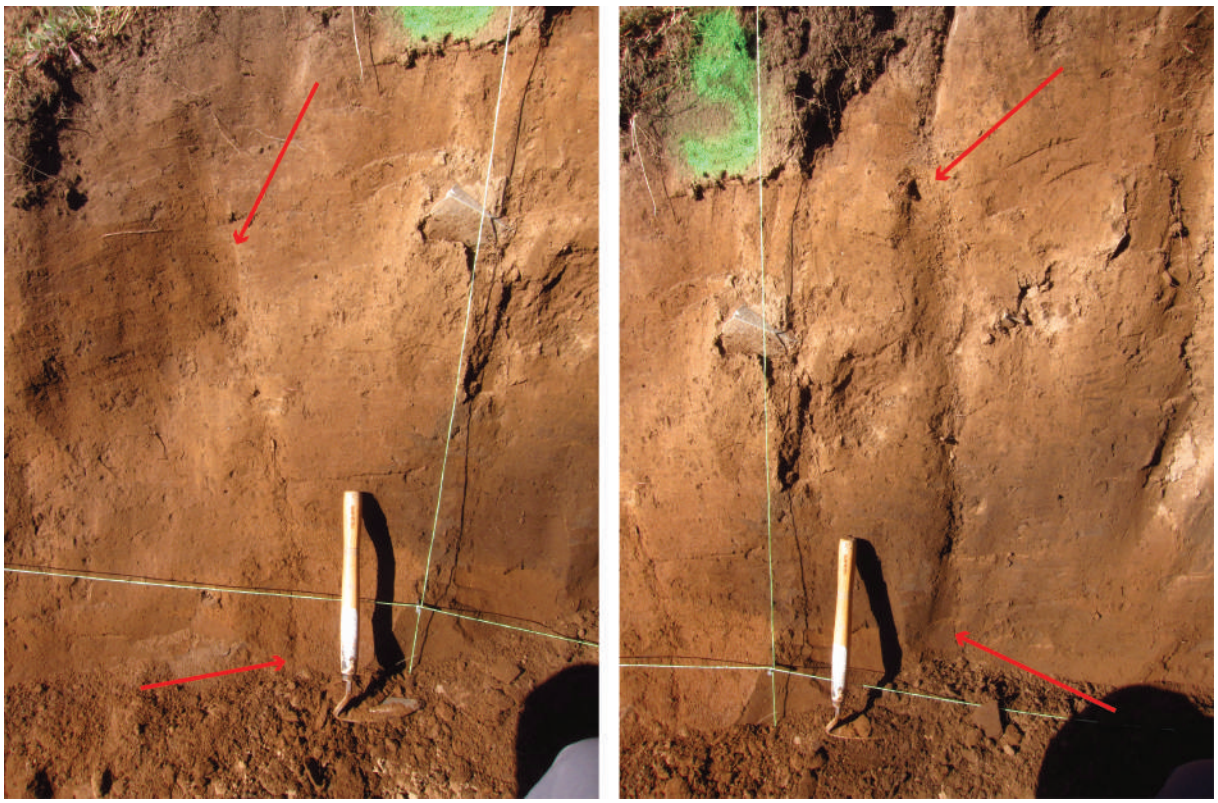

Figure 3.15: Trench photos showing initial evidence of fractures. The red arrows show the location of these fractures.

Upon returning to the trench with supervisor, Mark Quigley, clear unit boundaries were immediately visible (Figure 3.16). By following these boundaries, the subvertical features noted the day of logging showed clear offset, in some cases exceeding 15 cm, and were deemed to be tectonic in origin (Figure 3.16).

While offset was seen, because no gravel units were found, the original fan surface was not discovered. Therefore, while subsidiary fractures were visible, discrete fault plane rupture was not. Nonetheless, evidence of earthquakes was discovered and was documented. Because of the influx of new information, a new, more detailed photolog and trench log were created at the same scale (1:10) in order to accurately show the trench wall.

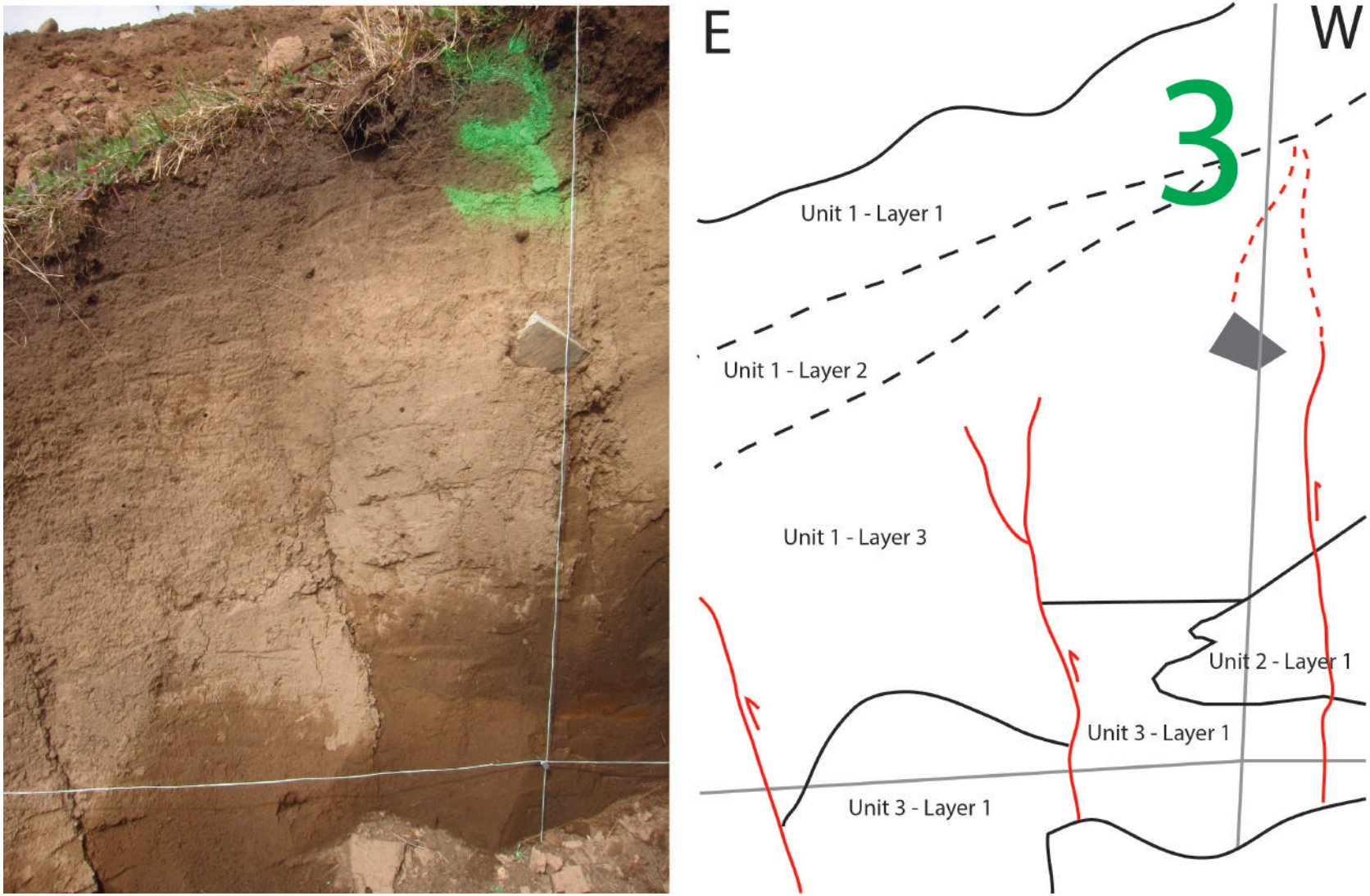

Figure 3.16: Trench photo showing clear evidence of faulting and offset.

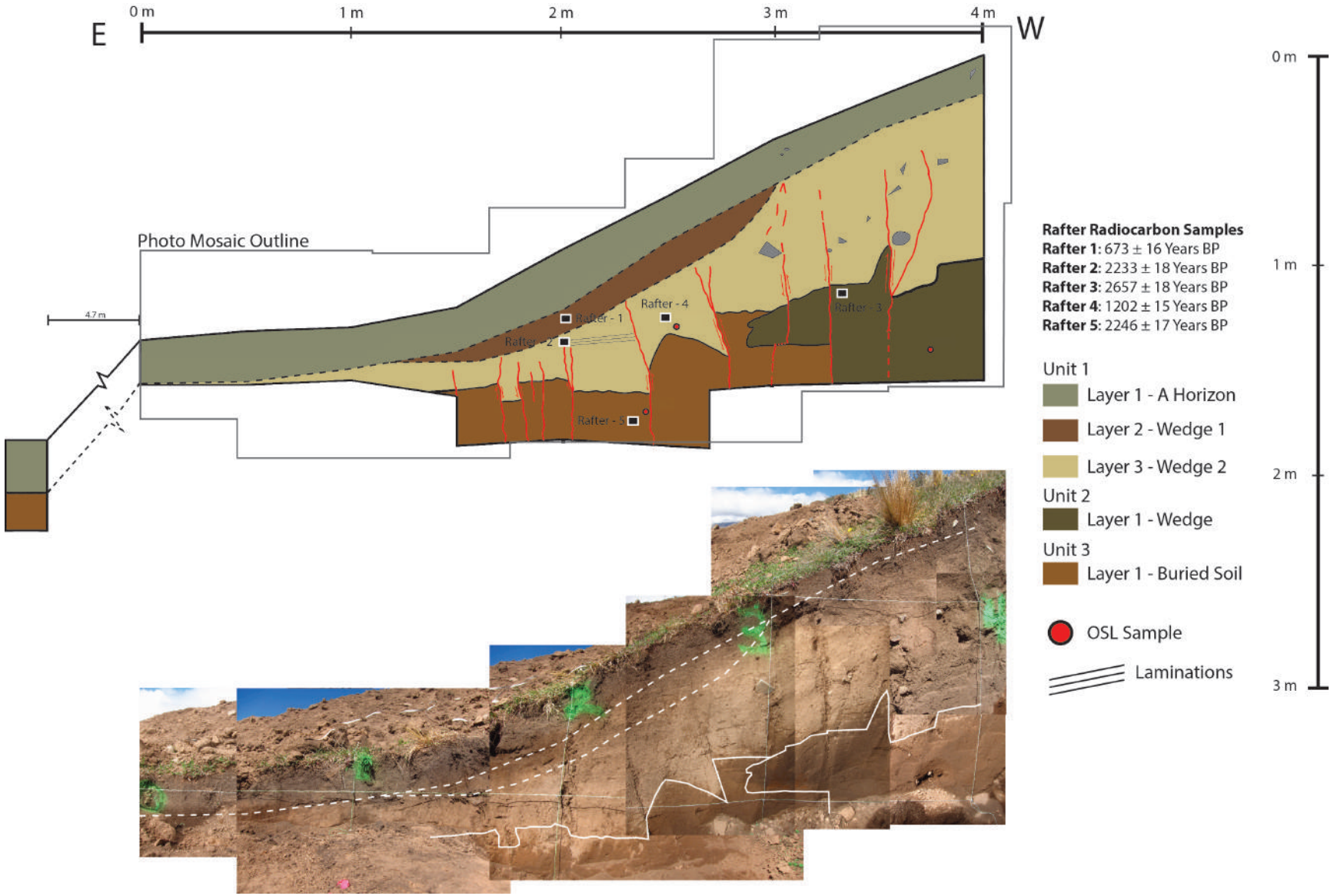

Figure 3.17: Trench log with accompanying photomosaic.

While trench stratigraphy consisted predominantly of silt, it could be subdivided into several units (Table 3.5)(Figure 3.17). Unit 1, which made up the majority of the trench, was subdivided into three layers, the topmost of which was an A horizon. This layer consisted of a light grey to brown fine silt. A Munsell color chart was also used to further classify color for each layer in both a wet and dry state. When wet, the A horizon was 10 YR 3/1, while when dry it was 10 YR 4/1. This layer contained a large amount of organic matter, it was not plant litter, which is why it was classified as an A horizon rather than on O horizon. This layer's lower contact was considered gradational, because while color changed, no definitive grainsize difference could be noted. Lastly, small, angular greywacke fragments were found, and there was no clear evidence of faulting. While some vertical fractures neared the layer, most appeared to terminate prior to the gradational contact.

Of the two other layers making up Unit 1, one (Wedge 2) was diagramed in the final log, while the other (Wedge 1) was interpreted following trench infill. Wedge 2 was made up of a fine-grained silt and was light brown in color (Munsell: Wet - 10YR 4/4, Dry - 10 YR 7/1). This layer showed clear evidence of faulting in the form of large cracks, and offset of the basal contact. Near the 2 m mark of the trench, subtle laminations were found, suggesting possible fluvial sheetwash. Like the overlying A horizon, angular greywacke fragments were found, though in this layer they were more abundant. Lastly, a significant amount of charcoal was found, and two samples were sent to the Rafter Radiocarbon lab at GNS Science (Full radiocarbon reports can be found in the Digital Appendices). The first sample (Rafter 2, Figure 3.18) contained 7805.7 mg of raw sample, and several pieces of angular charcoal were extracted. Using conventional radiocarbon ages (Years BP), this sample was dated at 2233 ± 18 years BP (Figure 3.19). The conventional radiocarbon age is reported as defined by Stuvier and Polach (1977). The charcoal taken from this location was located within small-scale fractures and a few centimeters east of the subtle laminations (Figure 3.18). For that reason, it is believed to represent remobilized charcoal. The second sample (Rafter 4) contained 274.41 mg of raw sample, and charcoal was dated at 1202 ± 15 years BP (3.19). This layer was deemed a colluvial wedge due in large part to its shape, and because it was absent in a test pit 4.7 m east of the trench (Figure 3.17).

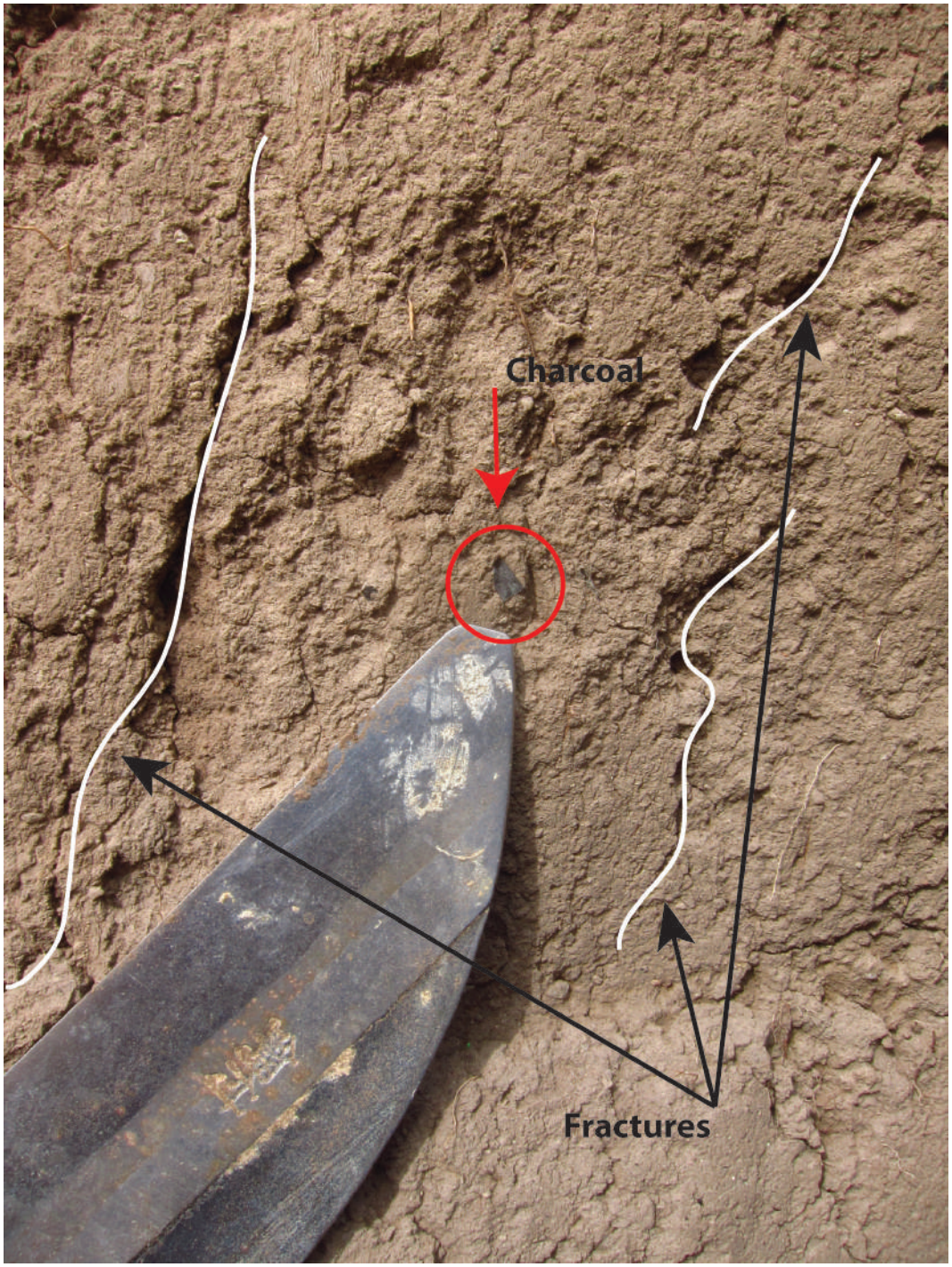

Figure 3.18: Charcoal used for radiocarbon dating of Rafter 2 sample.

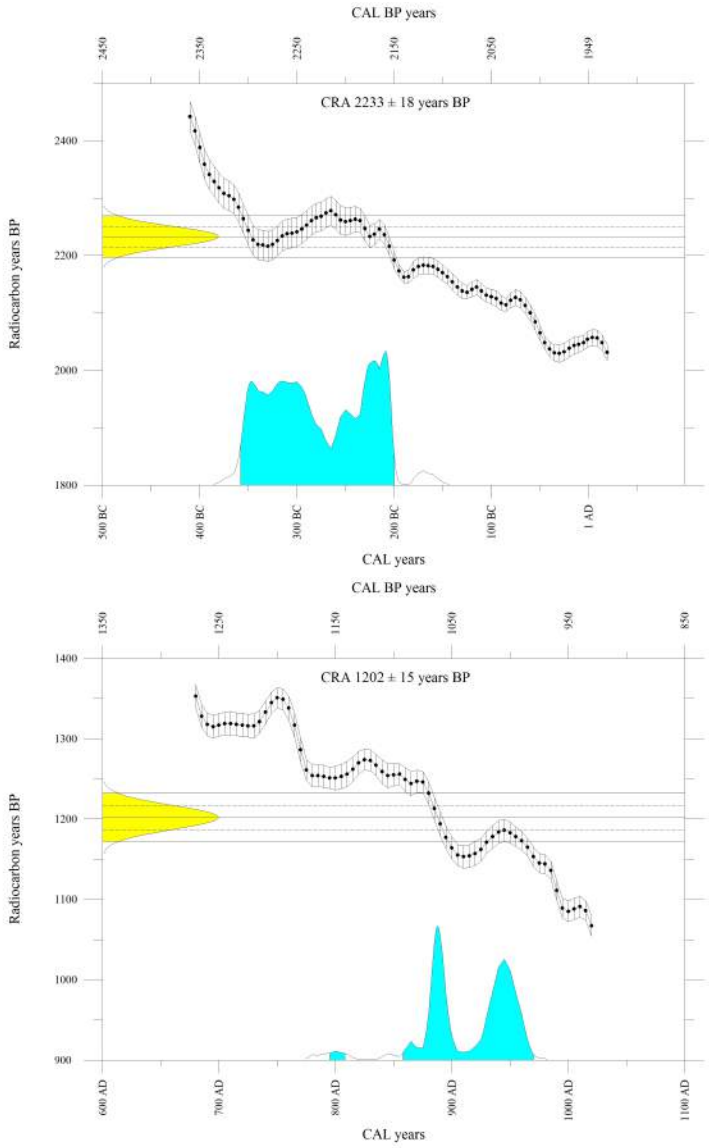

Figure 3.19: Radiocarbon calibration curves for Rafter 2 (Top) and Rafter 4 samples.

Wedge 1 on the other hand was identified predominantly through color and radiocarbon age analysis. Because interpretation came following trench infill, the same type of analysis was not done, though from examining photos, comparative analysis could be done. For example, it is darker in color than Wedge 2, and a gradational contact with Wedge 2 has a concave downward shape. Additionally, a single charcoal sample (Rafter 1) containing 5868.7 mg of raw sample, was dated at 673 ± 16 years BP (Figures 3.20 & 3.21). It is because of this significant age difference that this layer was differentiated from the rest of the unit.

Figure 3.20: Angular charcoal fragment used for Rafter 1 radiocarbon dating.

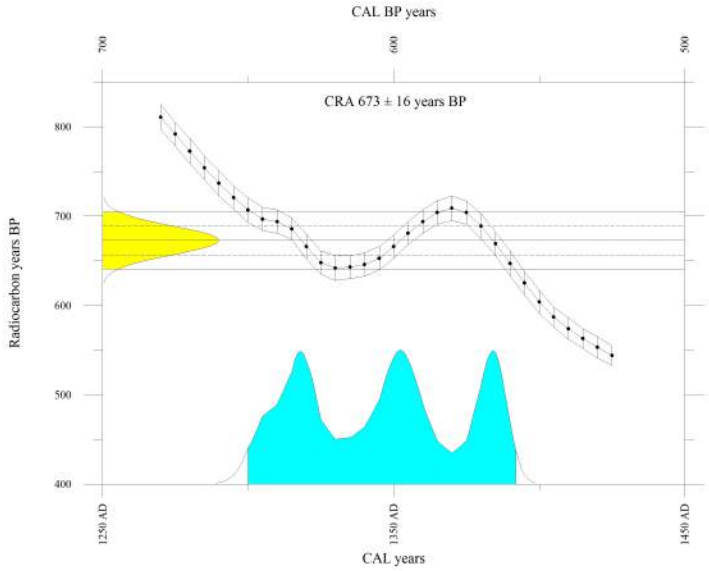

Figure 3.21: Radiocarbon calibration curve for Rafter 1 sample.

Unit 2 was only found on the western side of the trench, and was classified as a reddish-brown (Munsell: Wet - 5 YR 3/3, Dry - 5 YR 7/1) fine-grained silt. It was interpreted as having a higher proportion of fines to the layers in Unit 1, as it dried out slower, exposing offset of units. This unit was heavily fractured, and contained organic carbon (Rafter 3) (Figure 3.22). The 25.48 mg of raw sample, was dated to 2657 ± 18 years BP (Figure 3.23). Similar to the wedges in Unit 1, Unit 2 was also deemed a colluvial wedge because of its shape and limited extent.

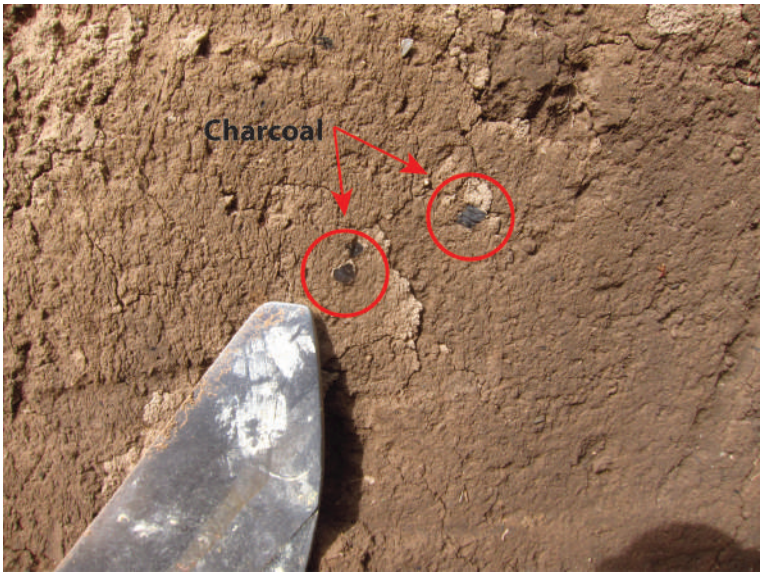

Figure 3.22: Rafter 3 charcoal sample used to date Unit 2.

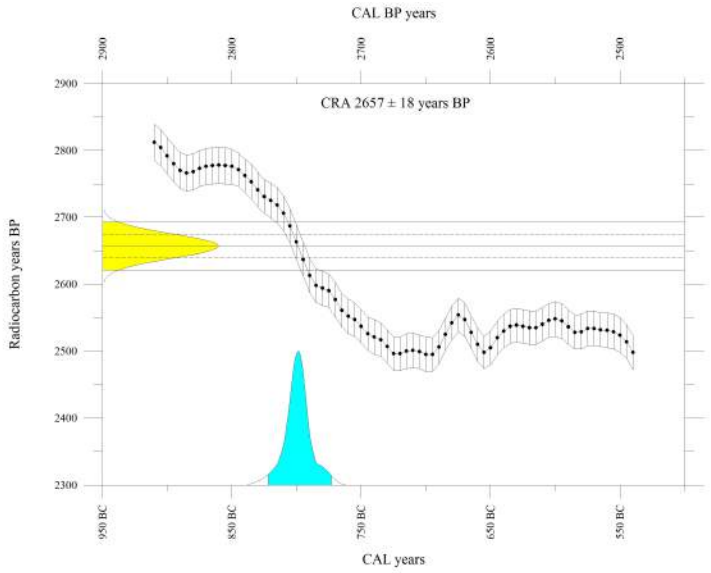

Figure 3.23: Radiocarbon calibration curve for Rafter 3 sample.

The final trench unit (Unit 3), underlay all units, and included the trench floor. Like the other units it was a fine silt, though much redder than any other layer (Munsell: Wet - 5 YR 4/2, Dry - 5 YR 6/3). Numerous fractures propagated through this unit, and while it contained some organic matter, it was sparse. A single charcoal sample from this unit (Rafter 5), was analyzed, yielding an age of 2246 ± 17 years BP (Figure 3.24). Within this unit, some fractures indicate the presence of normal faults. In a compressional area, it is more likely that they are reverse faults which have rotated due to footwall flexure described in Chapter 2 (Figure 3.17).

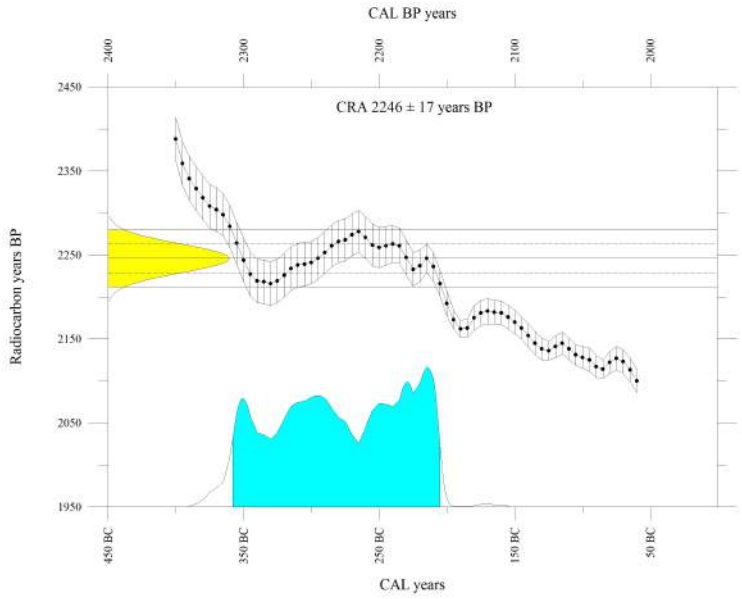

Figure 3.24: Radiocarbon calibration curve for Rafter 5 sample.

Unit Name	Deposit	Color	Texture	Notes
1 - A Horizon	Modern Soil	Wet: 10 YR 3/1 Dry: 10 YR 4/1	Fine Silt	-
1 - Wedge 1	Colluvial Wedge	-	Fine Silt	Concave downward shape
1 - Wedge 2	Colluvial Wedge	Wet: 10 YR 4/4 Dry: 10 YR 7/1	Fine Silt	Laminations and remobilized carbon
2 - Wedge	Colluvial Wedge	Wet: 5 YR 3/3 Dry: 5 YR 7/1	Fine Silt	Finer grained than Unit 1
3	Buried Soil	Wet: 5 YR 4/2 Dry: 5 YR 6/3	Fine Silt	Basal unit

Table 3.5: Trench unit descriptions.

Sample	Deposit	Notes	Radiocarbon Age (Years BP)
LHF-Unit1W-2m	Unit 1 - Wedge 1	Taken at 2 m mark	673 ± 16
LHF-Unit1W-NOSL3	Unit 1 - Wedge 2	Taken near OSL 3	1202± 15
LHF-Unit1W-FC	Unit 1 - Wedge 2	Charcoal within fractures	2233 ± 18
LHF-Unit3-NOSL2	Unit 3	Taken near OSL 2	2246± 17
LHF-Unit2-Wedge	Unit 2	Colluvial wedge charcoal	2657 ± 18

Table 3.6: Radiocarbon results from trench.

Because gravel was not found, several augers were put into both the floor and western wall of the trench in an attempt to find the old fan surface. Along the trench floor, augering reached depths of 0.6-1 m, while in the western wall they went in 0.77-1.35 m. These measurements likely indicate the location of the original fan surface, prior to soil formation, earthquakes, and additional deposition. Using this knowledge, a retro-deformation diagram was made showing a simplified history of the site (Figure 3.25). While the history depicted in this diagram shows the site with the maximum number of events possible (3), the third event, which created Unit 1 - Wedge 1, is debatable as it was identified through photo analysis and radiocarbon ages.

While this trench does illustrate an earthquake history along the Lake Heron Fault, it is unlikely to show the complete record. Because there is 20 m of total vertical deformation, and the events seen in this trench are along a 5-6 m high scarp, suggests rupture has been quite complex and distributed amongst numerous scarps. Nonetheless, stratigraphy and radiocarbon ages do show evidence of at least two, if not three events. From radiocarbon ages received, these events can be constrained to the last 2.6 ka, and possibly even further to 2.6-0.6 ka. Because of the potential variation in interpretation, a logic tree was created illustrating possible scenarios (Figure 3.26).

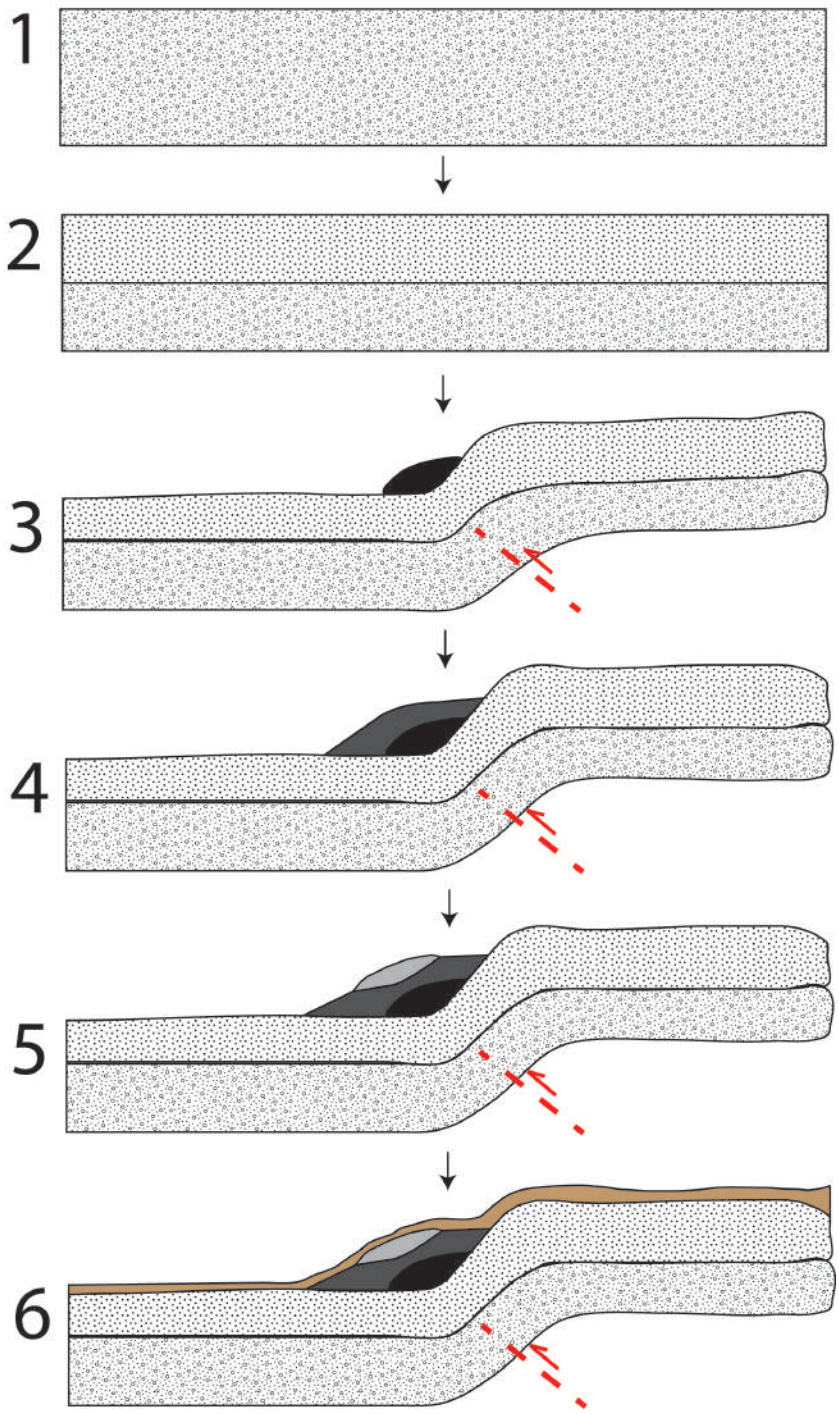

Figure 3.25: Retro-deformation sketch of trench location. The sequence is as follows: (1) Deposition of the lowest surface of the Paddle Hill Creek Fan (Unit not encountered in trench), (2) Abandonment of lowest surface allowing for soil formation, and occasional sheetwash and loess deposits (Unit 3), (3) Earthquake (EQ1) leading to the collapse of a colluvial wedge (Unit 2), (4) Light soil formation begins, until another earthquake (EQ2) causes additional colluvial wedge collapse (Unit 1 - Wedge 1), (5) More soil formation, until a possible third event (EQ3?) causes additional collapse, and (6) Soil formation (Unit 1 - A Horizon).

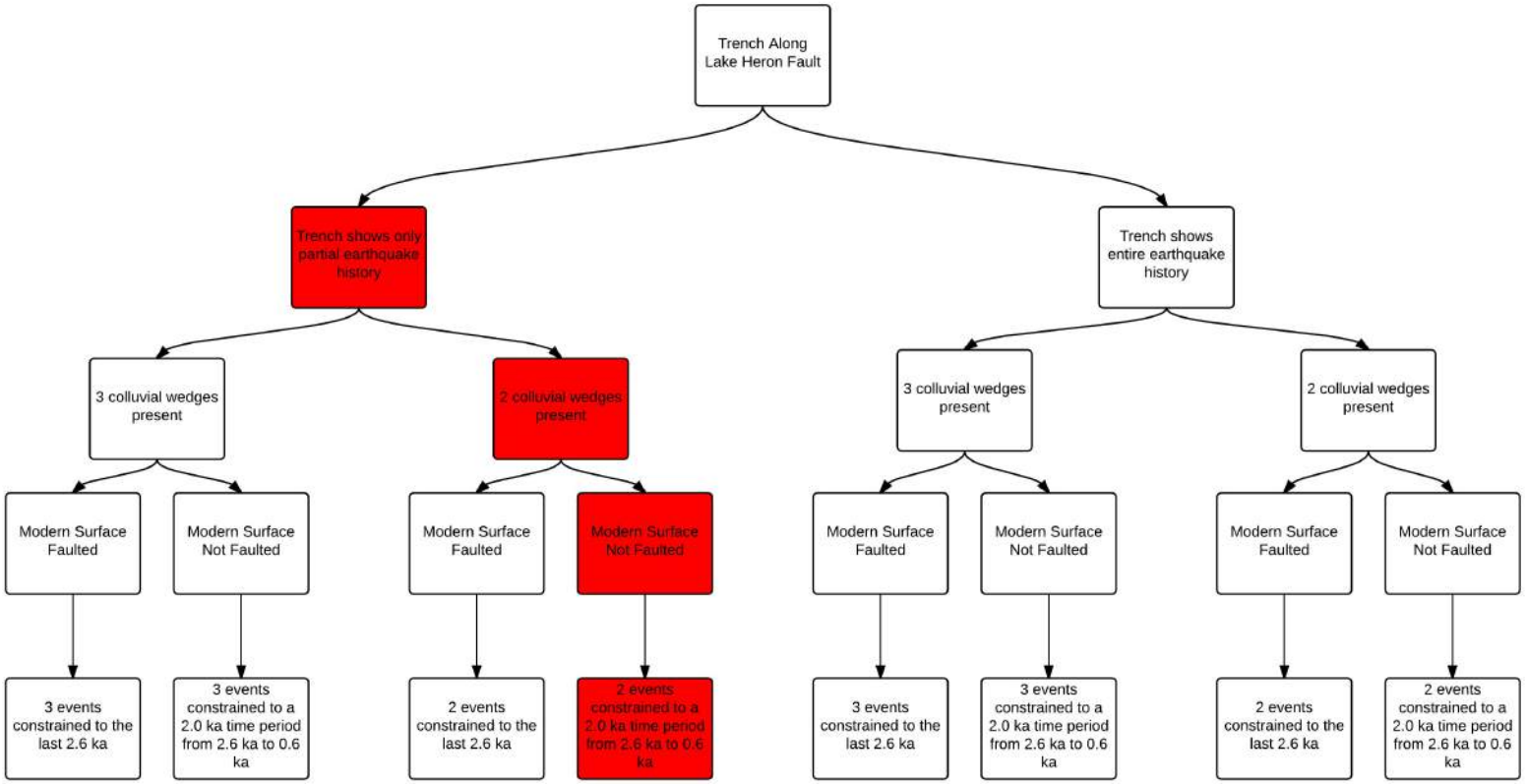

Figure 3.26: Logic tree illustrating possible scenarios interpreted from the Lake Heron Fault trench. The red boxes indicate the most plausible and conservative approach taken in this thesis.

3.3.5 Discussion

3.3.5.1 Single Event Displacement and Earthquake Magnitude

Based on data presented, and scenarios given in the logic tree, single event displacements and earthquake magnitudes can be estimated. While there is a significant range, emphasis will be placed on more probable, and often conservative interpretations. Additionally, while there are a variety of ways in which these can be calculated, greater weight will be given to more recent studies that have documented faulting within New Zealand. This was done as there is a discrepancy between how faults within New Zealand behave, when compared to regression formulae that summarize global data (Stirling et al., 1998).

The first way to estimate single event displacement is to assume a characteristic earthquake model. When this is combined with the number of events and scarp height, a rough estimation can be given. At the trench location, the fault scarp was 5.5 ± 0.5 m high, and evidence of 2-3 earthquakes was discovered. Using the more conservative interpretation of two events yields a single event vertical displacement of 2.75 ± 0.25 m.

Scaling relationships can also be used to calculate single event displacement. Wesnousky (2008) combines the type of fault (strike-slip, normal, reverse) with the surface rupture length to determine the average geologic slip per event. Although valuable, this method relies heavily on knowing the surface rupture length, which is not known for the Lake Heron Fault, and estimates place it anywhere between 18-80 km (If it connects with the Forest Creek Fault) (Pettinga et al., 1998, 2001; Upton et al., 2004; Upton and Koons, 2007; Upton et al., 2009; Barrell and Strong, 2009; Stahl, 2014). Even if it does not connect with the Forest Creek Fault, estimates still place it between 18-60 km long. This is in contrast to the definitively-mapped trace in this study, which only found a 10 km long surface trace of tectonic origin. Because of these uncertainties, a large range for single event displacement results (Table 3.7). Although a significant range is shown, it must be emphasized that the 10 km surface rupture length mapped in this study is not believed to represent the entire fault trace, and is instead shown to highlight issues surrounding the use of scaling relationships.

Length (Km)	Average Single Event Displacement (m)	Maximum Slip (m)
10	0.6	2.1
18	1.08	3.78
60	3.6	12.6
80	4.8	16.8

Table 3.7: Variation in single event displacement using Wesnousky (2008) scaling relationship for reverse faults applied to the Lake Heron Fault.

The average single event displacements were calculated using the equation $Slip(m) = C \cdot Length(km)$, where $C = 0.06$ for reverse faults (Wesnousky, 2008). From the values calculated, an average single event displacement of 2.7 ± 2.1 m was determined. While the error is significant, it is due to the uncertainty of the fault's length. However, because much of the trace is likely obscured by Quaternary deposits or trends parallel with geomorphic features (e.g. moraines and terrace risers) it cannot be limited. While this gives the average single event displacement, it is by no means the maximum slip possible, which is 2.1-16.8 m per event ($Slip(m) = C \cdot Length(km)$ where $C = 0.21$).

Similar issues are encountered when calculating a possible earthquake magnitude. Stirling et al. (2013) suggests that for reverse faults in a plate boundary tectonic setting, a Wesnousky (2008) scaling relationship be used. However, like the relationship for calculating average displacement, this one also uses surface rupture length. The equation, $Mw = A + B \cdot log(Length(km))$, where $A = 4.11$ and $B = 1.88$ for reverse faults helps give an indication of a fault's moment magnitude on a logarithmic scale. Using the potential range of surface rupture length for the Lake Heron Fault (10-80 km) yields a magnitude of 6.85 ± 0.85(Table 3.8). Having said that, Mw 7.0+ is more likely, as this is the likely minimum magnitude historically required to produce surface rupture in thick gravel sequences overlying greywacke bedrock in this region (e.g. Quigley et al. (2012)). In turn, this may indicate the Lake Heron Fault is at least 35 km long.

Length (km)	Earthquake Magnitude (Mw)
10	6.0
18	6.5
60	7.5
80	7.7

Table 3.8: Variation in earthquake magnitude using Wesnousky (2008) scaling relationship for reverse faults applied to the Lake Heron Fault.

From the calculated values, and coupling them with trench data, more detailed conclusions can be made about the single event displacement and earthquake magnitude of the Lake Heron Fault. Although scaling relationships are valuable, because they rely on knowing the length of a fault, large ranges result, some of which do not appear plausible. Therefore, the conservative single event displacement calculated using a combination of trench data and surveying of the scarp suggests that the Lake Heron Fault demonstrates an average single event displacement of 2.75 ± 0.25 m. Additionally, because generating surface rupture in Canterbury require a Mw 7.0+ earthquake, the same is likely the case here here, giving the Lake Heron Fault a likely magnitude of Mw 7.4 ± 0.3.

3.3.5.2 Recurrence Interval Implications

Based on interpretation of trench units, radiocarbon and Schmidt hammer ages, and the approximate single event displacement, a rough recurrence interval (RI) can be calculated. However, because the RI will depend on how many earthquakes are believed to be visible in the trench, and if the modern surface is faulted, values vary considerably. First, it must be reiterated that the lowest surface of the Paddle Hill Creek fan has undergone 19.3 ± 3 m of vertical deformation.

While the age of the lowest surface of the Paddle Hill Creek Fan is poorly resolved, Schmidt hammer ages calculated using the a-value generated in this study (279) will be given greater weight, and yield an age of 10.15 ± 2.95 ka. From here, the single event displacement calculated in 3.3.5.1 can be used to determine how many earthquakes there have been. Because this single event displacement includes the possibility of two or three events being preserved in the trench, the range in the number of events varies considerably. However, because Unit 1 - Wedge 1 was not unambiguously fault-generated, a more conservative approach was taken, and a single event displacement of 2.75 ± 0.25 m was used to determine that seven earthquakes were required to produce 19 m of vertical deformation.

By combining all of this information, a RI of 1.45 ± 0.42 ka over the last 13 ka is suggested for the Lake Heron Fault. Additionally, prior to this, there appears to have been little to no discrete surface slip as surfaces dated at up to 25 ka showed the same amount of vertical deformation (Figure 3.27). This figure brings up the possibility of temporal variability in slip along the Lake Heron Fault. By comparing surface age with vertical offset, it can be seen that areas which differ in age by up to 15 ka, have the same amount of vertical offset. In turn, this would mean a substantial decrease in the slip rate prior to 13 ka, and a period of seismic quiescence.

While the RI calculated for the Lake Heron Fault is shorter than the the nearby Forest Creek and Fox Peak faults which have recurrence intervals of 2.5 ± 0.5 ka and 3.95 ± 1.35 ka respectively, it is similar to the 1.8 ± 1.2 ka RI in Barrell and Strong (2009). Having said that, Barrell and Strong (2009) suggested the faulted surface is 18 ka, while this study found it was significantly younger.

In addition to the long-term RI, insight into the more recent history can be derived from radiocarbon ages. Because Unit 2 was dated to approximately 2.6 ka, and is interpreted to have formed in an earthquake, and showed subsequent offset prior to deposition of the sediment hosting the the Rafter 1 radiocarbon sample, suggests that at least two earthquakes occurred 2.6-0.6 ka. However, while fractures near the surface were not seen, some were

dashed in as approximate, and it could not be definitively stated that the modern surface wasn't faulted. Therefore, while this author believes two earthquakes occurred in a 2.0 ka period between 2.6 and 0.6 ka, it can be conservatively stated that the Lake Heron Fault has ruptured at least twice in the last 2.6 ka.

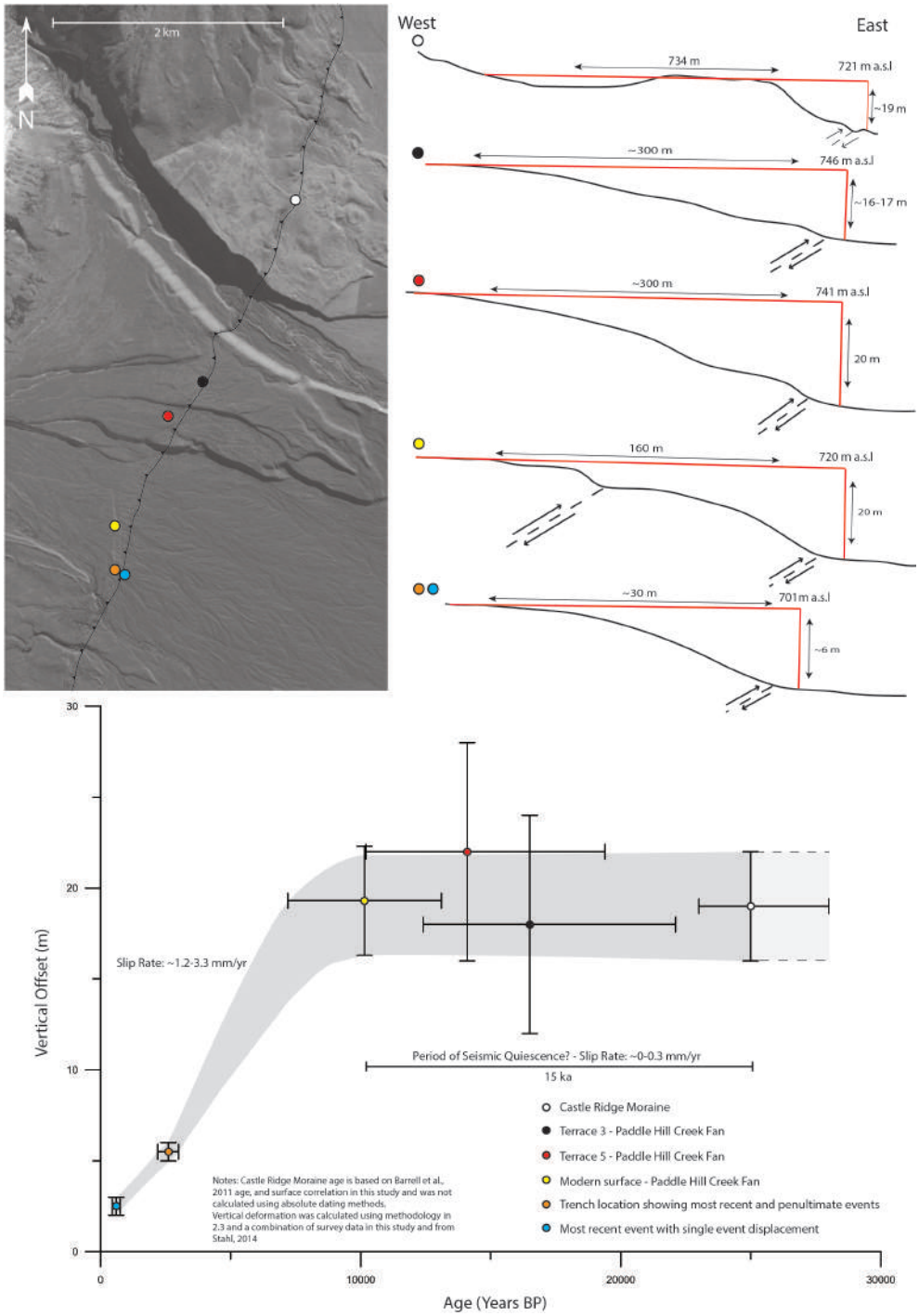

Figure 3.27: Age vs. Vertical Deformation Plot for the Lake Heron Fault, with accompanying simplified survey data. The blue and orange survey line only shows the solitary scarp where the trench was, illustrating the most recent and penultimate events (Total vertical deformation in this location is 19 m).

4 Discussion and Conclusions

From data presented in preceding chapters, it is clear that the Lake Heron Fault expresses geomorphology in the way of large fault scarps, topographic flexure, and crestal grabens. Additionally, along nearly it's entire length, tectonic deformation has resulted in approximately 20 m of vertical deformation. While 20 m is substantial, what makes the Lake Heron Fault particularly interesting is that all offset appears to have occurred in the last 10.15 ± 2.95 ka, using Schmidt hammer exposure age dating (SHD). Combining this with trench data and radiocarbon ages yields a recurrence interval of 1.45 ± 0.42 ka for the last 13 ka, with a vertical slip rate of 2.25 ± 1.05 mm/yr. This recurrence interval and slip rate are significantly lower and higher respectively than other faults in the rangefront and begs the questions of why or if this is the case, how the slip compares with geodetic slip rates, and how this helps or hinders the argument that the Lake Heron Fault may link with neighboring faults.

4.1 Episodic vs. Periodic Behavior of the Lake Heron Fault

Based on observations and field data, two possible scenarios can be given to explain the behavior of the Lake Heron Fault. One is that earthquakes are episodic, while the other is that they are periodic. The episodic approach implies that earthquake clustering has occurred in the last 10.15 ± 2.95 ka, while the periodic model suggests that behavior has remained more "regular," possibly dating back to 25 ka. Each of these scenarios has possible mechanisms, which will be highlighted throughout this section.

4.1.1 Episodic Behavior

Episodic fault behavior is a process which has been documented worldwide (e.g. Crone et al. 1997; Quigley et al. 2006, 2010; Gardner et al. 2009), and implies that a fault and/or region will experience episodes of multiple earthquakes in a relatively short period of time, separated in some cases by many thousands of years. While there are several reasons for this behavior, mechanisms include fault interaction, and changes in crustal stress.

Although it is a more stable continental environment, studies in Australia have shown that despite low long-term rates of tectonism, there is also evidence of high short-term rates of activity in regions considered aseismic (Crone et al., 1997). This reactivation of previously inactive faults is interpreted as a function of fault interaction and a changing stress field, causing instability and rupture in the forms of relative earthquake clustering (Crone et al.,

1997; Quigley et al., 2006, 2010; Gardner et al., 2009). Similar behavior has been see within New Zealand's central South Island, in the form of changing stress fields due to fault rupture, elevating the risk of earthquakes on other fault systems (e.g. Steacy et al. 2013).

Episodic fault behavior can also happen exclusively from changes in crustal stress such as unloading (e.g deglaciation) (Stewart et al., 2000). This theory (deglaciation seismotectonics), relies on the idea that in glaciated areas (such as New Zealand), following retreat, significant crustal deformation occurs, and earthquake clustering can result (Figure 4.1)(Patrick et al., 1999; Firth and Stewart, 2000; Muir-Wood, 2000; Lund et al., 2009; Kukkonen et al., 2010). While deglaciation seismotectonics has been noted in locations worldwide, it is seen to take the greatest effect where the maximum stress is horizontal (Stewart et al., 2000). Such is the case for New Zealand, and more specifically the Lake Heron Basin, where there appears to be no strike-slip motion across discrete fault rupture. These areas are most susceptible because as glaciers increase the vertical stress (σ^3), they can bring it into balance with σ^1. When this happens, fault stability ensues, and stress release is inhibited. However, as glaciers retreat, faults rapidly destabilize, and a succession of earthquakes can result.

Based on these examples, it seems possible that around 10.15 ± 2.95 ka, the eastern foothills of the Southern Alps experienced a changing stress field, resulting in significant instability and heightened earthquake activity. While the exact reason for this change may not be known, because such phenomenon has been documented worldwide emphasizes the need for it to be considered possible for this region.

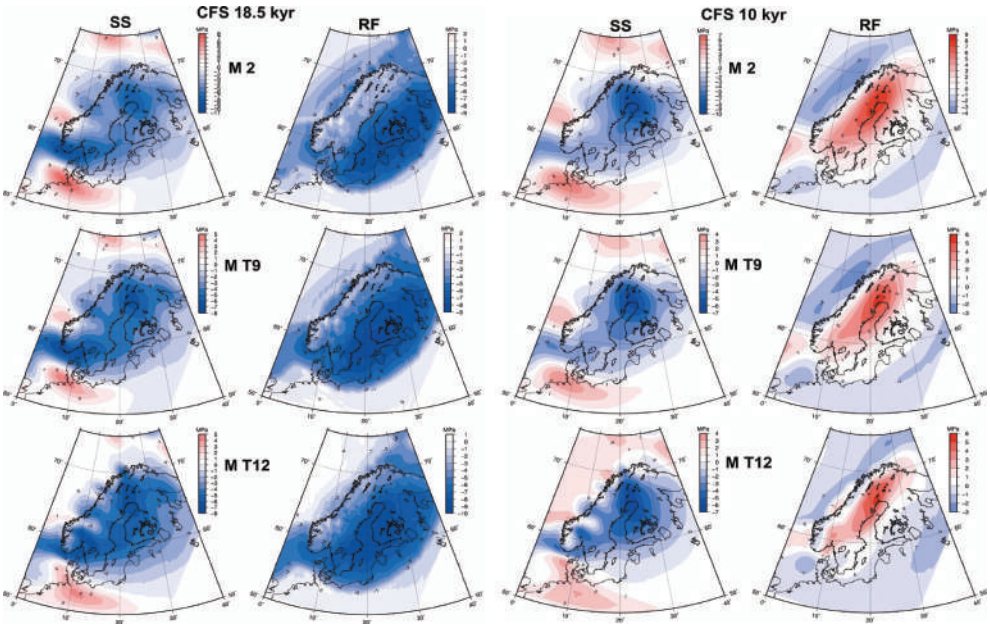

Figure 4.1: Comparison of fault stress in Scandinavia from 18.5 ka (left) to 10.5 ka (right). The left-hand column for each time period corresponds to strike slip faults, while the right column corresponds to reverse faults, which is of primary concern to this study. Figures from Lund et al. (2009).

4.1.2 Periodic Behavior

In comparison, periodic earthquake behavior implies that a fault will experience more "regular" earthquakes, which can exhibit time-predictable and/or slip predictable characteristics (McCalpin, 2009). Although this apparent behavior has been noted on faults, along the Lake Heron Fault, there is an apparent problem that surfaces dated at up to 25 ka, have the same amount of total vertical deformation as surfaces 10.15 ± 2.95 ka in age. However, strain dispersion could be responsible for the similarity seen. This concept relies on the idea that as a fault propagates through varying material, different surface structures can result (Roering et al., 1997). Through numerical modeling, Roering et al. (1997) found that both fault and bedding characteristics could significantly influence fault tip propagation in blind thrust faults. In some instances, these characteristics could caused a fault to not rupture through to the surface, despite numerous events.

Such behavior in the Lake Heron Basin is plausible, as the possibility exists that sediment thickness varies, and, where sediment is thickest, surface rupture in earthquake events was once inhibited, masking the evidence. However, over time, more earthquakes occurred, the surface ruptured, and evidence became clear. For example, on the young surfaces within the Spider Lakes and Paddle Hill Creek sections, there may be a thinner sediment veneer than there is in older portions of the basin. In turn, earthquakes in the last 10.15 ± 2.95

ka have propagated all the way to the surface. However, in the older sections (e.g. Castle Ridge), thicker sediment cover could have inhibited fault propagation prior to10.15 ± 2.95 ka. If this were to be the case, older areas with thicker sediment cover may display the similar vertical deformation to younger areas, not because all earthquake activity has been recent, but because of strain dispersion.

4.1.3 Conclusions

Overall, there are compelling arguments for both episodic and periodic behavior of the Lake Heron Fault. Although these mechanisms were not thoroughly examined within this thesis, this author believes that observations and data (e.g. survey line and dating techniques) are best explained by temporal variations in slip rate (Figure 3.27). This implies that the Lake Heron Fault is episodic in nature, and that there has been earthquake clustering in the last10.15 ± 2.95 ka as opposed to more "regular" behavior during the last 25 ka. However, because mechanisms were not examined, opens the possibility for future research, including numerical modeling of stress changes due to glacial rebound, and analysis of strain dispersion within alluvial sediment and glacial till.

4.2 Comparison of Slip and Geodetic Rates

From the evidence indicating the Lake Heron Fault has been more active in the last 13 ka than published reports suggest, also yields slip rate increases. From Monte Carlo simulations done in Chapter 3, and placing a greater emphasis on rates calculated using the Schmidt hammer a-value generated in this study, a vertical slip from 13 ka to present of 2.25 ± 1.05 mm/yr was calculated. This is significantly higher than the estimate of 1.1 mm/yr, in Barrell and Strong (2009), with even the lowest estimate in this thesis being higher than what is published.

While the slip rates calculated in this study are higher than published reports, they can also be compared with geodetic models. Models in Wallace et al. (2007), suggest that faults within the eastern foothills of the Southern Alps should collectively accommodate 2.5-7 mm of slip per year, broken up into contractional and strike slip components. As this represents net slip, to compare these values to the Lake Heron Fault, fault dip must be incorporated. Using a dip of 60° (Based on in situ greywacke measurements), and almost exclusive dip-slip motion (Based on the lack of strike slip motion across discrete fault scarps), the 2.25 ± 1.05 mm/yr of vertical slip translates to 2.6 ± 1.2 mm/yr of net slip, placing it at the lower end of geodetic models. This is in contrast to what is seen across the region, where geodetic slip

rates are 2-3 times higher than those derived geologically. Though the exact reasons for this overestimation is unknown, it could be for reasons such as unknown active faults within the eastern foothills of the Southern Alps, or that the geologically-derived rates underestimate slip rates (Wallace et al., 2007).

Although regional conclusions cannot be made from this estimate, as it only represent a single study, what can be stated is that unlike other geologic studies, this one has yielded slip rates within the range geodetic models suggest. Given there was a significant underestimation of the slip of the Lake Heron Fault, the same could be true for other faults as well.

4.3 Fault Segmentation and Linkage of Rangefront Faults

While the Lake Heron Fault represents a large structure within New Zealand's rangefront, there is a possibility that at depth it merges with other faults, capable of rupturing simultaneously. Such fault geometry was seen near the surface, and would not be unexpected at depth. Although fault segmentation is not a new concept, numerous factors inhibit a greater understanding.

On multiple scales, fault segment boundaries can be identified by a variety of characteristics including: (1) surface discontinuities (i.e. step-overs) or alterations in the geometry of the fault, (2) changes in the amount of relief (structural or topographic), (3) variability in the calculated slip rate and/or the timing of paleoearthquakes, and (4) the limit of past ruptures (Knuepfer, 1989; Depolo et al., 1991; McCalpin, 2009). Of primary interest to this study is if the Lake Heron and Forest Creek faults merge, representing an 80 km long segmented reverse fault capable of generating Mw 7.7 earthquakes (Based on Wesnousky (2008) scaling relationship).

While the idea that the Lake Heron and Forest Creek faults are the same structure has been postulated by others (e.g. Upton et al. (2004); Upton and Koons (2007); Upton et al. (2009)), only recently have paleoseismic studies been completed. In turn, this data can be used to interpret if a larger structure is possible and/or probable. Of primary interest are the timing of paleoearthquakes and recurrence intervals. As explained earlier, the recurrence interval of the Lake Heron Fault (1.45 ± 0.42 ka) is lower than other faults in the region, including the Forest Creek Fault (2.5 ± 0.5 ka) (Stahl, 2014).

Although there is no overlap in these recurrence intervals, because the Forest Creek Fault recurrence interval was difficult to determine, it is possible that with additional paleoseismic work, overlap may be seen (Stahl, 2014). This interval was difficult to determine as only a

few centimeters of throw was seen on discrete faults in trenches, and because the timing of earthquakes could only be constrained to timescales of several thousands of years.

For this reason it is also difficult to say if fault rupture could have been simultaneous. While the Lake Heron Fault has experienced 2-3 earthquakes in the last 2.6 ka, and 7 in the last 13 ka, the Forest Creek Fault has had 2-3 ruptures in the last 6 ka, with the first occurring before 5570 ± 611 years BP, while the next two were between 5.5 and 3.5 ka, likely closer to 5.5 ka, and between 3.5 and 0.5 ka, likely closer to 3.5 ka (Stahl, 2014). These ages possibly indicates variability in the timing of paleoearthquakes, supporting the argument of segmented faults, as it is one of their characteristics (Knuepfer, 1989; Depolo et al., 1991; McCalpin, 2009). Having said that, it is risky to assume a possible connection based on this data exclusively.

While paleoseismic investigation appears inconclusive, the difference in number of ruptures could be due to segmentation, and has been documented all over the world, including in New Zealand's rangefront. Howard (2001) determined that along the Porters Pass Fault, a segment boundary had inhibited fault propagation. This was discovered through trenching, as one trench showed evidence of four earthquakes, while another only showed a single event. Having said that, the possibility of a full length rupture was still acknowledged.

Given the differences seen between the Lake Heron and Forest Creek faults, a similar possibility exists that while they may primarily rupture individually, full length rupture is possible, and capable of generating Mw 7.7 earthquakes. However, to further examine the viability of this idea, both surface morphology and subsurface structures must be evaluated.

Through identification of past rupture limits it is seen that the two faults are separated by approximately 18 km. Between these limits is the Harper Range, a significant change in relief, possibly capable of inhibiting fault propagation. Additionally, within the Balmacaan Saddle, there is a small fault with a strike similar to the last known strike of the Lake Heron Fault, and which would project to the last known location of the Forest Creek Fault.

While a gap of 18 km may seem long, an almost identical distance was exhibited during the 2008 Wenchuan Earthquake (Xu et al., 2009) (Figure 4.2). During this event, two faults of the Longmenshan thrust belt, which merge at depth, ruptured simultaneously causing a Mw 7.9 earthquake. While these faults were separated horizontally, rather than vertically (In plan view) as is the case for the Lake Heron and Forest Creek faults, the same principles apply in terms of how they would merge at depth.

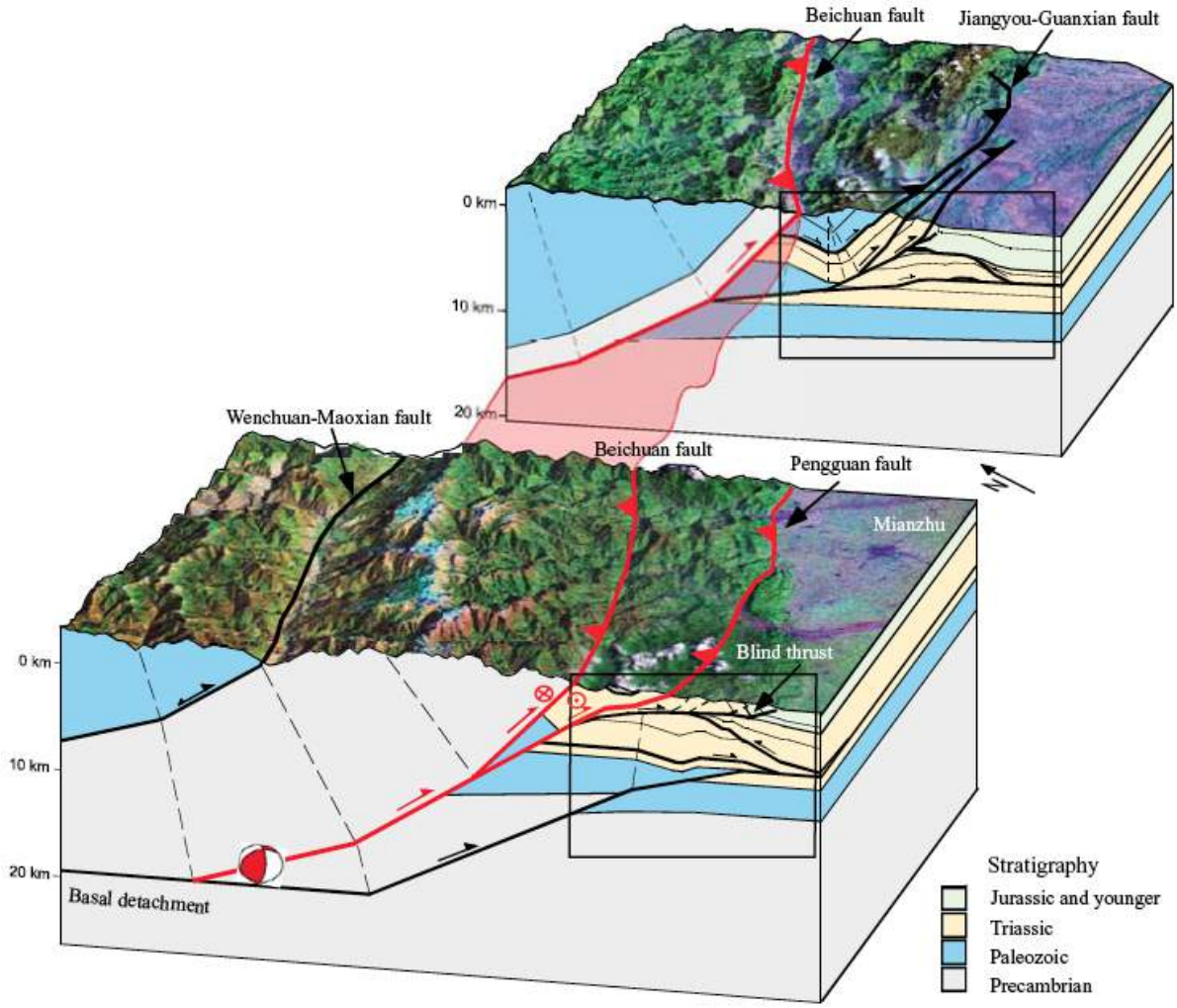

Figure 4.2: Schematic 3D diagram illustrating how multiple faults, separated by several kilometers at the surface, may in fact merge at depth. In turn, a resulting earthquake which ruptures both segments will be larger than an earthquake that only ruptures a single segment. Figure from (Xu et al., 2009).

A final piece of evidence suggesting the Forest Creek and Lake Heron faults represent an 80 km long segmented fault is the magneto-telluric survey across New Zealand's South Island. This survey, run through the Rangitata River, is where the 18 km void between the two faults lies. Based on current fault mapping, this is also where the Forest Creek Fault terminates, meaning one might expect it to only appear faintly on the survey. However, the structure is still clear at depth, as are possible near surface imbricate thrusts (Figure 4.3).

For a fault to appear so clearly near its apparent terminus seems unlikely. Therefore, based on the information provided, it it likely that the Lake Heron and Forest Creek faults represent a large segmented reverse fault at depth, while closer to the surface, it branches. Although there is variability in the timing of paleoearthquakes, calculated slip rates, and the limit

of past ruptures, these are all characteristics of segmented faults. Furthermore, while full length rupture (80 km) is possible, and capable of generating Mw 7.7 earthquakes, individual segments more frequently rupture in Mw 7.0+ earthquakes.

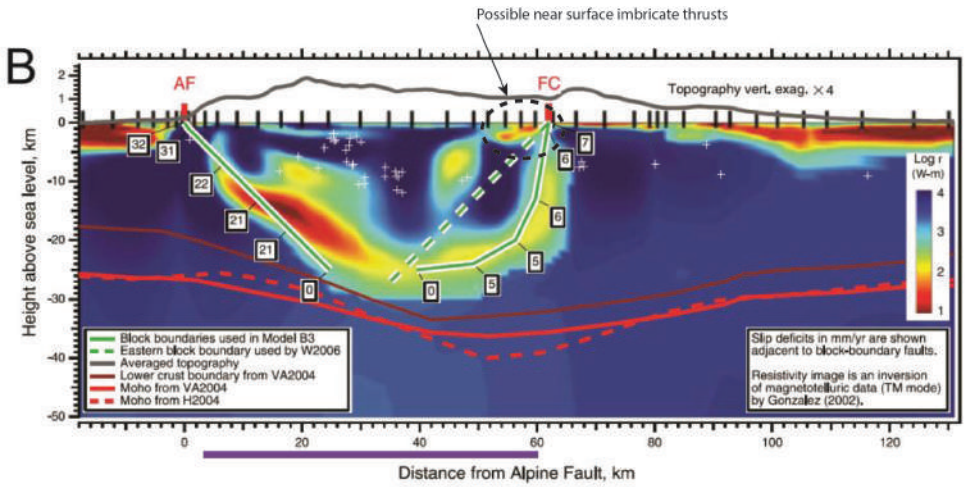

Figure 4.3: Magneto-telluric survey across the central South Island. AF and FC correspond to the Alpine and Forest Creek faults. This survey shows the Forest Creek Fault (solid green line) shallowing into a decollement at 15-20 km depth. It also suggests a linking with the Alpine Fault at depth, supporting the theory held by (Wannamaker et al., 2002) that numerous thrust faults within the Southern Alps at backthrusts off the Alpine Fault. Additionally, it appears to show near surface imbricate thrusts of the Forest Creek Fault.

Given the likelihood that the Lake Heron and Forest Creek faults represent a single structure brings in the question if it is possible that the entirety of this rangefront behaves similarly. If this information is combined with Stahl (2014), suggesting the Forest Creek and Fox Peak faults are segmented, suggests that at least three faults in the region are related. Additionally, the fact that the rangefront reverse faults are believed to be backthrusts off the Alpine Fault supports the idea they may be connected (Wannamaker et al., 2002). Although a significant amount of additional research would be required to support this theory the possibility exists that periodically New Zealand's rangefront destabilizes, resulting in earthquake clustering on a regional scale.

4.4 Key Findings

This thesis examined several aspects related to the tectonic geomorphology, structure, and paleoseismology of the Lake Heron Fault. Detailed field mapping, paleoseismic trenching, geophysics, surveying, topographic contouring, Schmidt hammer exposure age dating, and fault measurements were used to determine the deformation, rupture characteristics (e.g.

coseismic slip and fault motion), and paleoseismology of a previously unresearched fault. Below, key findings of this thesis are summarized.

Thesis Goal	Research Questions	Relevant Chapter
Determine slip rates and deformation to identify recent fault activity on the Lake Heron Fault. ✓	How is fault-associated deformation distributed along the fault?	Chapters 2 & 3
	How do ages calculated using Schmidt hammer exposure age dating compare with published ages?	Chapter 2
	How do calculated slip rates compare with geodetically derived ones?	Chapter 5
Obtain ages and single event displacement of earthquakes to determine a recurrence interval and potential earthquake magnitudes of the Lake Heron Fault ✓	How does sediment thickness/type/rheology effect fault behavior at/near the surface?	Chapters 2 & 3
	What type of motion is observed along the Lake Heron Fault and what are the implications?	Chapter 3
	Is it possible, that the Lake Heron Fault links with the Forest Creek Fault to the south-west? If so, what are the implications?	Chapters 4 & 5

Figure 4.4: Analysis of thesis aims.

4.4.1 How is fault-associated deformation distributed along the fault?

Field mapping and surveying were the most straightforward ways to determine how deformation was distributed along the fault. By using these techniques, it was determined that while the way in which vertical deformation is accommodated changes, total vertical deformation remains approximately 20 m. Additionally, this amount of deformation was seen to be consistent across surfaces differing in age by up to 15 ka.

The width of deformation throughout the Lake Heron Basin was reliant on the degree of topographic flexure. In some areas, topographic flexure was significant, in some cases forming crestal grabens, resulting in wide deformation zones. In other areas, discrete fault scarps dominated, and a narrower deformation zone resulted. In addition to these differences, this study found that numerous factors (e.g. fault dip, sedimentary strata) determine how a fault behaves at/near the surface.

4.4.2 How do ages calculated using Schmidt hammer exposure age dating compare with published ages?

Although Schmidt hammer exposure age dating (SHD) can yield significant error, because of its successful use on fluvial terraces (Stahl et al. (2013)), it was undertaken for this study. Ages in Barrell and Strong (2009), and Barrell et al. (2011) suggested that surfaces along the fault were 18-25 ka. While a single surface was dated to 25 ka using SHD, another surface yielded an age as young as 5.9 ka. The fact that the SHD in this study generated ages significantly younger than published reports has ramifications for both slip rates and recurrence intervals. Additionally, because surfaces dated at vastly different ages display the same amount of vertical motion indicates that there was likely a period of quiescence followed by significant activity in the last 13 ka.

4.4.3 How do calculated slip rates compare with geodetically derived ones?

Many geologic studies in this region (e.g. Amos and Burbank (2007); Amos et al. (2010); Stahl (2014)) show geologic slip rates significantly lower (2-3 times) than the geodetic models presented in Wallace et al. (2007). From Monte Carlo simulations to calculate slip rates, and integrating fault dip, the net slip for the Lake Heron Fault (2.6 ± 1.2 mm/yr) fell within the range expected for faults in the region (2.5-7 mm/yr). While this is only a single preliminary slip rate, which falls at the lower end of the scale, it does at least support the claim in Wallace et al. (2007) that fault-based geologic studies may underestimate slip.

4.4.4 How does sediment thickness/type/rheology effect fault behavior at/near the surface?

Based primarily on direct fault measurement at in situ greywacke, and comparing those with near surface dip calculations, it is clear that sediment overlying bedrock significantly effects fault behavior. At the South Branch of the Ashburton River, fault measurements at in situ greywacke indicated the fault dips approximately 60° within bedrock. When this is compared with near surface dip measurements along terrace risers, varying values were calculated (10-57°). This suggests that once the fault reaches the boundary, its dip can deflect by over 80%, influencing the near surface imbricate thrust network and effecting surface expression. Additionally, based on these measurement, it seems likely that some thrusts propagate through the overlying strata without experiencing deflection. While overlying strata can significantly reduce fault dip, a correlation could not be made between thickness of sediment and the type of fault expression. While some areas experience more flexure or

discrete scarps, because bedrock depth throughout the site remains unknown, more could not be determined.

4.4.5 What type of fault motion is observed along the Lake Heron fault, and what are the implications?

Using topographic contouring and measurements of piercing points, it was determined that across discrete fault scarps, the Lake Heron Fault is almost exclusively dip-slip. Although a small degree of lateral motion could not be discounted, because of the lack of strike-slip motion and the dominant fault strike (200°), compression can be assumed to have an orientation of 110°, almost identical to published reports (Pettinga et al., 1998, 2001; Beavan et al., 2002; Wallace et al., 2007).

While this appears to be the dominant stress, microtectonic stress measurements were also possible using crestal grabens. Although these features are extensional, created by fold hinge collapse, they also rely on deep compressional stress (Philip and Meghraoui, 1983). Nevertheless, instantaneous extensional stress can be assumed to be perpendicular to the orientation of each graben. From variability seen, it can be stated that superficial stress and localized surface rupture does not have to be representative of the structure at depth or regional stress.

4.4.6 Is it possible, that the Lake Heron Fault links with the Forest Creek Fault to the southwest? If so, what are the implications?

While a possible link between the Lake Heron and Forest Creek fault has been proposed by several (Upton et al. (2004); Upton and Koons (2007); Upton et al. (2009)), only recently has it been able to be more closely examined. By combining all methods and data in this thesis, it was determined that the Lake Heron Fault has a single event displacement of 2.75 ± 0.25 m, a recurrence interval of 1.45 ± 0.42 ka, and would generate Mw 7.4 ± 0.3 earthquakes. By comparing this information with the paleoseismology of the Forest Creek Fault, characteristics of segmented faults (including case studies), and magneto-telluric data, it seems likely that the two faults represent an 80 km segmented fault. Although there was overlap in the timing of events, because clear correlation could not be made, it is assumed that while full length rupture is possible, it is likely the segments more commonly rupture individually, rather than collectively in a Mw 7.7 earthquake. Furthermore, given a link between these two faults would mean three faults in the region are part of the same structure, as the Forest Creek and Fox Peak faults were shown to represent a segmented system (Stahl, 2014). Because of this,

the possibility exists that the entirety of New Zealand's rangefront represents a segmented fault network.

4.5 Research Summary

The tectonic geomorphology and paleoseismology of the Lake Heron Fault examined in this thesis has provided significant insight into a previously unresearched fault. This study has indicated that seismicity in the region is not as straightforward as many authors may suggest. Additionally, due to various uncertainties, scaling relationships such as those in Wesnousky (2008) often incur significant error. Therefore, individual measurements and paleoseismic investigation prove more valuable for estimating characteristics such as single event displacements and earthquake magnitudes.

Based on the research in this thesis, five conclusions are made regarding the Lake Heron Fault:

1. Near the surface, the Lake Heron Fault consists of imbricate thrusts, which result in a complex array of surface faulting and associated features. These thrust sheets, which likely merge at depth, are affected by sedimentary strata, which can in some cases deflect fault dip by up to 80%.

2. Through investigation of crestal grabens, significant variability was seen in near-surface instantaneous principle stress. These components of stress were both subparallel, and different to regional stress, showing that superficial stress and/or localized surface rupture does not need be be representative of regional forces.

3. Excluding the northernmost and southernmost mapped portions of the fault, vertical deformation remained consistent around 20 m. While the way in which this deformation was accommodated (discrete vs. distributed) changed, the total remained constant. This fluctuation is attributed to near surface variation in fault morphology, sedimentary strata, and localized stress.

4. Through various dating methods, paleoseismic investigation, and surveying, the Lake Heron Fault is believed to have a recurrence interval of 1.45 ± 0.42 ka over the last 10.15 ± 2.95 ka, each time generating Mw 7.4 ± 0.3 earthquakes. Additionally, a slip rate of 2.25 ± 1.05 mm/yr was calculated for this same time period.

5. Because of nearly identical vertical deformation seen across surfaces of different age, a period of seismic quiescence is suggested for the Lake Heron Fault (Figure 3.27). By

using radiocarbon, Schmidt hammer, and surface correlation ages, in conjunction with deformation plots, there is a significant argument for temporal variability in the slip rate of the Lake Heron Fault.

References

Amos, C. B. and Burbank, D. W. (2007). Channel width response to differential uplift. *Journal of Geophysical Research*, 112(F2).

Amos, C. B., Burbank, D. W., Nobes, D. C., and Read, S. A. L. (2007). Geomorphic constraints on listric thrust faulting: Implications for active deformation in the Mackenzie Basin, South Island, New Zealand. *Journal of Geophysical Research*, 112(B3).

Amos, C. B., Burbank, D. W., and Read, S. A. L. (2010). Along-strike growth of the Ostler fault, New Zealand: Consequences for drainage deflection above active thrusts. *Tectonics*, 29(4):n/a–n/a.

Amos, C. B., Lapwood, J. J., Nobes, D. C., Burbank, D. W., Rieser, U., and Wade, A. (2011). Palaeoseismic constraints on Holocene surface ruptures along the Ostler Fault, southern New Zealand. *New Zealand Journal of Geology and Geophysics*, 54(4):367–378.

Axen, G. J., Selverstone, J., Byrne, T., and Fletcher, J. M. (1998). If the strong crust leads, will the weak crust follow? *GSA Today*, 8(12):1–8.

Barrell, D. J. A., Andersen, B. r. G., Denton, G. H., and Science, G. N. S. (2011). Glacial geormorphology of the central South Island, New Zealand. Technical Report Report, Lower Hutt, N.Z.

Barrell, D. J. A. and Strong, D. T. (2009). General Distribution and Characteristics of Active Faults and Folds in the Ashburton District, Mid-Canterbury. *GNS Science Consultancy Report*, 2009(227):17.

Beavan, J., Ellis, S., Wallace, L. M., and Denys, P. (2007). Kinematic Constraints From GPS on Oblique Convergence of the Pacific and Australian Plates, Central South Island, New Zealand. In Okaya, D., Stern, T., and Davey, F., editors, *A Continental Plate Boundary: Tectonics at South Island, New Zealand*, pages 75–95. American Geophysical Union.

Beavan, J. and Haines, J. (2001). Contemporary horizontal velocity and strain rate fields of the Pacific-Australian plate boundary zone through New Zealand. *Journal of Geophysical Research*, 106(B1):741.

Beavan, J., Tregoning, P., Bevis, M., Kato, T., and Meertens, C. (2002). Motion and rigidity of the Pacific Plate and implications for plate boundary deformation. *Journal of Geophysical Research - Solid Earth*, 107(B10):2261.

Berryman, K., Webb, T., Hill, N., Stirling, M., Rhoades, D., Beavan, J., and Darby, D. (2002). Seismic Loads on Dams, Waitaki System: Earthquake Source Characterisation. Technical report, GNS Client Report 2001/129.

Burbank, D. W. and Anderson, R. S. (2012). *Tectonic geomorphology*. J. Wiley & Sons, Chichester, West Sussex ; Hoboken, N.J., 2nd edition.

Campbell, F. M., Ghisetti, F., Kaiser, A. E., Green, A. G., Horstmeyer, H., and Gorman, A. R. (2010a). Structure and evolution of the seismically active Ostler Fault Zone (New Zealand) based on interpretations of multiple high resolution seismic reflection profiles. *Tectonophysics*, 495(3-4):195–212.

Campbell, F. M., Kaiser, a., Horstmeyer, H., Green, a. G., Ghisetti, F., Gorman, a. R., Finnemore, M., and Nobes, D. C. (2010b). Processing and preliminary interpretation of noisy high-resolution seismic reflection/refraction data across the active Ostler Fault zone, South Island, New Zealand. *Journal of Applied Geophysics*, 70(4):332–342.

Cartwright, J. A., Trudgill, B. D., and Mansfield, C. S. (1995). Fault growth by segment linkage: an explanation for scatter in maximum displacement and trace length data from the Canyonlands Grabens of SE Utah. *Journal of Structural Geology*, 17(9):1319–1326.

Cox, S. C., Barrell, D. J. A., Suggate, R. P., and Science, G. N. S. (2007). Aoraki.

Crone, a. J., Machette, M. N., and Bowman, J. R. (1997). Episodic nature of earthquake activity in stable continental regions revealed by palaeoseismicity studies of Australian and North American quaternary faults. *Australian Journal of Earth Sciences*, 44(2):203–214.

Davis, K., Burbank, D. W., Fisher, D., Wallace, S., and Nobes, D. (2005). Thrust-fault growth and segment linkage in the active Ostler fault zone, New Zealand. *Journal of Structural Geology*, 27(8):1528–1546.

DeMets, C., Gordon, R. G., and Argus, D. F. (2010). Geologically current plate motions. *Geophysical Journal International*, 181(1):1–80.

Depolo, C., Clark, D., Slemmons, D., and Ramelli, a. (1991). Historical surface faulting in the Basin and Range province, western North America: implications for fault segmentation. *Journal of Structural Geology*, 13(2):123–136.

Elliott, A. J., Dolan, J. F., and Oglesby, D. D. (2009). Evidence from coseismic slip gradients for dynamic control on rupture propagation and arrest through stepovers. *Journal of Geophysical Research*, 114(B2).

Evans, M. D. (2008). *A geomorphological and sedimentological investigation into the glacial deposits of the Lake Clearwater basin, Mid Canterbury, New Zealand: a thesis submitted in partial fulfilment of the requirements for the degree of Master of Science in Geology at the U.* PhD thesis.

Firth, C. R. and Stewart, I. S. (2000). Postglacial tectonics of the Scottish glacio-isostatic uplift centre. *Quaternary Science Reviews*, 19(14-15):1469–1493.

Gair, H. S. (1967). *The question of post-Rangitata Peneplanation in New Zealand*. PhD thesis.

Gardner, T., Webb, J., Pezzia, C., Amborn, T., Tunnell, R., Flanagan, S., Merritts, D., Marshall, J., Fabel, D., and Cupper, M. L. (2009). Episodic intraplate deformation of stable continental margins: evidence from Late Neogene and Quaternary marine terraces, Cape Liptrap, Southeastern Australia. *Quaternary Science Reviews*, 28(1-2):39–53.

Ghisetti, F. C. (2006). Active Faulting During Positive and Negative Inversion : Examples from New Zealand and Italy.

Ghisetti, F. C., Gorman, A. R., and Sibson, R. H. (2007a). Surface breakthrough of a basement fault by repeated seismic slip episodes: The Ostler Fault, South Island, New Zealand. *Tectonics*, 26(6):n/a–n/a.

Ghisetti, F. C., Gorman, A. R., and Sibson, R. H. (2007b). Surface breakthrough of a basement fault by repeated seismic slip episodes: The Ostler Fault, South Island, New Zealand. *Tectonics*, 26(6):1–15.

Ghisetti, F. C. and Sibson, R. H. (2006). Accommodation of compressional inversion in north-western South Island (New Zealand): Old faults versus new? *Journal of Structural Geology*, 28(11):1994–2010.

Hornblow, S., Nicol, A., Quigley, M., Van Dissen, R. J., and Science, G. N. S. (2014). Paleoseismology of the 2010 MW 7.1 Darfield (Canterbury) earthquake source, Greendale Fault, New Zealand. Technical Report Report, Lower Hutt, New Zealand.

Howard, M., Nicol, A., Campbell, J., and Pettinga, J. (2005). Holocene paleoearthquakes on the strike-slip Porters Pass Fault, Canterbury, New Zealand. *New Zealand Journal of Geology and Geophysics*, 48(1):59–74.

Howard, M. E. (2001). *Holocene surface-faulting earthquakes along the Porters Pass fault: a thesis submitted in partial fulfilment of the requirements for the degree of Master of Science in Engineering Geology at the University of Canterbury*. PhD thesis.

Khajavi, N., Langridge, R., Quigley, M., Smart, C., Rezanejad, A., and Martin-Gonzalez, F. (2015). Late Holocene Rupture Overlap and Earthquake Clustering on the Hope Fault, New Zealand. *GSA Bulletin*.

Knuepfer, P. (1989). Implications of the Characteristics of Endpoints of Historical Surface Fault Ruptures for the Nature of Fault Segmentation. *U.S. Geol. Surv. Open File Rep.*, pages 193–228.

Kukkonen, I. T., Olesen, O., Ask, M. V., and the PFDP WORKING GROUP (2010). Postglacial Faults in Fennoscandia: Targets for scientific drilling. *Gff*, 132(1):71–81.

Langridge, R. M., Villamor, P., Basili, R., Almond, P., Martinez-Diaz, J. J., and Canora, C. (2010). Revised slip rates for the Alpine fault at Inchbonnie: Implications for plate boundary kinematics of South Island, New Zealand. *Lithosphere*, 2(3):139–152.

Lin, J. (2004). Stress triggering in thrust and subduction earthquakes and stress interaction between the southern San Andreas and nearby thrust and strike-slip faults. *Journal of Geophysical Research*, 109(B2).

Litchfield, N., Van Dissen, R., Sutherland, R., Barnes, P., Cox, S. C., Norris, R. J., Beavan, J., Langridge, R., Villamor, P., Berryman, K., Stirling, M., Nicol, A., Nodder, S., Lamarche, G., Barrell, D., Pettinga, J., Little, T., Pondard, N., Mountjoy, J., and Clark, K. (2013). A model of active faulting in New Zealand: fault zone parameter descriptions. Technical report, Lower Hutt, New Zealand.

Long, D. T., Cox, S. C., Bannister, S., Gerstenberger, M. C., and Okaya, D. (2003). Upper crustal structure beneath the eastern Southern Alps and the Mackenzie Basin, New Zealand, derived from seismic reflection data. *New Zealand Journal of Geology and Geophysics*, 46(1):21–39.

Lund, B., Schmidt, P., and Hieronymus, C. (2009). Stress evolution and fault stability during the Weichselian glacial cycle. *Waste Management*, (January).

Mabin, M. C. G. (1980). *The glacial sequences in the Rangitata and Ashburton valleys, South Island, New Zealand*. PhD thesis.

McCalpin, J. (2009). *Paleoseismology*. Number 95. Academic Press, Burlington, MA, 2nd edition.

Milsom, J. (2003). *Field Geophysics, The geological field guide series*.

Muir-Wood, R. (2000). Deglaciation seismotectonics: A principal influence on intraplate seismogenesis at high latitudes. *Quaternary Science Reviews*, 19(14-15):1399–1411.

Nicol, A., Institute of, G., Amp, Nuclear Sciences, L., New Zealand. Earthquake Commission Research, F., and University of Canterbury. Dept. of Geological Sciences. Natural Hazards Research, C. (2001). Paleoearthquakes on the Porters Pass Fault. Technical Report Report, Lower Hutt, N.Z.

Niedzielski, T., MigoÅĎ, P., and Placek, A. (2009). A minimum sample size required from Schmidt hammer measurements. *Earth Surface Processes and Landforms*, 34(13):1713–1725.

Norris, R. J. and Cooper, A. F. (2001). Late Quaternary slip rates and slip partitioning on the Alpine Fault, New Zealand. *Journal of Structural Geology*, 23(2):507–520.

Norris, R. J., Koons, P. O., and Cooper, A. F. (1990). The Obliquely-Convergent Plate Boundary in the South Island og New Zealand - Implications for Ancient Collision Zones. *Journal of Structural Geology*, 12(5-6):715–725.

Oliver, P. J., Keene, H. G., Crippen, T. F., Reay, M. B., and New Zealand Geological, S. (1990). Clearwater: 1:50 000 sheet J36 BD and part sheet J35.

Patrick, W., Johnston, P., and Lambeck, K. (1999). Postglacial rebound and fault instability in Fennoscandia. *Geophysical Journal International*, 139(3):657–670.

Pettinga, J., Chamberlain, C., Yetton, M., Van Dissen, R., Downes, G., and Council, C. R. (1998). Earthquake Source Identification and Characterisation. Technical report.

Pettinga, J. R., Yetton, M. D., Van Dissen, R. J., and Downes, G. (2001). Earthquake Source Identification and Characterisation for the Canterbury Region, South Island, New Zealand.

Philip, H. and Meghraoui, M. (1983). Structural Analysis and Interpretation of the Surface Deformations of the El Asnam Earthquake. *Tectonics*, 2(1):17–49.

Pugh, J. M. (2008). *The late Quaternary environmental history of the Lake Heron basin, Mid Canterbury, New Zealand*. PhD thesis.

Quigley, M., Van Dissen, R., Litchfield, N., Villamor, P., Duffy, B., Barrell, D., Furlong, K., Stahl, T., Bilderback, E., and Noble, D. (2012). Surface rupture during the 2010 Mw 7.1 darfield(canterbury) earthquake: Implications for fault rupture dynamics and seismic-hazard analysis. *Geology*, 40(1):55–58.

Quigley, M. C., Clark, D., and Sandiford, M. (2010). Tectonic geomorphology of Australia. *Geological Society, London, Special Publications*, 346(1):243–265.

Quigley, M. C., Cupper, M. L., and Sandiford, M. (2006). Quaternary faults of south-central Australia: Palaeoseismicity, slip rates and origin. *Australian Journal of Earth Sciences*, 53(2):285–301.

Roering, J., Cooke, M., and Pollard, D. (1997). Why Blind Thrust Faults do not Propagate to the Earth's Surface: Numerical Modeling of Coseismic Deformation Associated with Thrust-Related Anticlines. *Journal of Geophysical Research*, 102(B6):11,901–11,912.

Rother, H., Fink, D., Shulmeister, J., Mifsud, C., Evans, M., and Pugh, J. (2014). The early rise and late demise of New Zealand's last glacial maximum. *Proc Natl Acad Sci U S A*.

Schmidt, E. (1951). A non-destructive concrete tester. *Concrete 59*, pages 34–35.

Shakesby, R. A., Matthews, J. A., and Owen, G. (2006). The Schmidt hammer as a relative-age dating tool and its potential for calibrated-age dating in Holocene glaciated environments. *Quaternary Science Reviews*, 25(21-22):2846–2867.

Stahl, T. (2014). *Active Tectonics and Geomorphology of the central South Island, New Zealand: Earthquake Hazards of Reverse Faults*. PhD thesis.

Stahl, T., Winkler, S., Quigley, M., Bebbington, M., Duffy, B., and Duke, D. (2013). Schmidt hammer exposure-age dating (SHD) of late Quaternary fluvial terraces in New Zealand. *Earth Surface Processes and Landforms*, 38(15):1838–1850.

Steacy, S., Gerstenberger, M., Williams, C., Rhoades, D., and Christophersen, A. (2013). A new hybrid Coulomb/statistical model for forecasting aftershock rates. *Geophysical Journal International*, 196(2):918–923.

Stewart, I. S., Sauber, J., and Rose, J. (2000). Glacio-seismotectonics: Ice sheets, crustal deformation and seismicity. *Quaternary Science Reviews*, 19(14-15):1367–1389.

Stirling, M., Goded, T., Berryman, K., and Litchfield, N. (2013). Selection of earthquake scaling relationships for seismic-hazard analysis. *Bulletin of the Seismological Society of America*, 103(6):2993–3011.

Stirling, M., Langridge, R., Lamarche, G., Nodder, S., Reyners, M., Bradley, B., Rhoades, D., Smith, W., Nicol, A., Pettinga, J., Clark, K., McVerry, G., Jacobs, K., Gerstenberger, M., Litchfield, N., Van Dissen, R., Berryman, K., Barnes, P., Wallace, L., and Villamor, P. (2012). National Seismic Hazard Model for New Zealand: 2010 Update. *Bulletin of the Seismological Society of America*, 102(4):1514–1542.

Stirling, M., Rhoades, D., and Berryman, K. (1998). Evaluation of Wells and Coppersmith (1994) Earthquake and Fault Relationships in the New Zeland Context. Technical report, Institute of Geological & Nuclear Sciences.

Stuvier, M. and Polach, H. a. (1977). Reporting of 14C Data. *Radiocarbon*, 19(3):355–363.

Sumner, P. and Nel, W. (2002). The effect of rock moisture on Schmidt hammer rebound: Tests on rock samples from Marion Island and South Africa. *Earth Surface Processes and Landforms*, 27(10):1137–1142.

Sutherland, R., Eberhart-Phillips, D., Harris, R., Stern, T., Beavan, J., Ellis, S., Henrys, S., Cox, S., Norris, R. J., Berryman, K., Townend, J., Bannister, S., Pettinga, J., Leitner, B., Wallace, L., Little, T., Cooper, A. F., Yetton, M., and Stirling, M. (2007). Do Great Earthquakes Occur on the Alpine Fault in Central South Island, New Zealand. In Okaya, D., Stern, T., and Davey, F., editors, *A Continental Plate Boundary: Tectonics at South Island, New Zealand*, pages 237–254. American Geophysical Union.

Sutherland, R. and Norris, R. J. (1995). Late Quaternary displacement rate, paleoseismicity, and geomorphic evolution of the Alpine Fault: Evidence from Hokuri Creek, South Westland, New Zealand. *New Zealand Journal of Geology and Geophysics*, 38(4):419–430.

Thompson, S. C. (2002). Late Quaternary slip rates across the central Tien Shan, Kyrgyzstan, central Asia. *Journal of Geophysical Research*, 107(B9).

Upton, P. and Koons, P. O. (2007). Three-Dimensional Geodynamic Framework for the Central Southern Alps, New Zealand: Integrating Geology, Geophysics and Mechanical Observations. In Okaya, D., Stern, T., and Davey, F., editors, *A Continental Plate Boundary: Tectonics at South Island, New Zealand*, pages 255–273. American Geophysical Union.

Upton, P., Koons, P. O., Craw, D., Henderson, C. M., and Enlow, R. (2009). Along-strike differences in the Southern Alps of New Zealand: Consequences of inherited variation in rheology. *Tectonics*, 28(2):n/a–n/a.

Upton, P. d., Craw, D., James, Z., and Koons, P. O. (2004). Structure and late Cenozoic tectonics of the southern Two Thumb range, mid Canterbury, New Zealand. *New Zealand Journal of Geology and Geophysics*, 47(1):141–153.

Van Dissen, R., Barrell, D., Litchfield, N., Villamor, P., Quigley, M., King, A., Furlong, K., Begg, J., Townsend, D., Mackenzie, H., Stahl, T., Noble, D., Duffy, B., Bilderback, E., Claridge, J., Klahn, A., Jongens, R., Cox, S., Langridge, R., Ries, W., Dhakal, R., Smith, A., Hornblow, S., Nicol, R., Pedley, K., Henham, H., Hunter, R., Zajac, A., and Mote, T. (2011). Surface rupture displacement on the Greendale Fault during the M w 7 . 1 Darfield (Canterbury) earthquake , New Zealand , and its impact on man-made structures. *Earthquake*, (186):1–8.

Van Dissen, R., Hornblow, S., Quigley, M., Litchfield, N., Villamor, P., and Nicol, a. (2013). Towards the development of design curves for characterising distributed strike-slip surface fault rupture displacement: an example from the 4 September, 2010, Greendale Fault rupture, NZ. *19th NZGS Geotechnical Symposium*.

Van Dissen, R. J., Hull, A. G., and Read, S. A. L. (1993). Timing of some large Holocene earthquakes on the Ostler Fault, New Zealand. In *Proceedings of the Eighth International Symposium on Recent Crustal Movements (CRCM93), Kobe*, pages 381–386.

Wallace, L. M., Beavan, J., McCaffrey, R., Berryman, K., and Denys, P. (2007). Balancing the plate motion budget in the South Island, New Zealand using GPS, geological and seismological data. *Geophysical Journal International*, 168(1):332–352.

Wannamaker, P. E., Jiracek, G. R., Stodt, J. A., Caldwell, T. G., Gonzalex, V. M., McKnight, J. D., and Porter, A. D. (2002). Fluid generation and pathways beneath an active compressional orogen, the New Zealand Southern Alps, inferred from magnetotelluric data. *Journal of Geophysical Research - Solid Earth*, 107(B6):2117.

Wells, D. L. and Coppersmith, K. J. (1994). New Empirical Relationships among Magnitude, Rupture Length, Rupture Width, Rupture Area, and Surface Displacement. *Bulletin of the Seismological Society of America*, 84(4):974–1002.

Wesnousky, S. G. (2008). Displacement and Geometrical Characteristics of Earthquake Surface Ruptures: Issues and Implications for Seismic-Hazard Analysis and the Process of Earthquake Rupture. *Bulletin of the Seismological Society of America*, 98(4):1609–1632.

Winkler, S. (2005). The Schmidt hammer as a relative-age dating technique: Potential and limitations of its application on Holocene moraines in Mt Cook National Park, Southern Alps, New Zealand. *New Zealand Journal of Geology and Geophysics*, 48(1):105–116.

Xu, X., Wen, X., Yu, G., Chen, G., Klinger, Y., Hubbard, J., and Shaw, J. (2009). Coseismic reverse- and oblique-slip surface faulting generated by the 2008 Mw 7.9 Wenchuan earthquake, China. *Geology*, 37(6):515–518.